

Development of a steer-by-wire demonstration facility



Prepared by:
Masase Netshituka

Prepared for:
Azeem Khan
Dept. of Electrical and Electronics Engineering
University of Cape Town

Submitted to the Department of Electrical Engineering at the University of Cape Town in partial fulfilment of the academic requirements for a Bachelor of Science degree in Mechatronics Engineering

May 24, 2025

Declaration

1. I know that plagiarism is wrong. Plagiarism is to use another's work and pretend that it is one's own.
2. I have used the IEEE convention for citation and referencing. Each contribution to, and quotation in, this report, from the work(s) of other people has been attributed and has been cited and referenced. Any section taken from an internet source has been referenced to that source.
3. This report is my own work and is in my own words (except where I have attributed it to others).
4. I have not paid a third party to complete my work on my behalf. My use of artificial intelligence software has been limited to Quick calculations and assisting me to find relevant sources for the information I am seeking. I also used it to as a way to validate whether ideas I thought about implementing were feasible and keeping track of said ideas later on. (specify precisely how you used AI to assist with this assignment, and then give examples of the prompts you used in your first appendix).
5. I have not allowed and will not allow anyone to copy my work with the intention of passing it off as his or her own work.
6. I acknowledge that copying someone else's assignment or essay, or part of it, is wrong, and declare that this is my own work.

Word count: 20379.....

Signature:



Name: Masase Netshituka

Date: May 24, 2025

Acknowledgments

I would like to express my sincere gratitude to my supervisor, Professor Azeem Khan, for his invaluable guidance, support, and encouragement throughout the course of this project. His insights and feedback were instrumental in shaping the direction and execution of this work, and I am truly thankful for the opportunity to learn under his supervision. I would also like to give special thanks to Riyaad and Uzair. They have been a major help in this attempt. Helpful advice and someone to discuss concepts with was always a help.

I also wish to extend my deepest appreciation to my family, whose unwavering support and understanding made it possible for me to complete this project. Their encouragement, patience, and belief in me have been a constant source of strength throughout my studies. Here's to 2 times the charm. This one is for you guys.

To all those who go unnamed, your support is still felt.

Abstract

This project presents the development of a compact, pseudo-realistic Steer-by-Wire (SBW) demonstration facility aimed at showcasing the core concepts and operational principles behind modern vehicle steering systems. The model replicates the structure and function of commercial SBW implementations, emphasizing modular design, electronic control integration, and mechanical realism within a scale-appropriate prototype. Core subsystems include a steering input module, an electronic control unit (ECU), and a steering actuation module, all designed with real-time signal interchange and actuation dynamics. The model prioritizes educational value, system scalability, and ease of future enhancement. Comprehensive testing and literature integration guide the design process, balancing mechanical accuracy with cost, space, and feasibility constraints. This facility serves as both a learning platform and a foundation for further research into steer-by-wire technologies.

Contents

List of Figures	vii
List of Tables	ix
1 Introduction	1
1.1 Study background	1
1.2 Objectives	1
1.2.1 Scope and limitations	1
1.3 plan of development	1
1.4 Problem statement	2
2 Literature Review and Comparison Study	3
2.1 Introduction	3
2.2 Development of steering over the years	3
2.2.1 What is improvement in steering	3
2.2.2 Origins of steering	4
2.2.3 Synchronous steering	4
2.2.4 Rack and pinion	6
2.2.5 Intervention of electrical assistance	9
2.3 Steer-by-wire (SBW)	11
2.3.1 How it works	11
2.3.2 Research and Development around SBW	13
2.3.3 Current applications of SBW	14
2.3.4 Advantages and disadvantages of SBW compared to conventional steering	14
2.3.5 Future possibilities due to SBW	15
2.4 Comparison of Steering Systems	16
2.5 Conclusions	16
2.5.1 Research application to the model	16
3 Theory Development	19
3.1 Ackermann theory	19
3.2 Gears	20
3.3 Lead screw dynamics and principles	20
3.4 Rotary encoders	21
3.5 Control principles	22
3.5.1 PID	22
4 Model Design	24
4.1 Design overview	24
4.1.1 Design objectives	24
4.2 Model Sensors and Actuators	24
4.2.1 Motor	25
4.2.2 Encoder	26
4.3 Steering wheel module	27
4.3.1 Gears	28

4.3.2	Steering wheel	29
4.3.3	Screw box mechanism	29
4.3.4	Motor and sensor support	34
4.4	Steering actuation module	34
4.4.1	Base frame and supports	35
4.4.2	Steering visualization	37
4.5	Electronic Control Unit (ECU)	42
4.6	Control development	43
4.6.1	System modelling	44
4.6.2	Steering actuator model	48
5	Testing, Results and Discussion	52
5.1	Testing and Results	52
5.2	Discussion	53
5.2.1	Overall system performance	54
6	Conclusions and Recommendations	57
6.1	Future recommendations	57
Bibliography		59
A	Github	61
B	Parameter values	62
B.1	Gear values	62
B.2	Modelling	62
B.3	Bill of Materials	62
C	Additional pictures	65
D	Matlab Controller calculations	71
E	AI prompts	77

List of Figures

2.1	Bell-crank steering system [1]	4
2.2	Synchronous steering mechanism	5
2.3	Synchronous steering ratio [2]	5
2.4	Top view of various synchronous steering configurations [2]	6
2.5	A comparison of the steering ratio curves for various rack and pinion-based motor vehicles [2]	7
2.6	Varying tooth rack and steering ratio curve [2]	8
2.7	Top view of various rack and pinion based steering configurations	8
2.8	Steering torque vs vehicle speed and steering angle [3]	13
3.1	Ackermann steering principle	19
3.2	Grey code pattern	21
3.3	Absolute and incremental encoder diagram [4]	22
3.4	Basic PID closed loop configuration	22
4.1	Basic Steering wheel module flow	27
4.2	Steering wheel module design and printed version	28
4.3	Steering wheel gear design and printed version	29
4.4	Steering wheel motor gear design and printed version	29
4.5	Steering wheel motor gear design and printed version	30
4.6	Steering wheel motor gear design and printed version	30
4.7	Shaft bushing	31
4.8	Shaft sliding mechanism model	32
4.9	Slider spacer model	32
4.10	Printed shaft and slider	33
4.11	Annotated housing sectioned views	33
4.12	Printed housing	34
4.13	Printed housing	35
4.14	Assembled actuation module	36
4.15	Steering actuator leg model	36
4.16	annotated steering diagram	37
4.17	Printed housing	38
4.18	Steering actuator motor holder	38
4.19	Internal wheel hub diagram	39
4.20	Rack and pinion pair	40
4.21	Left wheel hub 3D model	41
4.22	Top(left) and bottom (right) support spacers	41
4.23	Rack and steering arm relation	42
4.24	Tie-rod model	42
4.25	ECU circuit layout	44
4.26	System Diagram (Steering wheel left, Steering Actuator right)	45
4.27	Steering wheel control loop	46
4.28	Input phase of the Steering wheel controller	46
4.29	Control phase of the Steering wheel controller	47
4.30	PD step response for Steering wheel motor	48
4.31	PID step response for Steering wheel motor	48

4.32 Steering actuator loop	49
4.33 Input phase of the steering actuator controller	50
4.34 Control phase of the steering actuator controller	51
4.35 Steering actuator step response	51
5.1 Test 4 results for Steering wheel sensor	53
5.2 Test 4 results for Steering actuator sensor	54
C.1 Fully assembled SBW Model	66
C.2 Arduino signal inputs	67
C.3 Steering wheel motor driver commands	68
C.4 Steering Actuator motor driver commands	69
C.5 Current analysis of motor under stress	70

List of Tables

2.1 Stakeholder-Oriented Comparison of Steering Systems	18
4.1 Table of model design requirements	25
4.2 Motor comparison table	26
4.3 Rotary encoder comparison	26
4.4 Optical encoder comparison	27
4.5 Compression spring comparison	33
4.6 Front axle system parameters	35
4.7 Motor driver comparison	43
5.1 Rack testing results	52
5.2 Steering limit testing results	53
5.3 Specifications assessment	56
B.1 Gear specifications for pinion, steering wheel, and steering motor	62
B.2 Parameters Table	63
B.3 Parts list for the Steer-by-Wire model	64

Chapter 1

Introduction

1.1 Study background

With the automotive industry shifting toward software-defined and electrically actuated systems, Steer-by-Wire (SBW) technology emerges as a transformative alternative to traditional mechanical steering. Unlike conventional systems that rely on physical linkages, SBW replaces these with electrical signals and actuators, enabling more flexible, compact, and efficient steering architectures. This project explores the feasibility and implementation of a scaled SBW demonstrator designed to simulate core functionalities such as angular feedback, rack actuation, and user torque response. It aims to provide both an educational tool and a foundation for further research into mechatronic control systems in modern vehicles.

1.2 Objectives

1.2.1 Scope and limitations

This project focuses on the design and implementation of a compact, scaled-down steer-by-wire (SBW) model, intended primarily for educational demonstration and foundational research. The system emulates key functions of SBW architectures, including electronically controlled steering input, rack actuation, and angular feedback. Emphasis is placed on mechanical clarity, cost-effectiveness, and modularity rather than full-scale integration or high-speed performance. The model is intended for interactive use, particularly at academic outreach events such as UCT Open Day.

Several constraints influenced the project's design and execution. The development timeline was limited to a 12-week period, restricting the extent of iterative testing and refinement. Additionally, access to manufacturing equipment was limited: only one 3D printer was available at any given time, and its use was confined to standard working hours (08:00–16:30, Monday to Friday). This significantly impacted component turnaround times and limited the feasibility of large or repeated print jobs. Financial resources were also restricted to a budget of R2000, necessitating the selection of low-cost components and materials, which in some cases limited precision, durability, or performance. These constraints required strategic compromises in system complexity, component quality, and control accuracy.

1.3 plan of development

The development of this project is structured across six key chapters, each building upon the previous to document the full scope of the steer-by-wire model's design and implementation.

Chapter 1: Introduction This chapter introduces the concept of steer-by-wire technology, outlines the motivation behind the project, and presents the central problem being addressed through the development of a functional, scaled demonstrator.

Chapter 2: Literature Review and Comparison Study A comprehensive review of historical and modern steering systems is provided, including mechanical, power-assisted, and steer-by-wire configurations. The chapter

highlights key advantages, limitations, and future trends, contextualising the project's relevance.

Chapter 3: Theory Development Core theoretical principles relevant to the model are discussed, including Ackermann steering geometry, gear and lead screw dynamics, encoder functionality, and PID control principles used for closed-loop response.

Chapter 4: Model Design This chapter details the mechanical and electrical design of the system, including CAD modelling, material selection, and the physical construction of the steering wheel, actuation module, and rack system. It also outlines the sensor and actuator configurations.

Chapter 5: Testing, Results and Discussion A series of tests are described to validate the system's performance against the defined objectives. Results are discussed in terms of steering accuracy, system sensitivity, centring effectiveness, and overall compliance with design specifications.

Chapter 6: Conclusions and Recommendations The project's outcomes are summarised, with a critical evaluation of successes and limitations. Recommendations for future improvements and research directions are provided to guide further development of the SBW model.

1.4 Problem statement

Steer-by-Wire (SBW) is an emerging technology in the automotive sector that replaces traditional mechanical steering linkages with electronic control systems. By using sensors, actuators, and embedded software to interpret driver inputs and command wheel angles. SBW offers advantages such as improved safety, reduced mechanical complexity, enhanced performance, and integration potential with advanced driver assistance systems (ADAS) and autonomous driving technologies. However, the implementation of SBW systems introduces complex challenges related to real-time control, sensor precision, actuator reliability, and mechanical-electronic integration.

This project focuses on the development of a scaled, pseudo-realistic SBW model that emulates the core functionalities of commercial SBW systems. The aim is to demonstrate how electronically controlled steering can replicate or enhance conventional steering performance, while also highlighting the practical design, manufacturing, and control challenges involved. Supported by a comprehensive review of existing SBW technologies and a comparative analysis with mechanical steering systems, the study explores system modelling, simulation, prototyping, and testing of a functional demonstrator.

As part of UCT Open Day, this working prototype serves both educational and outreach purposes. The model is designed to be visually engaging and technically robust, providing prospective engineering students with a tangible example of cutting-edge automotive mechatronics. Mechanical components are fabricated using 3D printing facilities at UCT, while actuators, encoders, and controllers are integrated to showcase real-time control in action. This project thus not only investigates the feasibility of scaled SBW implementation but also aims to spark interest and awareness in automotive systems engineering.

Chapter 2

Literature Review and Comparison Study

2.1 Introduction

Transportation has become a vital part of everyday life and has undergone many transformations since the horse-drawn carriage days. Since the inception of the motor vehicle in the late 1800s to early 1900s [5], motor vehicles have undergone many advancements and evolutions. This was achieved by developing the technology behind motor vehicles. More specifically, it's sub-systems. One of the most vital subsystems is the ability to control the direction in which the vehicle is travelling. In the case of 4-wheeled motorised vehicles, this is achieved through a steering mechanism attached to a wheel that the driver can manually rotate to induce a turning movement, steering towards the desired direction of travel. This review investigates the development of the systems involved with steering and how they have previously been developed and may continue to develop in the future.

Motor vehicles are largely complex mechanical systems, with the effects of changes having an intersectional impact. Due to this, there is research into the kingpin and caster angles (longitudinal and latitudinal, respectively), alternative suspension structure, different tire design and tread, etc., that improve vehicle manoeuvrability, stability and turning ability. However, they do not affect how the driver's steering intent is executed and thus are not considered for this study.

This research instead focuses on the prominent forms of steering actuation that have developed over the years and their further development. Historical steering improvements can be tracked from horse-drawn carriage carts to different 4-wheel motor vehicle steering mechanisms and eventually the inception of electromechanical power steering. From that point, the tangible future of steering through Steer-by-wire technology is explored. Comparisons are drawn throughout the review between the most prevalent modern conventional steering methods and the expected performance of practical steer-by-wire implementation. The differences between the various steering mechanisms and methodologies will be directly compared.

2.2 Development of steering over the years

2.2.1 What is improvement in steering

What constitutes an improvement in steering largely depends on the perspective from which the system is evaluated. Drivers, manufacturers, and designers prioritise different performance, usability, and practicality characteristics.

For the driver, enhancements of steering precision and controllability are highly valued. Reduced steering effort contributes to a more accessible and comfortable driving experience, particularly in urban or low-speed scenarios, such as parking or driving in traffic. The type of driver, however, plays a critical role in defining these improvements. For everyday drivers, suppressing road-induced disturbances, such as vibrations and minor road irregularities, enhances comfort and reduces steering fatigue. However, performance-oriented drivers desire increased tactile feedback from the steering system, as this is crucial in vehicle control at high speeds and under demanding conditions, improving both safety and performance.

From a manufacturer's and brand perspective, improvements are often linked to the design, production, and

operational characteristics of the steering system. Reduced manufacturing complexity and lower component costs enhance scalability and profitability. Additionally, system reliability, responsiveness, and crash safety are key to brand reputation and consumer trust. The ability to fine-tune or customise the steering characteristics, such as responsiveness, damping, feedback or layout, adds value during vehicle development and allows for better alignment with various vehicle classes, market needs and design objectives.

Evaluating improvements in steering systems requires a multidimensional approach. Many of the above factors are considered when assessing and comparing the steering systems to be expanded in the review.

2.2.2 Origins of steering

Some of the first steering mechanisms developed were intended for horse-drawn carriages. The design, developed in the late 18th century, used a trapezoid-based steering mechanism [5]. Later on that century, the first self-propelled vehicle was developed in France by Nicolas-Joseph Cugnot [6]. The Fardier à vapeur, using steam engine propulsion, had a 3 wheel configuration, one in front and two behind. A design still used today for tricycles. Due to the direction being determined by a single wheel, a simple pivot point between the wheel and handle is sufficient, similar to that of a bicycle.

Eventually, vehicle designs incorporated a 4th wheel. This addition increased vehicle stability, but presented a challenge for aligning the front wheels. At this point, many principles developed for horse-drawn carriages were implemented for motor vehicles. Primarily, one devised by a Bavarian carriage builder, Lenkensperger, to improve the steering ability of carriages. This was achieved through increasing the relative steering angle of the internal wheel. This method was patented by Rudlof Ackerman and is known as the Ackerman criteria, a fundamental design principle for steering mechanisms utilised to this day [7] (The Ackerman principle is further explored in Chapter 3).

The next step signified the beginning of mechanical leverage used to a significant extent for steering. In the late 19th century, the bell crank steering system was developed by Amédée-Ernest Bollée[1], depicted in Figure 2.1. The system uses a vertical steering column, with the steering motion executed by a pinion gear pushing a curved rack, inducing a swinging motion in the central rod structure. While this design is mechanically advanced, it did not gain popularity.

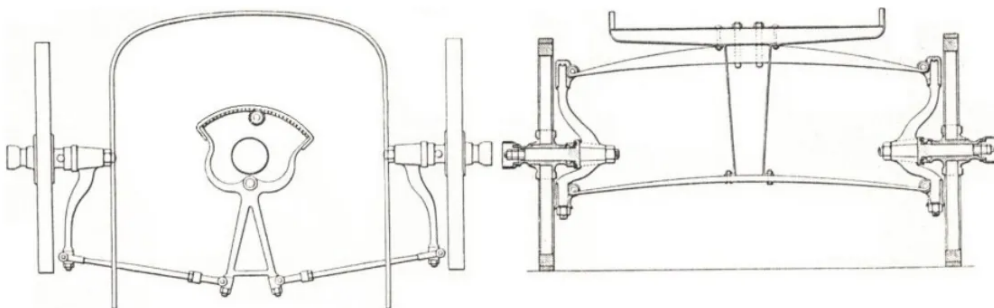


Figure 2.1: Bell-crank steering system [1]

The early 20th century brought the first use of a tilted steering column, power screw steering box and trapezoidal steering linkage in automotive vehicles. P. Mooers trapezoidal mechanism and Du Quet's winch-and-rope mechanism (for ship rudders) would form the basis for the earliest form of rack-and-pinion steering as it currently exists, which was patented by Gustave Dumont in 1922 [1].

2.2.3 Synchronous steering

As technology advanced, the use of leverage became more popular. Synchronous steering is a modern technique that utilises multiple lever arms to improve the driving experience. The name is due to the steering execution

2.2. Development of steering over the years

being carried out by 2 arms moving synchronously, the pitman and idler. It is also referred to as recirculated ball steering, after recirculated ball joints that translate the rotational movement of the steering column to the pitman, the primary driving arm. Synchronous steering operates on the same principle as a lever, with greater torque exerted the longer the radius of rotation is. Rotational movement is the primary type of movement throughout the system. Through this, the effort required by the driver to achieve the desired steering output is greatly decreased.

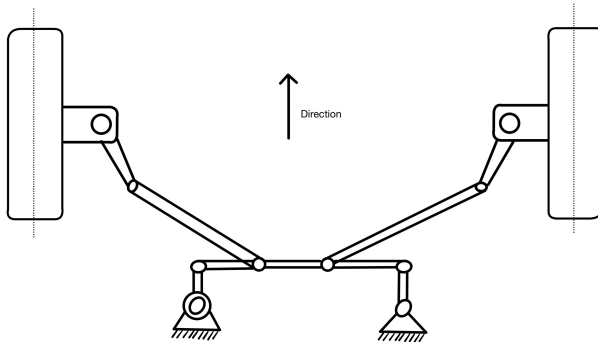


Figure 2.2: Synchronous steering mechanism

Figure 2.2 shows the general structure of this mechanism. The steering shaft is connected to the pitman. Parallel and adjacent to the pitman is the idler arm fixed to the frame with a pivot joint. The pitman arm and the idler are connected by an intermediary bar to keep their rotary movement synced. Connected to this intermediary bar are two arms referred to as tie-rods that connect the syncing bar to the fixed steering arms of the wheel hub. As the driver steers, the pitman arm is, in turn, rotated. This rotation induces a near-linear translation of the intermediary bar, pushing & pulling the tie-arms and their associated steering arm. This creates the rotation of the wheels around their kingpin.

This system enabled manufacturers to tune the steering experience for drivers, increasing the amount of steering wheel rotations required in exchange for less physical effort. The difference between the steering wheel angle and the resulting steering angle of the vehicle is referred to as the steering ratio. Reimpell created a graph comparing the steering ratios of different car models that use synchronous steering, seen in Figure 2.3. While the achieved steering ratios are considered low, they remain fairly linear within a $\pm 25^\circ$ range from the centre in either direction and drop off at a low gradient. In the case of the BMW, the ratio remains fairly linear with a 425° input resulting in a 25° mean steering output.

While the synchronous bar's movement may seem linear, it is not. The significance of this is demonstrated when comparing the steering ratio curves of this and rack-and-pinion mechanisms.

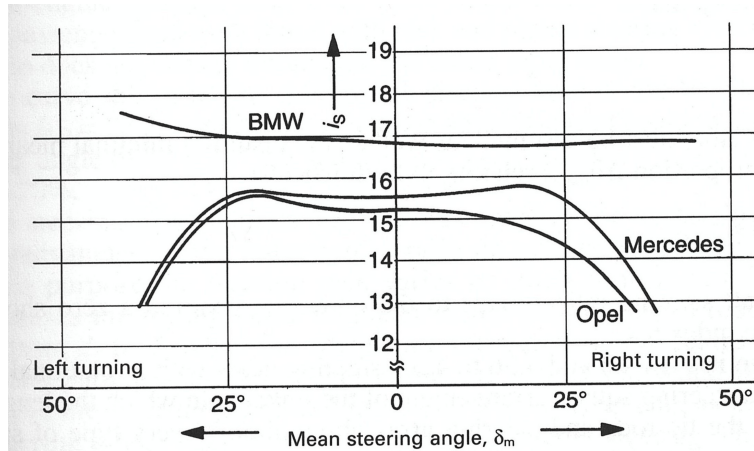


Figure 2.3: Synchronous steering ratio [2]

Configurations

Synchronous steering has 4 main configurations. These are all based on the positioning of the pitman and idler arms, and the tie rods relative to the wheel axle. These different arrangements are shown in Figure 2.4 below.

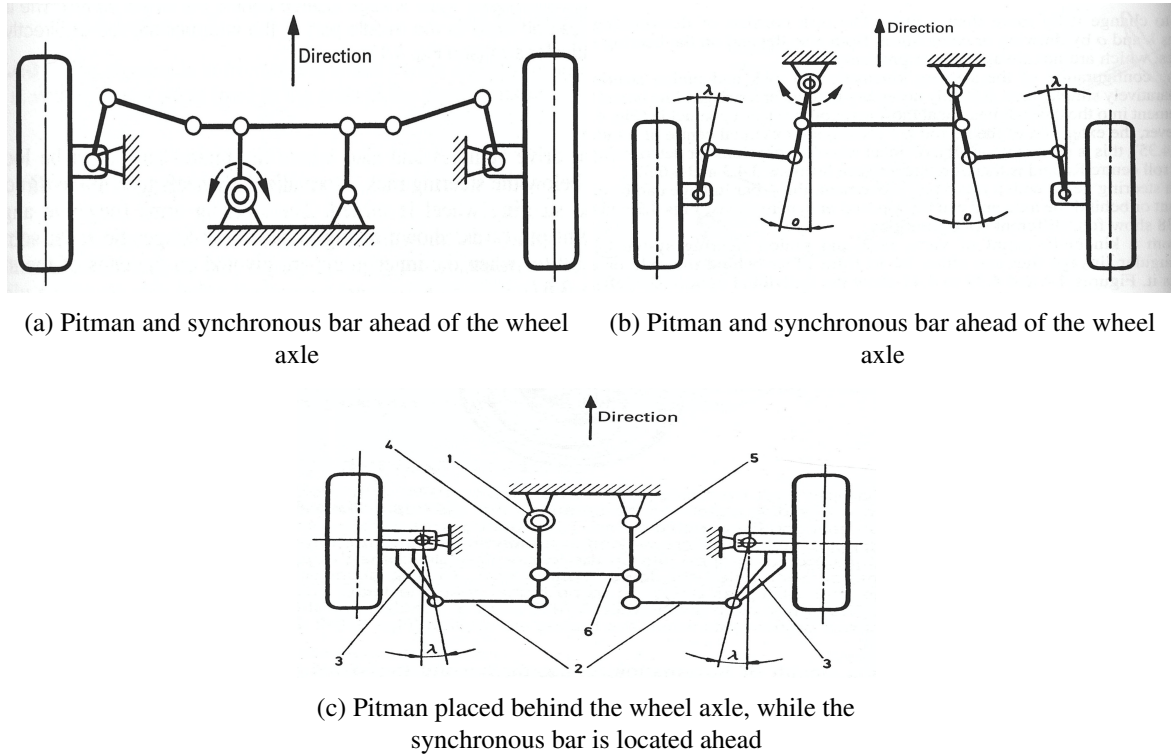


Figure 2.4: Top view of various synchronous steering configurations [2]

Advantages and Disadvantages

Synchronous steering has quite a few advantages. One being that the system is suitable for vehicles using a rigid axle. The other advantages relate to the lengths of the rotating arms. Due to the lever principle, this system can transfer high loads between its arms and the driver. The functionality grants a high level of flexibility regarding the lengths of tie-rods and steering arms, the idea being that the longer, the better. Longer arms reduce the force on the pitman and intermediate arms. The lengths of the tie rods can and are often set to different lengths to create more customised steering ratio curves.

The disadvantage is that the system requires a lot of space, even in its most compact form. This makes it difficult to implement in front-wheel passenger cars. Due to the number of long members, the vehicle needs an independent suspension for each wheel to prevent damage to the system. They also create a higher steering elasticity than other systems, although this elasticity can be good, depending on the desired steering feel. A major reason this system isn't popular is the system's complexity due to the high number of individual moving parts. This makes it more expensive to manufacture and implement.

2.2.4 Rack and pinion

Rack and pinion steering uses the rack and pinion gearing system, as the name suggests. The steering wheel that the driver interacts with is connected through a shaft to the actuating pinion. The pinion drives a sliding rack through the meshing of the tooth patterns along the pinion gear and rack. This mechanism translates a rotational force (through the pinion) into a translational force (carried through the rack) and vice versa. The initial concept mentioned in the Origins of steering was based on a 4-bar steering system. However, this proved inefficient,

requiring large amounts of force to steer, as highlighted by Zhao J, Liu X, et al. [8]. Their paper highlights the limitations of 4-bar linkage systems, motivating the conversion to a 6-bar steering system. A key point is the increased ability to achieve the ideal Ackermann principle. 2 tie rods connect the rack to the steering arms fixed on the wheel hub. The push/pull of the tie rods on the steering arms rotates the wheel around the kingpin. This is how steering is achieved. Figure 2.7a shows an example of this mechanism.

Due to being a gear-based relationship, the desired steering characteristics can be tuned. The gearing ratios between the rack and pinion allow for a reduction in turning speed in exchange for a larger linear force output. This decreases the effort needed to steer the vehicle, but requires more wheel rotations to get the same turning result. In the case of the rack and pinion system, the steering ratio is not fixed nor linear, having more variance compared to synchronous steering. Figure 2.5 displays the curve of a traditional rack and pinion steering configuration. As the mean steering angle of the wheels increases, the steering ratio decreases significantly. This means fewer wheel rotations are needed, but more effort is required at more extreme steering angles. This presents challenges in situations such as parking, which often requires sharp steering angles while moving at a low velocity. These also happen to be circumstances that would require the most steering effort.

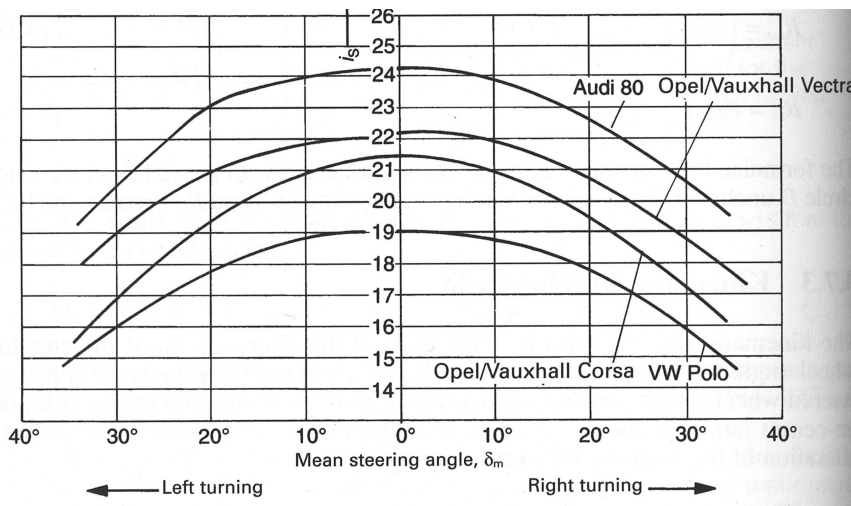


Figure 2.5: A comparison of the steering ratio curves for various rack and pinion-based motor vehicles [2]

This eventually led to the development of variable steering ratio racks. These racks were manufactured such that the width of the teeth would change towards the ends of the rack, effectively changing the gearing ratio and resulting steering ratio (Figure 2.6a). While this is a costly and intricate component to manufacture, it significantly improved the steering ratio curve of the early rack-and-pinion system. The generic form of the altered steering ratio is shown in Figure 2.6b. This improvement meant steering at high angles would be significantly easier, improving parking and emergency steering manoeuvrability.

While the number and type of components for this steering style are standardised, their configuration can vary depending on different factors, such as the desired steering performance and available space due to general vehicle design.

Configurations

Rack-and-pinion steering has quite a few ways to design the mechanism. The overall linkage layouts are mostly categorised by the rack and tie-rod positions relative to the axle. The more standard layouts have the rack and tie rod on the same side of the axle, such as in Figure 2.7a and 2.7b. This often results in shorter tie-rods, with the steering arm being angled outwardly. However, it's not uncommon for the rack to be behind the axle, while the tie-rods extend ahead of the axle or vice versa. These configurations often result in longer tie-rod connections and the steering arms being angled internally, such as Figure 2.7d and 2.7c. The decision of which configuration to use depends on space constraints and the associated suspension system. Each has different factors to account

2.2. Development of steering over the years

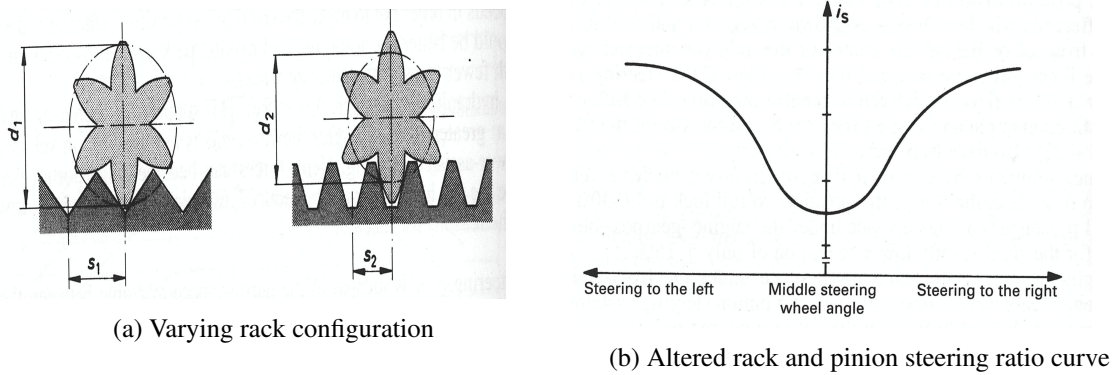


Figure 2.6: Varying tooth rack and steering ratio curve [2]

for in terms of support and function, which will be expanded on ahead.

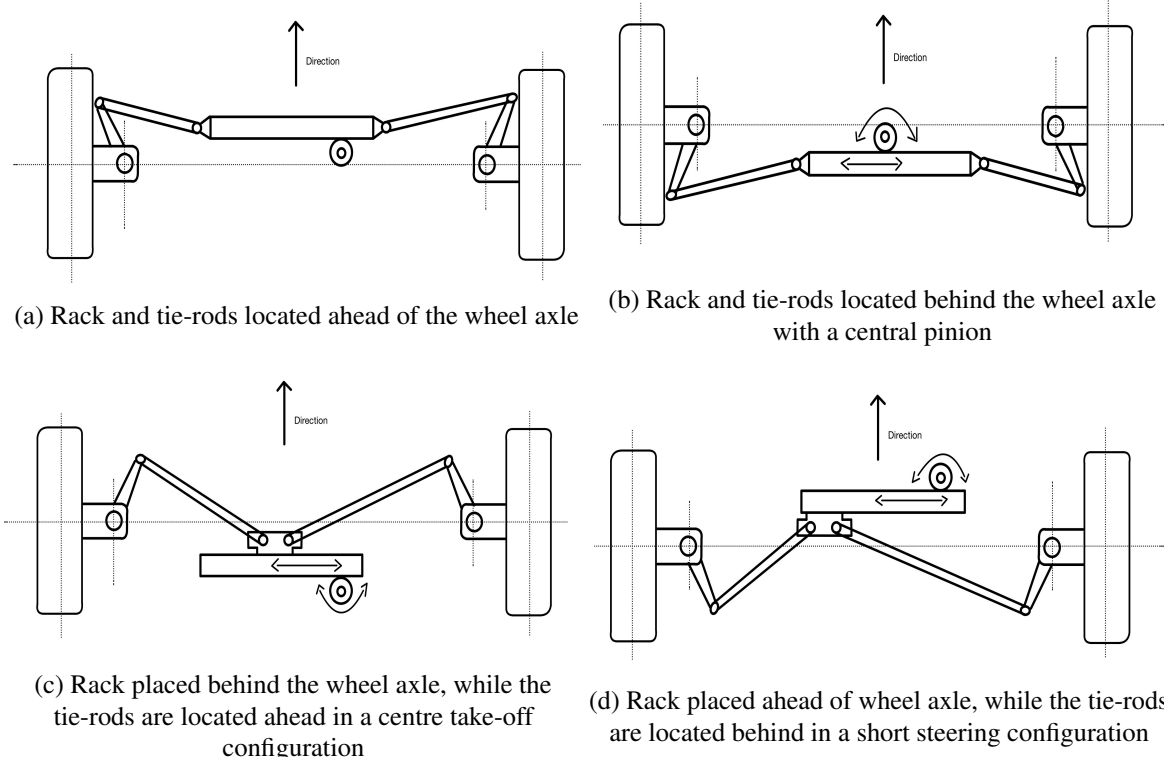


Figure 2.7: Top view of various rack and pinion based steering configurations

Additionally, pinion and tie-rod positions along the rack can differ. The pinion and tie rod placement comes in 4 standardised configurations [2]. Type 1, Figure 2.7a - 2.7b, has the pinion placed off centre of the rack when in a neutral steering position (right or left side depending on right or left side drive respectively); additionally the tie rods are connected on the ends of the rack. This is referred to as a ‘side tie rod take-off’. Type 2 has the pinion placed in the centre of the rack, with the tie rods connected on the ends. Type 3 has the pinion off-centre, while the tie rods are connected in the centre of the rack, much like figure 2.7c. This is known as ‘centre tie rod take-off’. Lastly, the Type 4 configuration, known as ‘short-steering’, has the pinion placed on one end of the rack with both tie rods connected on the other end.

Of these configurations, Type 1 is the most popular. This is largely due to its simplicity and compact nature. Additionally, no rotary moment is induced that could turn the rack around its centre line, resulting in 1 less factor

to worry about compared to types 3 and 4. In conventional steering, the off-centre nature of the pinion allows for easy alignment with the steering shaft.

Type 3, the second most popular configuration, incorporates McPherson struts and strut dampeners. This configuration is suitable when the steering gear has to be located fairly high, hence the long length of the tie rods for reliable steering. While this is a key characteristic of the configuration, additional care needs to be taken to ensure the steering rack cannot twist due to rotary moments when driving. The steering system also has worse precision and responsiveness than its Type 1 counterpart due to the steering forces happening far from the connection points on the steering axle. These forces cause elastic deformations on the suspension and shock-absorber struts and induce additional strain on the tie rods.

While Types 2 and 4 are more niche, they are fairly prevalent and are favoured by particular vehicle brands. The Type 2 configuration is present in some Porsche vehicles, and the Type 4 is found in vehicles produced by the Volkswagen Motor Group.

Advantages and disadvantages

Rack and pinion is the most commonly used steering configuration, especially among European and Japanese front wheel drive vehicles, and for good reason [2]. Its simple nature is translated into the ease of construction. This simplicity leads to good manufacturing efficiencies, saving time and cost. While some considerations need to be taken, the overall design has a good degree of efficiency. This is partly due to the tie-rods being connected directly to the steering rack, leading to a compact form factor and ease in limiting the rack travel distance and steering angles.

While rack and pinion is the most commonly used steering mechanism, it is not without its faults and limitations. One limitation is the inability to use a rigid front axle. Using one leads to unintended steering behaviours, especially when encountering bumps/impurities in the road, known as ‘bump steering’. Thus, when making use of Rack and pinion, an independent suspension needs to be accounted for. Despite this, rack and pinion steering is still the most sensitive to impacts as the tie-rods are subject to greater stress through angular forces. Depending on the configuration, particularly with outward angled steering arms, the steering arms need to be short enough to fit in the wheel hub. Shorter steering arms translate into more force on the steering system through the tie rods. Since the steering actuation is carried out through the rack, the potential steering angle depends on the available travel space. Thus, for increased steering, more space needs to be left vacant. Lastly, Rack and pinion steering experiences an increasing reduction in turning ratio the further the wheels are turned. Thus, more effort needs to be exerted the greater the turning angle. This disadvantage becomes most apparent in situations requiring high turning angles at low speeds, like parking the vehicle. This was initially improved due to the intervention of the variable steering rack and later by power steering advancements.

2.2.5 Intervention of electrical assistance

As vehicle engines became larger, increasing the front axle load of cars, there was an increased demand for improvements to steering. This came in the form of power steering. Power steering functions as an additional support to the existing system. This means the steering ability of the vehicle would not be dysfunctional should the power steering fail. Power steering works by detecting the input steering torque through the steering shaft and supplementing it with additional force. The amount of force is determined according to a predetermined curve, using input torque and sometimes vehicle speed as factors [2]. There are currently 3 main variations of power steering commonly implemented, with varying degree of intervention.

Hydraulic Power-Assisted Steering (HPAS)

The first power steering system to be commonly implemented was Hydraulic Power-Assisted Steering. HPAS uses a pressurised oil and pump system to exert additional steering force. The system is efficient at reducing the sensitivity of the system from road impacts and vibrations, especially for the rack and pinion steering system.

This self-damping effect allows the removal of a shock absorber for HPAS Rack and pinion compared to a traditional rack and pinion system.

The hydraulic pump is driven by the engine directly, using V-belts. Flow-limiting valves within the pump ensure fast steering movements are supported by hydraulics. When on centre, the pressure in both chambers is equal. However, when a steering motion occurs, a set of valves open, and others close. This causes pressurised oil to apply pressure to a piston, assisting the steering motion in the desired direction [9]. In rack and pinion systems, a separation disk is located in the working cylinder to divide the pressure used to move the steering mechanism. For recirculating-ball steering, torsion bars detect the amount of input torque via the steering bar. The bar's twisting motion opens valves depending on the direction of rotation, resulting in a pressure difference within the main chamber [2].

HPAS has the benefit of maintaining a mechanical link between the shaft and steering mechanism, so if pressure is lost, the vehicle can still be steered. However, the system is always fully operational. This causes an unsatisfactory light steering effect at high speeds and increases the vehicle's energy consumption to a large degree. The additional fuel consumption due to hydraulics can be 0.2 - 0.71 L per 100 km [2].

Electro-Hydraulic Power Assisted Steering (EHPAS)

EHPAS was developed to improve the control and efficiency of the hydraulic system while reducing the form factor. The oil pump is no longer driven by the engine, but rather electronically by a 'power pack'. The use of a power pack improved the space constraints of the system, as the pack could be placed separately and connected by cables, additionally, a cooling system was no longer required [2]. The power packs have controllers utilising steering data such as input torque, steering angle and rate of rotation to calculate the appropriate release of oil. The oil is stored in an accumulator, released by the pump during steering motions and returned upon the completion of said motion.

Aside from the saved space, the pack provides a few functional benefits. One such benefit is the engine does not need to run to activate the power steering. Another being the precise control of oil release, resulting in a $\pm 20\%$ reduction in energy consumption during steering and turning off the hydraulic system during non-steering operation [10]. This refined control also opened the door to customised steering characteristics, by adjusting the release of oil according to vehicle behaviour.

A. Pawlak, D. Gruber et al, took an alternate approach. They created a combined system using a magnetic system electronically augmented to supplement the torque provided to the hydraulic system [11]. While their system does not interface directly with the hydraulics, the electrically controlled magnetic actuator makes this an EHPAS.

While EHPAS improved the functionality and fuel efficiency of HPAS, the addition of various components and system complexity made it significantly more expensive to manufacture [9].

Electrical Power Assisted Steering (EPAS)

The next progression in PAS is the complete removal of the hydraulic system. While EHPAS was an improvement in functionality, the cost drawback made it unreasonable as a final solution [9]. EPAS uses a motor and power amplifier combination coupled to the steering column and rack system to replace the hydraulic aspect of HPAS. The assistive motor can be placed on the steering column, coupled to the pinion (pinion stress increases directly with additional force) or directly on the gear rack (suitable for high axle loads and steering forces) [2]. Much like EHPAS, an Electronic Control Unit (ECU) uses data from appropriate sensors to control the force generated by the motor. The architecture for this system is more complex than EHPAS, but the physical package is smaller, lighter and simpler to assemble, solving the main issues posed by both prior power-assisted systems. The motor system is also a lot more responsive than EHPAS, offering more performance customisation.

Adwest Engineering designed their own EPAS system, using a 12 V 4 Nm motor, driven through 5:1 gearbox, to convert a 5 Nm input to a 25 Nm steering output [9]. The choice was made to optimise force output, without

requiring a motor with higher base output as it would become too expensive. Steering axle loads can vary in intervals from 650 Kg - 1300 kg with associated maximum gear rack loads of 6000 N - 10 000 N, so the gearing ratio and motor selection will depend on placement and expected loads.

In its current form EPAS is mainly used for smaller vehicles, due to their limited power output 12 V motors being the popular choice with 42 V looking to be introduced, but it takes the first step to integrating the steering systems with future vehicle network and control systems. This could be used to refine the dynamic performance and provide useful diagnostic information as well.

2.3 Steer-by-wire (SBW)

Steer-by-wire represents the highest degree of electrical assistance, resembling an evolution of EPAS. However, while other power assist systems amplified and augmented the drivers force through the steering shaft, SBW eliminates the steering shaft entirely. Thus, it is beneficial to see SBW as the birth of an entirely new steering system that borrows many elements from power assisted systems like EPAS.

2.3.1 How it works

'By-wire' refers to using electrical controllers to replace mechanical connections. While fully electric steering assist is a recent development, by-wire technology has been present for a long time. Many planes and large boats use steer-by-wire technology, and in the car context, throttle and brake systems have already begun transition to by-wire technology [12]. Generally, SBW systems can be broken up into 3 subsystems: The steering wheel and feedback module, the steering actuation module and the Electronic Control Unit (ECU), which facilitates the control and communication between the two subsystems and the various vehicle state sensors. The main objective of these systems is to improve steering performance while still recreating the same responsive feeling as a real car performance, and they are thus modelled after real, mechanically based vehicles.

Steering input module

The steering input module of SBW still uses a steering wheel attached to a steering column. However, this shaft is significantly shorter and is connected to some sensors, with a motor commonly placed on the end, instead of being attached to the actuation system. The motor is present due to the understanding that despite being disjointed, the steering sensation of SBW should mimic that of conventional steering as much as possible. The objective is to eliminate the need for a re-learning period when transitioning from conventionally steering vehicles. To this end, much of the research surrounding SBW technology emphasises the need to translate a resistive feedback force from the road to the driver. Conventionally, this force is a by-product of the stiffness and translation of forces acting on the wheels when steering. This is one of the most vital input stimuli used by the driver while driving, particularly when steering, visual and 'centrifugal' forces being second and third, respectively. This enables the driver to deduce the wheel's interactions with the road. This informs the driver of the road's conditions and how to adjust the steering angle for an optimal steering result. Additionally, these forces are responsible for the steering wheel returning to centre as the car straightens after a turn.

A brushed DC motor is the most commonly used actuator for steering torque feedback, translating the force to the shaft through gearing or belt drive configurations. However, Masahiko et al. [13] suggest that a controller paired with an electric power steering module would perform better than a motor. Their main criticism is the stiffness of the motor response, accompanied by a low on-centre handling. This is especially present at high speeds, when minimal turning angles are used, but high sensitivity is required.

Traditionally, the steering shaft is a torsion bar with a torque sensor attached to it. As the driver steers towards the desired direction, a torque is induced along the length of the shaft. This is detected by the sensor and communicated to the ECU. The ECU then sends a signal to the feedback motor. Depending on the signal received, the motor will either attempt to match, resist or drive the rotation of the shaft. This combination of

motor interaction creates a varying feedback and centring sensation. Some designs for the Steering module use rotary encoders in combination with the torque sensors for improved steering angle detection.

Electronic control Unit (ECU) and control methods

The ECU is a dedicated microcontroller connected to the various motor drivers, sensors and protection circuitry. In that sense, it fulfils the same role as the ECU in EPAS systems, but with even greater complexity. Park et al. use a 68HC912 made by Motorola, a microcontroller already prevalent in vehicle electronic control [14]. It is responsible for receiving and interpreting the data from multiple sensors, assessing the vehicle state and the intended steering result and sending control signals to the steering actuator and feedback motors. As was mentioned, the ECU will receive the torque input from the steering module and calculate the desired steering angle using known material and design parameters. This angle is then adjusted according to the configured steering ratio and compared to the current angle of the car's wheels. The controller then calculates the appropriate signal to send to the actuation motor to achieve the desired angle. Simultaneously, the torque experienced by the car's wheels is calculated based on the steering error and data from other sensors, such as vehicle speed and actuating motor currents. A signal to simulate the effect of this force is then communicated through motor drivers to the torque feedback motor. The motor drivers are commonly H-bridge MOSFET circuits due to their fast responsiveness and the need to operate the motors in all 4 quadrants (forward and reverse motoring/braking). This feedback torque is then communicated to the driver through the motor on the steering input module. This process is cyclical and highly complex, happening at a high, constant rate. The more advanced and complex the system is, the more sensors are integrated, leading to a more refined feedback and steering result. More advanced systems also account for data such as the car's yaw, pitch and roll, etc.

The control algorithm of the ECU is an intricate and tailored endeavour, as the optimisation and performance of these controls depend on the use case and specifications of the vehicles they are implemented for. While the precise tuning of these algorithms forms the core of proprietary intellectual property for companies that develop high-performing controllers; generally, PI, PD and PID control serve as the most commonly used methods of control by researchers. Yih et al. [12] and Se-Wook et al. [3] use feed-forward techniques to improve the closed-loop control of the steering response. Feed-forward techniques help reduce tracking error without the downsides of other methods like using an integrator term or the increase of gain constants, which slow down the system response and reduce overall system stability respectively. Another benefit is a reduction in the system's cost, as fewer sensors are required for operation. The downside is that the forces/disturbances being accounted for need to remain fairly constant and/or predictable throughout vehicle operation. While PID is the most common, improvements to this and other control methods are still being researched.

Steering actuation module

Due to SBW having an independent/isolated actuation subsystem, there is a lot more freedom for design compared to traditional steering. Research has been conducted into various forms of actuation, primarily rack, tie-rod and steering knuckle (wheel hub) based actuation [14]. Despite this, most of the research and development around SBW, as well as its few implementations, have currently been focused on rack based actuation. This is largely due to the usage of the 6-bar mechanical linkage system that is already prevalently used in conventional vehicles. This makes the process of converting/redesigning current vehicle models to SBW simpler for research and manufacturing purposes. Additionally, actuation through the rack only requires a single driving motor to function with a more simplistic control logic when compared to tie-rod and knuckle based methods that require an individual motor per wheel. This in turn also makes it the most cost effective of the 3 to implement.

While the specific configurations may vary, much like in traditional non-SBW vehicles; the general architecture is the same as EPAS. A motor takes the place of the steering shaft, providing a rotational force through a pinion to the rack that drives the steering movement. On this front, there is not much else that is different on how the vehicles behave in comparison vehicles equipped with EPAS, some researchers even choosing to make use of existing PAS in conjunction with a motor, like Yih, Gerdes et al. [12]. The main difference being that the motor is directly controlled by the ECU. The motor selected for this purpose would depend on the requirements of

the vehicle and the needed performance. The most common is a 12 V DC brushless motor, as these are already standardized due to EPAS. However, some designs do use an AC brushless motor.

A major benefit of SBW actuation is that steering ratios that would've been fixed, or partially dynamic through the use of specialized rack designs, as shown earlier; are now able to be controlled to a much more customizable degree than was previously possible even in PASs. Depending on the parameters, configurations, objectives and presets determined by the manufacturer, a much more tailored approach can be taken to designing the driver's experience.

2.3.2 Research and Development around SBW

While by-wire technology has been present for a long time, SBW is still fresh and as such, there is a lot of research currently being completed and being proposed for the future. The main focuses currently are the refinement of the control theory behind the system overall system and feedback torque in particular. Another aspect is the safety systems surrounding SBW. PAS are able to continue steering should the system fail, but due to the lack of steering shaft, this is not an option for SBW. These points of research are expanded on below.

Handling control and optimisation

Yih, Gerdes et al. delve into the possibility of using SBW technology in order to alter the handling of a vehicle electronically[12]. They successfully convert a traditional hydraulic power steering vehicle into one using SBW as a basis, still making use of the hydraulic power steering as mentioned earlier. They developed and confirmed a second-order system model for their SBW steering mechanism, which was used for the development and simulation of their control algorithm. PD feedback control principles formed the basis of the system with the addition of feed-forward techniques to reduce the tracking error of the system. The developed system was tested against an altered ‘bicycle model’ that would approximate the dynamics of a vehicle in linear motion. In the end they were able to prove their system and control methodology could effectively control the handling response; akin to changing the front tire stiffness of a car. The result was producing handling ranging from understeer to oversteer tendencies through the adjustment of 2 gain variables. This would allow drivers to customize their experience to their liking.

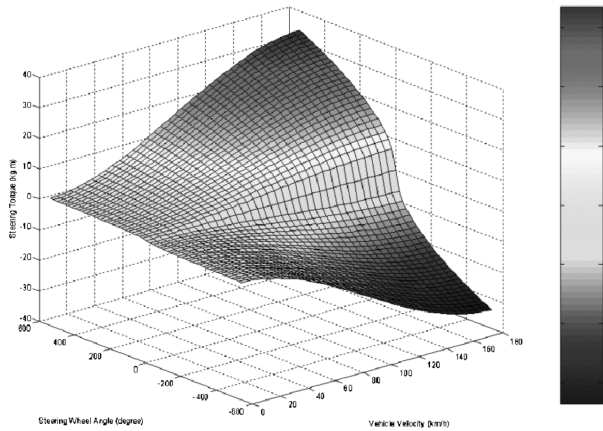


Figure 2.8: Steering torque vs vehicle speed and steering angle [3]

Se-Wook, Ho-Chol et al.[3] follow a similar approach as the one taken by Yih. They both make use of full PID and feed forward control, however Se-Wook developed a torque that dynamically adjusts between under and oversteering, with varying feedback torque, on the fly based on the speed of the vehicle and steering angle as seen in Figure 2.8. This is an improvement on the feedback response used by Park et al. [14] who use a linear relationship between driver and feedback torque. The turning angle produced would tend towards oversteering with minimal reactive steering torque when the vehicle was at low speeds to allow for easier manoeuvrability when parking etc. While at higher speeds, the steering would operate similar to understeering with high reactive

torque in order to maintain vehicle stability. This was done by adjusting the amount of displacement the rack would have, effectively altering the steering ratio paired with the varying feedback. Similarly to Yih's control system, the characteristics of the developed torque curve can be readily adjusted from the altering of a few gain variables configured in the control algorithm. This research served as a first step, with the hope of evolving their algorithm into one that incorporates Active Roll Stability Control(ARSC).

Guangyu Zhu, Haohan Yang and Fan Yu [15] take a different approach to control. Instead of PID, they researched the alternative use of Internal Model Control (IMC) in combination with a slide mode controller (SMC). IMC is common in industrial uses, favoured for its robustness, with the SMC focusing on tracking the vehicles desired yaw rate (rate of rotation about the z-axis), shifting between various gearing ratios to provide easier steering and control through active steering. According to their tests, performing a double lane change procedure using a hardware-in-the-loop configuration, the IMC and SMC combination outperformed PID control under the same conditions. While both tracked the desired steering inputs well, PID control was less robust to disturbances requiring increased driver effort to correct steering. IMC performed trajectory tracking and anti-interference to reduce driver workload, while SMC varied the steering gear ratio for increased turning stability at low and high speeds.

2.3.3 Current applications of SBW

While SBW is a new and cutting edge concept in the realm of auto mobiles, it is the main form of navigation control for large ships and aeroplanes.

There are a few vehicles that have been designed to/already incorporate full SBW control. While the GM Sequel was designed to have it, the Tesla cybertruck is one of the first commercial vehicles to make use of a full SBW system without a steering column [16] [17]. Unlike most of the cases spoken of in earlier sections, these vehicle use SBW for both front and rear wheel steering. Due to the ability to freely manipulate the steering ratio, the need for multiple wheel rotations and a hand-over-hand steering manoeuvre is eliminated as alluded to earlier. As such, a steering Yoke is used as opposed to a wheel, with rotation end stops representing the end of steering motion of the car. The actuation is done through a rack and pinion with component redundancy (2/3) as the basis of fail-safe protocols. The system and motors of the Tesla all operate and communicate on a base 48 V using Ethernet for power and communication transfer, while the Sequel uses 42 V and a fail proof communication referred to as FlexRay. This is in comparison to the 12 V used for conventional vehicles.

2.3.4 Advantages and disadvantages of SBW compared to conventional steering

Advantages

SBW has a unique advantage over other systems due to its flexibility. From the easy implementation of a variable steer ratio, to the availability of unconventional steering devices such as a steering yoke. This is made possible by freely controlling both the allowed and necessary steering limits needed to adequately steer the vehicle. This flexibility is further extended to aspects such as driver seating position and steering actuation configuration. Not only is this sense of flexibility extended to manufacturers, but possibly the end customer as well through adjustments to driver feel independent of tire choice, suspension adjustment etc.

Drive-by wire systems also serve to improve vehicle safety, convenience and functionality. Due to their reduced weight, size and number of assembly parts, these lead to improved energy efficiencies both in manufacturing and in everyday use. Safety benefits are made prevalent with SBW creating space for the involvement and intervention of autonomous steering and vehicle stability control; and in the case of head-on collisions, the absence of a steering column also serves to better protect the driver [3] [15]. Additionally, since all of the steering configuration is done through software, a lot more electronically based features are easier to develop and implement with the correct sensor data, such as automatic lane keeping, park assist and advanced vehicle dynamics control. Should there be any issues upon initial launch, or if better operating configurations are designed for the vehicle, a simple software update would be all that is required to adjust the existing system; unlike conventional vehicles.

Disadvantages

While SBW may be a step in the improvement of steering systems, there are some disadvantages created by its inherently disconnected nature. The most prevalent and detrimental of these being the lack of steering feedback and the need to regenerate this artificially. The quality of said artificial response being directly correlated to the quality for the driving experience. While there are many studies that look into how this can be improved, the resulting forces do and will continue to differ depending on the methodologies used to simulate it.

Additionally, there is the concern of safety in the event that the electronic components fail or run out of power while functioning and the inherent loss of vehicle control due to it. Currently, there are two main methods of addressing this. They are referred to fail-safe and fail-proof protection methods. Fail-safe makes use of redundancy in order to protect against component failure; however this results in a large increase of costs as it is essentially 2 steering systems per vehicle. Fail-proofing involves having a mechanical system underlying the SBW one, enabling steering to still be possible should an electrical component fail. The downside being that due to its presence, the weight and safety advantages (like the lack of a steering column in a collision) of SBW are then effectively nullified. Thus a lot of work still needs to be done in order improve the reliability of these systems in effective ways.

2.3.5 Future possibilities due to SBW

Increased steering control

The intervention of steer by wire opens the door to a lot of possibilities in the future. Above the advancements currently being researched and alluded to above, there are also some other possibilities that have not been getting attention for various reasons. One such case is the use of independent steering for vehicles in the future.

As mentioned before, there are many circumstances where it is beneficial for the vehicle to operate under different handling conditions depending on the situation. Currently this comes in the form of dynamic steering ratios and creating a sensation of under/oversteer for the driver.

Current SBW research is mainly focused on single motor, rack and pinion steering for the reasons mentioned earlier. However, this may be a limitation of the true benefits SBW could provide. The translation of steering to an electrical and computerized system create a range of new possibilities for independent steering. Systems such as ABS in breaking and torque vectoring through acceleration, as planned for use in the Koenigsegg Gamera, have demonstrated the improvement in performance as a result of greater freedom of control of the vehicle as opposed to synchronous steering as it currently exists with a central axle.

Integration of racing simulation technology into standard vehicles

One aspect of SBW that is continually emphasized and researched in the spirit of getting it correct is the feedback of road sensations to the driver. This also happens to be the primary challenge when it comes to simulation racing, creating the realistic sensation that they are driving the vehicle.

Most of the research utilized DC motors, creating feedback torque through gear/belt systems. While this does work to an extent it falls short of the real thing. When looking to the gaming and simulation racing communities, these methods of translating force have long since been viewed as obsolete. Currently the best rigs make use of direct drive motors.

Direct drive motors remove the need for a medium, reducing losses and eliminating gaps in sensation due to meshing or the stretching of belts. Additionally, they are a lot more precise in their movement and delivery of force, with some rigs capable of 12 Nm of feedback torque.

2.4 Comparison of Steering Systems

The development of vehicle steering systems has evolved from fully mechanical linkages to complex electronic systems. Each system introduces unique advantages and limitations based on technological capability and intended application. This evolution has altered vehicle behaviour but has also changed the way ‘improvement’ can be assessed. While drivers may value comfort and responsiveness, engineers prioritise system redundancy and control, designers seek packaging freedom, and manufacturers seek cost effectiveness. Table 2.1 outlines a comparative evaluation of the major steering systems: Hydraulic Power-Assisted Steering (HPAS)(including EHPAS), Electric Power-Assisted Steering (EPAS), and Steer-by-Wire (SBW) from a stakeholder-focused criteria. These systems are compared on the basis of the Rack-and-pinion system, as SBW currently is not incorporated with synchronous steering mechanisms.

This comparison illustrates that while HPAS offers mechanical reliability and natural feedback, it is inefficient and offers little flexibility. EPAS provides a compromise, delivering energy efficiency and partial electronic control while retaining a mechanical fallback. Steer-by-Wire, however, redefines the vehicle steering architecture. For the driver, it offers the possibility of tailoring the steering experience; for the designer, it allows more creative freedom in layout; and for the engineer, it unlocks advanced control possibilities. Yet, the high safety demands, cost, and technical complexity mean that SBW comes at a significant detriment to manufacturers. It must be implemented carefully with robust fault tolerance, and component costs must be reduced before widespread adoption becomes viable.

2.5 Conclusions

The progression of steering systems has consistently trended towards increased precision, reduced mechanical complexity, and greater integration with electronic vehicle control systems. Hydraulic PAS brought the first wave of steering ease, EPAS improved on efficiency and controllability, and now Steer-by-Wire systems represent the next leap—entirely removing the mechanical linkages and shifting control into the digital domain.

SBW provides numerous benefits, including reduced weight, improved energy efficiency, advanced control possibilities, and enhanced integration with driver-assistance systems and autonomous driving technologies. Its flexibility also allows for significant innovation in driver experience, vehicle design, and vehicle dynamics. However, challenges remain. The absence of a physical link between driver and wheels necessitates highly reliable electronics and artificial feedback mechanisms. Ensuring safety through redundancy or fallback systems adds complexity and cost, and the driving feel depends heavily on accurate and responsive feedback models.

Despite these limitations, SBW is already being applied in cutting-edge commercial vehicles and is expected to be at the core of future vehicle control strategies. As research on controller performance, feedback realism, and safety architecture improves, Steer-by-Wire is poised to become the standard steering system in future electric and autonomous vehicles.

2.5.1 Research application to the model

While feedback torque mechanisms are critical to practical Steer-by-Wire (SBW) implementation, the approach for it is often subjective and context-dependent. Feedback torque requirements vary significantly with vehicle dynamics, driver expectations, and control objectives. Many studies, such as those by K. Eisenhauer and J. Andrew [18], as well as R.J. Hazelden [19], have proposed various sensing techniques to capture steering input torque, angular displacement, and velocity. Despite the diversity in approach, most effective systems converge on using sensor arrays in combination with torsion bars for accurate steering feedback.

However, torsion bars and the associated sensor hardware introduce cost and complexity that exceed the project scope. Given that this model aims to demonstrate the fundamental architecture and principles of an SBW system, rather than to replicate its closed-loop torque feedback behaviour, such functionality has been excluded from active implementation. Nevertheless, placeholders and design provisions for feedback elements have been

2.5. Conclusions

incorporated into the 3D-printed model to ensure structural compatibility. This not only supports the educational and demonstrative value of the prototype but also establishes a foundation for future work, where more advanced feedback features can be added.

In this way, the project balances realism and feasibility, acknowledging key elements of SBW systems while adapting them to the constraints of time, cost, and available resources. The result is a representative, scalable platform that can evolve with further development and research.

Table 2.1: Stakeholder-Oriented Comparison of Steering Systems

Criterion	HPAS	EPAS	SBW
Steering Feel and Comfort	Good natural feedback, but heavy at low speeds	Generally lighter with variable assist; feedback can feel artificial	Feedback is simulated; can be tailored, but realism depends on controller design (still requires significant research)
Customisability[experience]	little to None (heavily pump reliant)	Limited—static &/or load-sensitive assist maps	Fully customisable: steering ratio, feedback level, damping
Packaging and Integration	Bulky (requires pump, lines, reservoir) and heavy	Compact, but retains mechanical linkage	Highly compact; mechanical link removed, allowing more freedom in layout and cabin design
Energy Efficiency	Poor - efficiency Slightly improved by EHPAS, but still bad	Good — motor only runs when needed	Good — minimal parasitic losses, but more power drawn by motor
Electronic Control and ADAS Integration	Very limited—mechanically dominant	Moderately integrated with ESC, lane keeping, etc.	Fully software-defined; seamlessly integrates with autonomous driving, ADAS, and dynamic stability control
Redundancy and Reliability	Mechanical fallback always available	Mechanical link retained; moderate electronic dependency	High dependency on electronics and sensors; must implement full redundancy and fail-safe/fail-proof strategies
Complexity and Production Cost	tried, tested and well-understood; moderately expensive	Cost-effective for modern cars	High initial cost due to sensors, motors, controllers, and backup systems
Functional Safety and Standards	Conforms easily due to mechanical nature	Needs functional safety validation for electric components	Subject to many safety requirements and validations; systems are more complex but progressing

Chapter 3

Theory Development

This section expands on the specialized theoretical concepts applied while designing the model.

3.1 Ackermann theory

Ackermann's theory is a fundamental principle regarding the optimal turning angles of the right and left front wheels when steering a vehicle. The optimal steering result is achieved when the steering wheels experience minimal slippage by making pure rotations about an instantaneous centre of rotation [8]. This point is observed by drawing a line perpendicular to the face of the wheels during the turning motion. When Ackermann's theory is fulfilled, all these lines should meet at a common point, i.e., the turning point. Since the rear wheels ordinarily do not turn, this turning point is aligned with the rear wheel axle. As seen in Figure 3.1, the angle created by the inner steering wheel to intersect with the turning point is larger than that of the outer wheel. The average of these two wheel angles is the vehicle's turning angle, and the distance between the vehicle centre and the turning point is the turning radius.

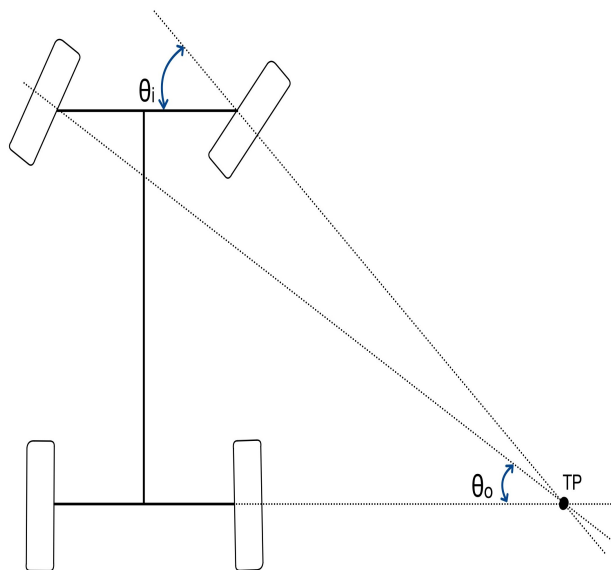


Figure 3.1: Ackermann steering principle

The Ackermann principle is generally accepted and utilised as a guideline in many steering mechanism designs and research. That being said, W. Milliken, D. Milliken, and M. Olley note that while the principle is grounded, it fails to account for the kinematics of the vehicle when in motion [20]. Primarily, the centrifugal force of the car tilts it at an attitude angle (nose down/up, etc.), inducing slippage on the tires when turning. This results in the turning point position moving off the rear wheel axle line. The point tends towards the front axle when the vehicle moves at higher speeds, while tending towards the theoretical Ackermann position at lower speeds.

Most mechanisms are designed around a shifted turning point to account for this; the offset distance is calculated based on the intended vehicle dynamics.

Another variation that manufacturers make relates to the wheel angles. While the Ackermann principle indicates the optimal turning angles for a smooth turn, some designers and manufacturers add an offset angle to the inner or outer wheels. The offset induces an inherent under-/oversteer characteristic to the vehicle's handling. A positive offset creates oversteer, and a negative one results in understeer [20].

3.2 Gears

Gears are mechanisms used to transfer torque/power between rotating shafts. They can also translate/change the rotational velocity of shafts relative to each other. Traditionally, they can be seen as disks with tooth profiles along their circumference.

Gears are designed according to Equations 3.1 - 3.4. Equation 3.1 calculates p , the circular pitch, which defines the distance between gear teeth, and is measured along the pitch circle of diameter d . N being the number of teeth along the gear's circumference. The optimal mesh and operation of two or more gears requires that their module m is equal. The calculation of the module is defined in Equation 3.2. A gear's power, H , is the product of its angular velocity w and Torque T . Subsequently, the relationship between the speed and torque of two meshed gears in an ideal system is demonstrated by Equation 3.3. It is worth noting the inverse proportional relation between the torque and velocity. This is the base principle behind gear boxes as speed reducers and torque amplifiers.

$$p = \frac{\pi d}{N} \quad (3.1)$$

$$m = \frac{d}{N} \quad (3.2)$$

$$H = Tw \quad (3.3)$$

$$\frac{w_2}{w_1} = \pm \frac{d_2}{d_1} = \pm \frac{N_1}{N_2} = \pm \frac{T_1}{T_2} \quad (3.4)$$

Gears come in multiple forms, the design changing based on their intended use. The most common and easiest to construct is a simple spur gear. Other notable rotational gears include helical gears and internal/ring gears. Rack and pinion systems follow the same design theory, only differing in translating rotational movement into linear movement along the same plane. Other gear systems do exist, to account for different angles etc, but they are irrelevant for this paper.

3.3 Lead screw dynamics and principles

While a rack and pinion converts rotational movement into linear movement along the same plane, lead screws perform the same purpose for perpendicular planes. The shaft's rotation results in movement parallel to the screw shaft. Lead screws are externally threaded, with their interacting components, normally nuts, are internally threaded. Equation 3.5 defines the distance d_{lead} travelled along the shaft per rotation. The pitch p is the distance between threads, similar to that of gears, and N_{starts} is the number of threads along the circumference of the shaft. The more starts there are, the greater distance d_{mov} is covered per revolution, N_{rev} as shown in Equation 3.6.

$$d_{lead} = pN_{starts} \quad (3.5)$$

$$d_{mov} = d_{lead} N_{rev} \quad (3.6)$$

Equation 3.7 calculates the resulting torque produced along the shaft of a lead screw due to a liner force $F_{applied}$ acting against the threads.

$$T = \frac{F_{applied} d_{Lead} \mu_{efficiency}}{(2\pi)} \quad (3.7)$$

3.4 Rotary encoders

Rotary encoders are sensors used to detect object rotation. They are categorised according to whether they only detect rotation (incremental encoder) or rotation relative to a particular reference point (absolute encoder), the medium used to detect this rotation (optical, magnetic, voltage), and the signal generated to indicate rotation.

Functionally, the encoder is a spinning disk capable of generating 1 and 0 signals. In the case of optical encoders, this is done using an IR emitter/s on one side of the disk and one or more photodiodes on the other. Gaps in the disk cause the diode to give off a 1 signal when light is detected and a 0 signal when no light is detected. Resistive encoders achieve this with a conductive plate and insulation segments to create the break in signal.

Incremental encoders have a simple, yet periodic pattern of these breaks along the face of the disk. These breaks are known as detents and define the encoder resolution. The more detents there are, the smaller the angle represented per detent. Some incremental encoders can indicate the direction of rotation through a method known as Grey Code. Grey code functions by comparing the signals of two detectors. One method to implement this is to have 2 detectors placed along the disk with a common ground. The detectors are offset, so they do not detect a '1' signal simultaneously. When the two signals are compared, one will be ahead of the other. The leading signal indicates the direction of rotation as seen in Figure 3.2. Alternatively, the disks are made with 2 rows of detents, one offset from the other, as shown in Figure 3.3; while the detectors are aligned. Encoders that utilise grey code are also known as Quadrature encoders.

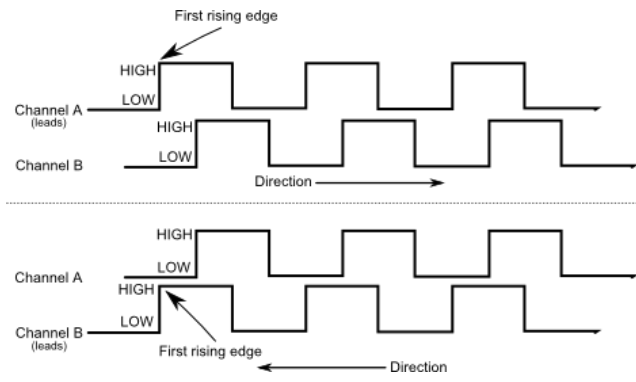


Figure 3.2: Grey code pattern

The signal produced by these encoders is digital, but analogue/continuous encoders do exist. Servo potentiometers are a good example, but they are considered absolute encoders as the voltage could be used to indicate the relative rotation of the shaft. Digital absolute encoders have a more complex pattern and construction, as shown in the left image of Figure 3.3. Detectors are aligned along the disk radius, while the detents are set up to create a signal when the disk is in a particular position. This is often a binary signal, but manufacturers sometimes create a customised sequence and include the key in the datasheet.

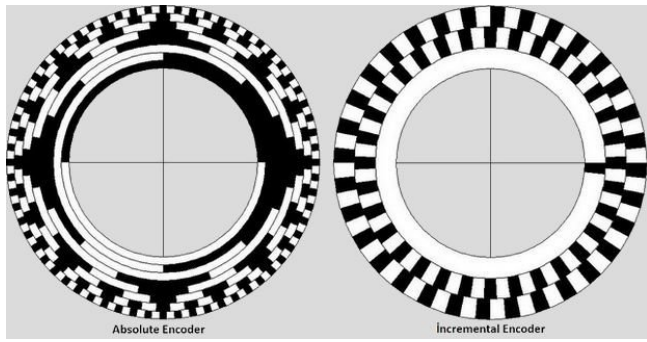


Figure 3.3: Absolute and incremental encoder diagram [4]

3.5 Control principles

3.5.1 PID

PID (Proportional Integral Derivative) control is a control principle widely used and implemented in various closed-loop control applications. This principle is based on reducing the difference between a desired state and the current state of the object to be controlled, referred to as the plant. Figure 3.4 below shows a basic closed-loop implementation of a PID controller. This is done by having a weighted gain multiplied to a characteristic of the error. The overall principle can be described using Equation 3.8.

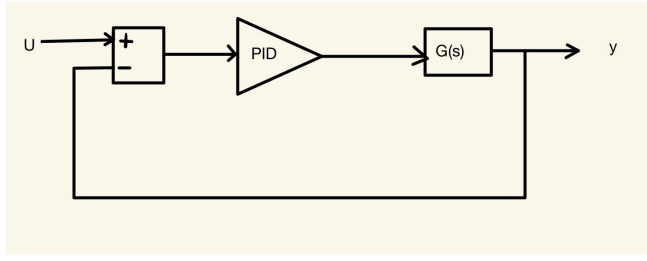


Figure 3.4: Basic PID closed loop configuration

$$u(t) = K_p e(t) + K_i \int_0^t e(\tau) d\tau + K_d \frac{de(t)}{dt} \quad (3.8)$$

The subject of control is represented by a transfer function derived from its behavioural characteristics, often the Laplace transformation of its equation of motion. The input of the transfer function is the control variable, and the output is the desired result. $e(t)$ is the error between your desired value and the current value of the system output; K_p represents the gain, P, directly proportional to the error; K_i is the gain, I, associated with the integral of the error over time; and K_d the gain, D, associated with the derivative. PID, P and PI control are the most popular, with PD control less commonly implemented due its tendency for erratic behaviour. Each gain parameter plays a different role in controlling the output, and their relative weighting will change depending on the desired response. A higher proportional gain will result in a faster response; however, too high a gain will result in the response overshooting the target, causing oscillations around the desired set point. The integral gain reduces the accumulated error over time, increasing steady-state tracking. While this does add stability, it can slow down the response to the point of being sluggish while increasing processing time and resources. The derivative gain focuses on the transient state of the response. The gain scales the rate of change of the error to predict the next point; increasing tracking speed, reducing overshoot and dampening the response. However, if too high, it amplifies signal noise and could induce erratic behaviour.

The tuning of these gain values is notoriously a trial and error method. Often once a system of this control is safely implemented, it is improved by making small tweaks to the current values and analysing the resulting response. For new systems, it is advised to begin with a low proportional gain and slowly incorporate the other gain values

as desired. PID control can be implemented with any combination of the gain variables. Simulink/Matlab does, however, have a tool made to assist with tuning these values by providing a step response/Bode plot representation of the input/detected plant. The tool then allows the adjustment of the response, providing suggested gain values based on the desired combination to try to achieve this response. From then on, it is an iterative process to fine-tune the response.

Chapter 4

Model Design

4.1 Design overview

The SBW model developed is intended to draw the attention of prospective students who attend the UCT open day. It must be compact enough to set up and operate freely on a table. The steering actuator of the model is designed to be small-scale, while clearly showing the working mechanisms. To this end, certain liberties in the relative proportioning of components are taken to maintain legibility, ease of assembly, and handling. The mechanism is designed to mimic the characteristics of the Suzuki Fronx 2024 model.

Most of the mechanical components are custom-designed and 3D printed. The university facilities have 3 Prusa Mini 3D printers using PLA material of various colours. The printed parts are completed with a 25% - 30% infill (a higher infill for more stress-prone components) and an average of 6 outer layers, using a 0.15 mm nozzle. The printer has a rated build volume of 18cm^3 , but practically it is closer to 16cm^3 when accounting for stability supports. While printing individual parts in sections and assembling them is possible, there is a risk of misalignment during assembly and a reduction in the strength and integrity of the parts. Misalignment becomes especially prevalent when combining parts from different printers &/or using different colours. Since the model would be interacted with often during and after the demonstration, parts are designed to be printed as whole components to ensure the model is durable. All 3D printed parts are designed using the web-based OnShape CAD software, and their files are accessible on the GitHub link in Appendix A.

4.1.1 Design objectives

Table 4.1 lists the design objectives for the model and the specifications derived to achieve them. The UCT White lab is the main venue for project demonstrations. These lab benches can accommodate 2 students, leading to specification M-1. M-4 and M-7 are based on P. Yih and J. Gerdes's [12] analysis of standard steering behaviour. They relate that the average person exerts 0-2 Nm of torque, steering as fast as 2 rotations per second under particular manoeuvres. To ensure the model is durable, it is designed to handle a scaled input equivalent to 2.5 Nm of torque on a standard-size steering wheel, the additional 0.5 Nm functioning as a safety overhead.

One aspect of SBW brought up in the literature review is the need to recreate the centring phenomenon in standard vehicles. In conventional steering, this is done intuitively due to the dynamics of the wheels and the road. The method researchers use to tackle this is achieved through a similar means, just electronically instead of physically. However, a different method is needed, as the model will not be in motion. This led to specification M-6.

4.2 Model Sensors and Actuators

While most of the components are custom-designed, the sensors and actuators are ordered. Thus, the priority was component selection to identify and design around their limitations. Aside from component functionality, delivery times, stock availability, and pricing were strong selection factors.

Table 4.1: Table of model design requirements

No.	Objective description	Acceptance criteria
M-1.	The model must be small	Model should fit in a 0.6 m x 0.6 m area
M-2.	The model should be low cost	Model components < R2 000
SA-1.	The model must have realistic steering capacity	Ackermann compliant angle within $\pm 10^\circ$ error
SA-2. & SM-1.	The model should be sensitive to steering inputs	1° angle resolution (detection and actuation)
SA-3 & SM-2.	A fast steering speed	120 rpm steering wheel rotation
SM-3.	The model must be rugged	Should endure a scaled input torque (2.5 Nm)
SM-4.	replicate common steering experience	Upon release of steering wheel must centralise
C-1.	The steering response should be smooth	<5% transient state overshoot
C-2.	Steering input should be translated to the wheel quickly	<2 s delay

4.2.1 Motor

The motors are one of the key points of the functionality for SBW, as without the motors, there is no movement execution. As noted in the literature review, 12 V DC motors are the standard selection for the steering module motor. For the Actuation system, both AC and DC motors are viable options, but a DC motor is chosen for uniformity of control and power supply. While brushless motors are more precise, they are also significantly more expensive than their brushed counterparts within the same performance range.

Regarding the steering module, the motor must handle the driver's torque input and achieve the desired turning rate as noted in the design objectives. The 2.5 Nm input is applied to a 36 cm - 40 cm standard wheel diameter. Due to the limitation of the Prusa build plate, the model wheel diameter is 15.5 cm. The relative scale between the model and the median wheel size is 0.41:1. The resulting input torque to be designed for is 0 - 1.03 Nm. The objective maximum speed for input and feedback is 120 rpm. Thus, it was necessary to select a motor with rated values as close to this as possible.

$$T_{model} = T_{standard} \frac{d_{model}}{d_{standard}} \quad (4.1)$$

For the actuation module, an estimate of the minimum required torque output was calculated based on early component designs. The assumed friction points in the system are: A, Kingpin friction; B, Steering arm and tie-rod connection; and C, Rack and tie-rod connection. An estimated torque of 0.2325 Nm is calculated using Equation 4.3 and the friction values derived from Equation 4.2. This is used as a baseline value for the required motor torque.

$$F_{friction} = (u_{static})(9.8)(\rho_{PLA}V_{component}) \quad (4.2)$$

$$T_{total} = (2(F_A) + 2(F_B) + 2(F_C))(r_{pinion}) \quad (4.3)$$

Picking a high-speed motor, using a speed reducer to obtain the desired speed, and inadvertently increasing torque output was considered. Especially since they are a lot more affordable and readily available. However, advisors expressed caution against picking motors with overly high speeds. Due to the weight and friction of the high-speed reducer gears, the effectiveness of the motor could be affected to the point of potential stalling. It was thus beneficial to consider low-speed motors that require minimal speed adjustment. The list below in Table

4.2 of various motors from different suppliers was compiled and compared. The focus was on low-speed motors with the highest available torque output.

Table 4.2: Motor comparison table

	Component Name	Voltage supply (V)	Speed (rpm)	Torque (Nm)	Price (R)
1	RS PRO Brushed Geared DC Geared Motor, 7 W, 6 mm Shaft Diameter	12	60	0.59	R453.61
2	RS PRO Brushed Geared DC Geared Motor, 1.71 W, 4 mm Shaft Diameter	3	72	0.1	R338.16
3	RS PRO Brushed Geared DC Geared Motor, 1.3 W, 4 mm Shaft Diameter	12	27	0.12	R411.90
4	Nidec Components Geared DC Geared Motor, 6 mm Shaft Diameter	24	70	0.2	R631.29
5	MOTOR GEARED 12VDC 1A6 6mm DIA=37mm	12	270	0.52	R251.00
6	MOTOR GEARED 12VDC 0A3	12	65	0.59	R496.85
7	MOTOR GEARED 12VDC 0A3	12	10	0.59	R392.00

Motors 1, 5 and 6 were the main 3 considered for the steering module. These were the focus due to their high rated torque of 0.52 - 0.59 Nm while needing the lowest adjustment to speed to achieve an output of 120 rpm ($\pm 2:1$ for 1 & 6 at ± 60 rpm or $\pm 1:2.25$ for 5 at 270 rpm). Motor 5 was selected over the other 2 as the reduction in speed would increase the torque capacity to ± 1.196 Nm, putting it over the objective minimum torque. In contrast, the other two would have their torque capacity reduced, putting them well below the objective. For the actuator, the considered motors were 1, 4 and 6 for the same reasoning as the steering module. While the specific speed was unknown at this stage, the objective of completing a full steering motion within 1 second was used as an estimate. As such, the choice was to select a moderately fast motor with a suitable torque margin when driven at a 1:1 gear ratio. Motor 1 was the initial choice, but due to a lack of stock availability, motor 6 was the one ordered.

4.2.2 Encoder

The encoder senses the rotational movement of the shaft as the wheel turns, i.e. the driver's steering intention. As such, the sensor needs to be as precise as possible. Research indicates a preference for torque detectors as the steering input, subsequently calculating the intended input angle. However, as mentioned in the literature review, these devices are expensive and thus were not considered. An alternative approach was a combination of an incremental rotary encoder to track the scale and rate of angle change, paired with a potentiometer to track the change in direction/relative position. This combination of components is also a significantly cheaper alternative. The list of rotary encoders in Table 4.3 was made for consideration.

Table 4.3: Rotary encoder comparison

	Component Name	Actuation method	Encoding form	Output	Voltage (V)	Rotary range (°)	Number of detents	Price(R)
1	Seeed Studio Grove Rotary Angle Sensor	Resistive	incremental	analogue	5	300	N/A	R72.73
2	F12E-S4H4BF724	Resistive	incremental	digital	5	360 cont	20	R38.67
3	EN18ABHB11A0F26	Shaft	Absolute	Binary	12	360 cont	12	R38.03
4	PAC18R1-43D19F	Shaft	Absolute	Grey Code	10	360 cont	16	R64.11
5	EN16ABVM22B0F20	Shaft	Absolute	Binary	12	360 cont	16	R48.86
6	Rotary Encoder Module	shaft	incremental	Grey-Code	5 V	360 cont	20	R28.00

The most precise of the available encoders are 1&6 with 20 detents. This correlates to an 18° resolution every step or 9° every half step. This is further increased to 4° when the sensor is connected to the smallest speed reducer gear. Regardless, this is still not precise enough, as any wheel rotation less than 4° would go undetected. Under standard driving conditions, a steering dead zone of 4° is unacceptable.

A custom encoder is developed to achieve the required precision. The design is based on the theory behind optical encoders covered in Chapter 3, utilising the gear faces as disks. Due to precision being the driver of this decision, the objective is to create an encoder with a 1° resolution. Using the change in sensor output to indicate a degree of rotation, 180 slots as detents are required for the steering wheel encoder. Several gap detector sensors were compared for the sensing aspect of this encoder and listed in Table 4.4.

Table 4.4: Optical encoder comparison

	Component Name	Actuation method	Encoding form	Output	Voltage (V)	Rotary range (°)	Number of de-tents	Price(R)
1	HKD MINI SPEED SENSOR -74HC14	optical	incremental	digital	3.3 - 5	gap counter	N/A	R26.00
2	170202	optical	incremental	digital	3.3-5	gap counter	N/A	R19.35
3	EE-SX4081 Omron	optical	incremental	digital	4.5 - 16	gap counter	N/A	R145.00
4	TCST2103	optical	incremental	analogue	5 V	gap counter	N/A	R24.28

Considering the gears are load-bearing for all modes of operation, the sensor needs sufficient space between the emitter and detector terminals, while having a significantly small detection gap, to allow for the most gear material possible. The sensor chosen from the selection is the 3rd one, 170202, as this sensor has the largest space of 10 mm between the diode and sensing terminals, and a detection slot of 1 mm. Additionally, the sensor comes preconfigured with an Op-amp comparator to eliminate noise potential, increasing accuracy. There is an added benefit of this being the cheapest of the selected sensors, contributing to the goal of being low-cost.

To supplement the gap sensors, a Bourns 6639 precision servo potentiometer is employed to detect the direction of rotation by measuring voltage variation as the shaft rotates. This component is readily available in the UCT White Lab.

4.3 Steering wheel module

As noted in the literature review, the steering wheel rig is composed of a steering wheel and shaft, for driver interaction; a motor, for feedback torque; a shaft and gear combination, to translate movement between the wheel and the motor; and a rotary encoder, to send the position and rotation speed of the wheel to the ECU. This can be represented as Figure 4.1. This module is designed to model and operate under conditions that would be considered for practical implementation, scaled to suit the model's size. This includes aspects such as an expected driver input of 0 - 1.22 Nm as indicated in the design objectives.

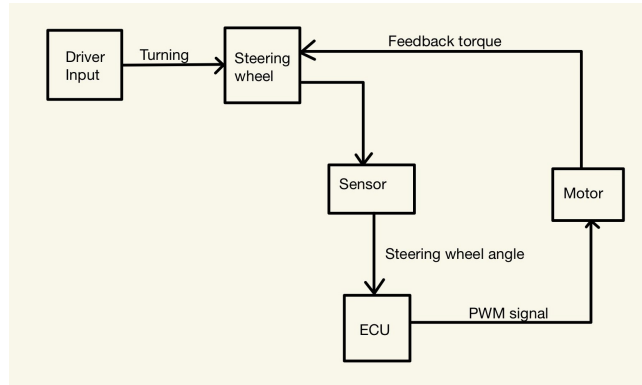


Figure 4.1: Basic Steering wheel module flow

The final design can be viewed in Figure 4.2. The following subsections expand on each of its subsections and how they were designed.

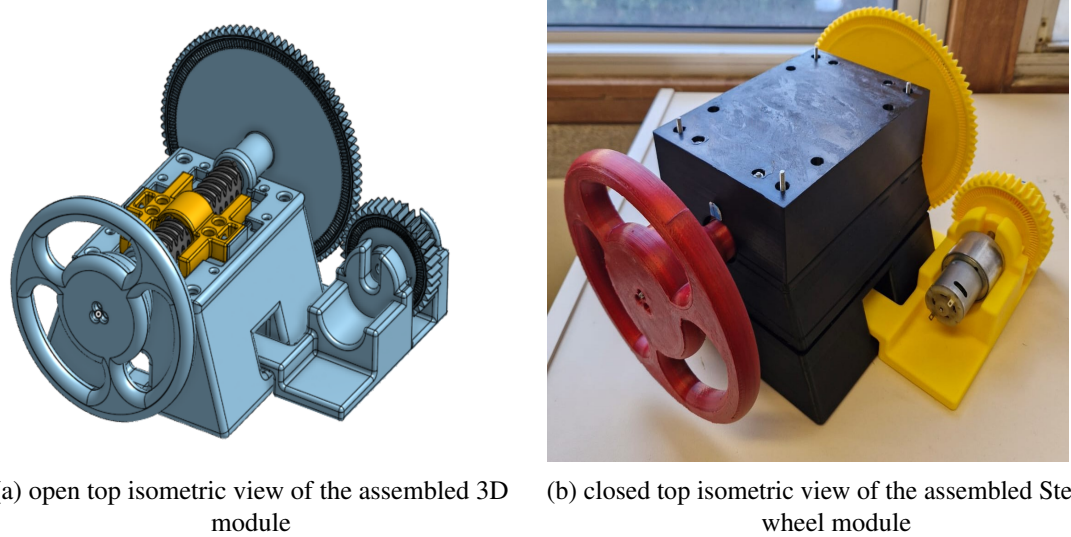


Figure 4.2: Steering wheel module design and printed version

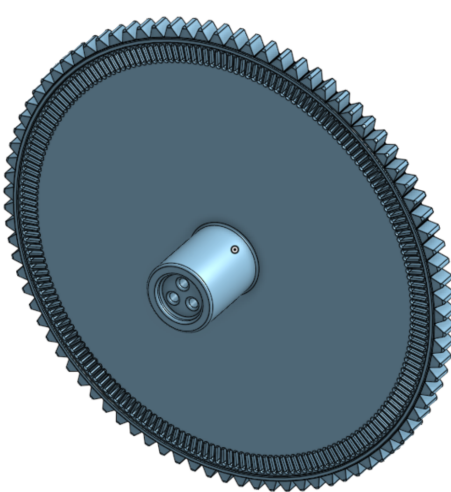
4.3.1 Gears

As per the motor selection, a 1:2.25 gear ratio between the steering input and the steering motor is needed. One of the two would also need to function as the disk of the encoder. The larger gear (the one attached to the driver shaft) is chosen as the disk, as the increased surface area allows for the necessary number of slots, while accounting for the required gap size and maintaining the gear's structural integrity as much as possible. Considering that for adequate detection, the gaps and the detents between them must be at least 1 mm wide each at the detection point, the minimum radius of 57.29 mm is calculated according to Equation 4.4. The final gear radius is larger than this when accounting for the gear's teeth.

$$r_{gear} = \frac{180 \times d_{gap} \times d_{detent}}{2\pi} \quad (4.4)$$

A diameter of 114.58 mm is used as the central point of the detection slot, the slots being 5 mm long. Standard gears have a pressure angle of 20° to 25°. However, as the gears are 3D printed, additional leeway was added to account for a phenomenon known as 'elephant foot'. This is when prints bulge around corners due to the plastic settling as it cools. Thus, a pitch of 6 mm and a pressure angle of 30° were selected for this gear relationship. These are used with Equation 3.1 & 3.2 to calculate the number of teeth and module. These parameters are then input to a website for calculating gear parameters[21] to attain the missing parameters needed for modelling, such as addendum and dedendum sizes. These, and all other gear parameter values, can be found in Appendix B ???. A centre shaft is extended from the gear to provide space for the sensor between the support box and the gear face. This shaft is 25 mm in diameter and 30 mm long. Three holes 3.5 mm in diameter, 4.25 mm offset from the centre and 120° apart go through the entire gear. This is to provide space for the 3 mm threaded rods that would serve as the compression force for the steering shaft components (gear, threaded shaft and steering wheel), and the means for carrying out rotation between them. The final design is seen below in Figure 4.3a.

A similar process is followed to derive the motor gear using the gear ratio of 1:2.25 according to Equation 3.4. As this gear is the primary driver of the motor and does not pass through the encoder, it was possible to make it thicker. Doing this reduces the possibility of the gears disconnecting during operation due to misalignment or warping. While the gaps are not needed for a sensor, they are kept for uniformity in the gear's appearance. This gear has a connection shaft of 25 mm in diameter and 8.5 mm long protruding from both faces. One side provides a connection for the motor as seen in Figure 4.4a, and the other for the potentiometer as seen in Figure 4.5b. Grooves suited to each component's shaft are incorporated into the surfaces.

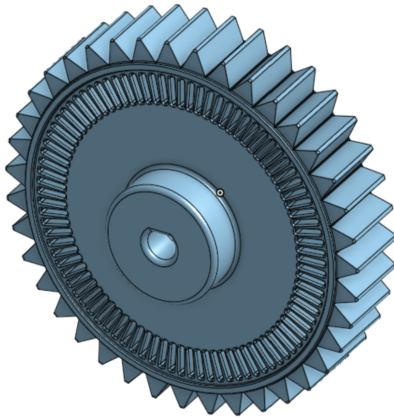


(a) Steering wheel gear model



(b) Printed steering wheel gear

Figure 4.3: Steering wheel gear design and printed version



(a) Motor side view of the steering wheel motor gear model



(b) Potentiometer side view of the printed steering wheel motor gear

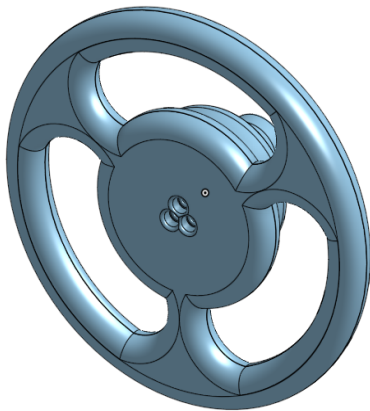
Figure 4.4: Steering wheel motor gear design and printed version

4.3.2 Steering wheel

The steering wheel is designed to be as large as possible to provide a suitable point of interaction. The wheel has an outer diameter of 155 mm, limited by the build area of the 3D printer. The final design is visible in Figure ???. The wheel has a 3-arm design to mimic a traditional steering wheel. The same accommodations for threaded rods made in the steering wheel gear are made for the steering wheel.

4.3.3 Screw box mechanism

D. Cesiel, M. Gaunt and B. Daugherty speak on the need to simulate the end stop of the steering motion due to the lack of a mechanical one. They use 15 - 20 Nm feedback torque to simulate the end stop of the steering range available [17]. This is 6.15 - 8.2 Nm when scaled down using Equation 4.1. This is linearly applied over a steering range of 5° from the configured end stop. This solution's benefit is the ability to change the desired steering range as the steering ratio changes. Alternatively, A Liu and S. Chang use a mechanical solution to create end-stops. They have physical barriers in place with the addition of springs to create a linear resistance torque feedback, reaching a maximum when the wheel reaches its intended limit. The selected motor does not



(a) Isometric view of the steering wheel model



(b) Printed steering wheel

Figure 4.5: Steering wheel motor gear design and printed version

have a high enough output torque (even with the gearing ratio), so a combination of both methods was needed.

The shaft, shown in Figure 4.6a, is 153 mm long, the thread taking up the centre 126 mm span. The centre shaft has a diameter of 16.7 mm and a threaded diameter of 26.5 mm. The thread is designed with a 0.008 m pitch and 2 starts. While OnShape does not have a native feature to create this pattern, an add-on feature was adapted from their tutorial model. This initial design of the shaft was printed vertically to maintain the round shape of the screw pattern. Printing it on its side would result in the screw becoming oblique as the weight on the support material increases, deforming the screw pattern.



(a) Version 1 of Lead screw shaft



(b) Version 2 of the Lead screw shaft

Figure 4.6: Steering wheel motor gear design and printed version

Unfortunately, printing the shaft vertically did not eliminate the issue and merely transferred it. The threads of the shaft, while circular, sagged along the length of the shaft slightly. This deformation made rotation easier in one direction, but more difficult in the other. After further research it was found that this is a fairly common issue for printing screw patterns in the 3D printing community. A solution to this, as shown in a post made by a 3D creator, Nackhabitat, on Instagram [22] is to flatten the thread of one side of the screw and print it horizontally. The flattening of the side allows the screw to rest on the build plate eliminating the need for supports on the

curve of the thread. This resulted in the second version of this shaft seen in Figure 4.6b.

Initially, bearings were ordered as a medium for reducing friction between the housing box and the rotating steering shaft. However, the bearings had a higher friction than the PLA sliding on itself. As such, bushings are designed and printed to fulfil this purpose. The bushings, in Figure 4.7, have an inner diameter of 17 mm, an outer diameter of 34 mm, and a 10 mm width. They are positioned flush against the threading of the shaft.

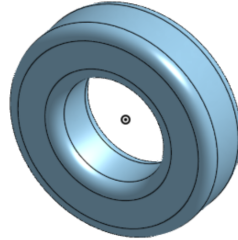


Figure 4.7: Shaft bushing

The slider is designed with the base dimensions shown in Figure 4.8a. The core structure is 30 mm thick, with the legs protruding 32 mm off the surface. The purpose of these legs is to function as the mechanical limit stops for steering. When the steering wheel completes a $\pm 360^\circ$ rotation, the legs stop on the housing walls. The 13 mm extensions on the sides are compressors for the springs and the housing for 5 mm bearings. The bearings are intended to act as rollers to reduce friction during the slider's operation. On the bottom of the slider, as seen in Figure 4.8b, there is an extrusion that functions as an additional spring compressor and a guide for the slider along the housing base.

The initial print was done vertically for the same reason as the initial shaft. As these threads were internal, cleaning the supports effectively was extremely difficult. To overcome this, the slider was redesigned to be slightly thicker and printed as 2 half sections split along the middle. The two halves were then printed with the thread exposed on the top, removing the need for supports on the threading. The 4 holes visible on the top of the slider were accommodations for M3 10 mm bolts to hold the 2 halves together, while the holes on the side are for the spacer in Figure 4.9.

The spacer, shown in Figure 4.9, is designed to perform 2 purposes. The first is to hold the bearings in place to elevate the slider slightly above the housing surface. The second is to reduce the space between the slider and the housing wall. This helps keep the slider linear during its function. Both of these aspects are done to keep the slider aligned with the shaft to optimise the motion transfer between the two and reduce the possibility of wedging between their threads. The spacer shaft is 5 mm in diameter and 13 mm long. The base is designed to match the profile of the compressor's side and is 29 mm x 14 mm. Figure 4.10 shows the assembled shaft mechanism.

When selecting the springs for the screw system a few factors were considered. Firstly, the springs should produce enough force to centre the steering wheel. The second factor is that they should not output more torque at maximum compression than the motor could produce. Onshape can return the moment of inertia of an assembly if you input each component's material. This feature determined that the shaft assembly (steering wheel, lead shaft, slider and steering wheel gear) had a rotational inertia J of 0.001 Kgm^2 around its centre axis. Equation 3.7 & 4.5 were used to calculate the torque produced by the springs listed in Table 4.5 at maximum compression. K_{spring} and N_{spring} represent the spring constant and number of springs, respectively.

$$F_{spring} = K_{spring} * d_{compression} * N_{spring} \quad (4.5)$$

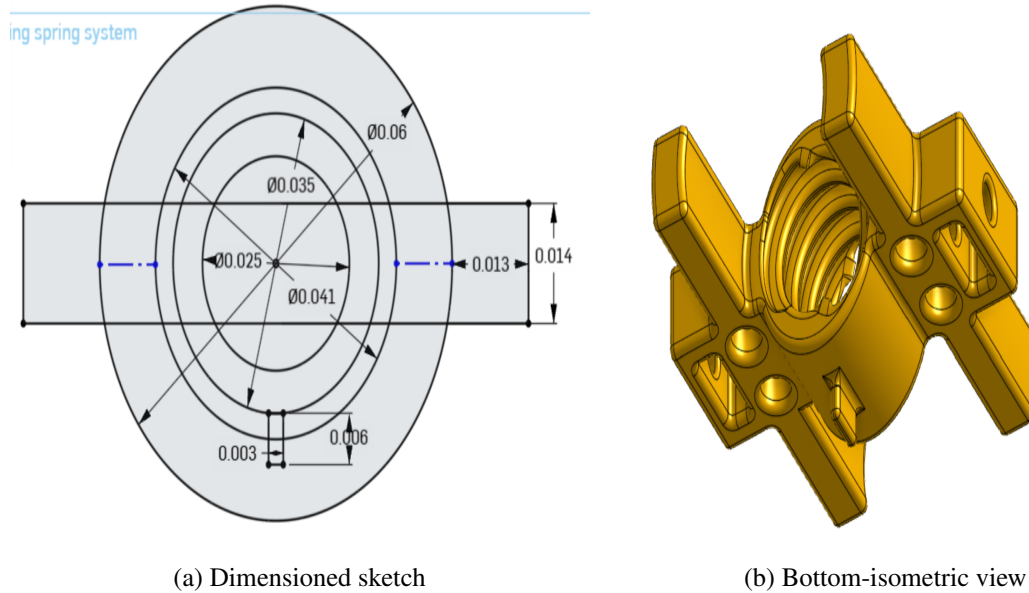


Figure 4.8: Shaft sliding mechanism model

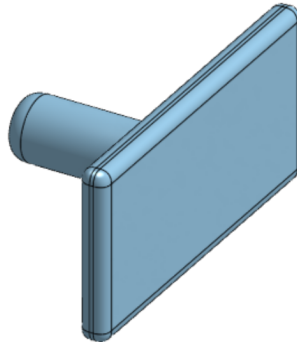


Figure 4.9: Slider spacer model

$$\alpha = \frac{T}{J} \quad (4.6)$$

The springs came in packs of 10, so to minimise cost, the plan was to incorporate all 10 springs into the design (5 for either side) to minimise waste. Based on Equation 4.6, springs that produced a total torque $> 0.001 \text{ Nm}$ would induce an acceleration and subsequently a rotation. Spring 2 had a small form factor and would output 0.03 Nm of torque under maximum compression with 5 springs. This was also the cheaper of the springs available and was thus selected.

The housing unit is designed to use the full build plate in a single print, to maximise its size for stability and strength. It's designed to support the rotating shaft, steering wheel, and steering wheel gear at a suitable height to fit the gap sensor below the steering gear. Figure 4.11 depicts annotated section views of the base's design. The line coincident with the circles' centre is the top surface of the housing's base. The base's height is 93 mm to account for the 57.29 mm radius of the steering gear. The housing is designed to limit the rotation of the steering wheel to 2 revolutions from end-to-end. Equations 3.5 & 3.6 were used with the shaft's dimensions to determine that for a maximum of 2 revolutions, the slider's movement should be limited to 32 mm. Sections A and C are thus 62 mm and 94 mm, respectively. Segment D (35 mm diameter) is the space to account for the

4.3. Steering wheel module



Figure 4.10: Printed shaft and slider

Table 4.5: Compression spring comparison

	Material	min length (mm)	Free length (mm)	working range (mm)	spring rate (N/mm)	Load at min length (N)	price (R)
1	RS PRO stainless Steel	17.4	65	47.6	0.11	5.47	R21.48
2	RS PRO Stainless Steel	9.5	41.9	32.4	0.08	2.57	R18.30
3	RS PRO Stainless Steel	12.8	53	40.2	0.09	3.64	R19.40
4	RS PRO Alloy Steel	33	71	38	6.69	253.99	27.44

shaft bushing. Section E is a cutout from the base to allow the core of the slider to move uninterrupted without friction. Segment B is the dedicated space for the springs. Initially, this was just a groove in the housing, but as the springs came under compression, they would pop out of their positions, even when the box's top was in place. To correct this, section B was filled and a groove incorporated. This groove is inlaid 24 mm from A's surface. The four grooves would have 2 springs each, with the last 2 placed in the 5 mm x 5 mm groove below section E.

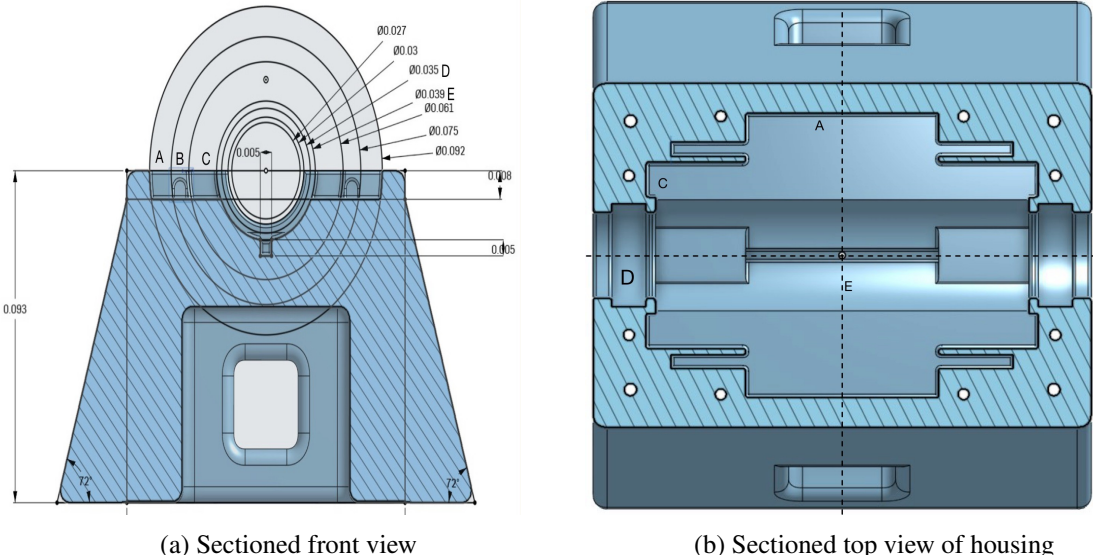


Figure 4.11: Annotated housing sectioned views

A volume of $0.426 \times 10^{-3} m^3$ and a 25 mm x 25.5 mm block on each side of the base were hollowed out to reduce the filament used and reduce printing time. The side spaces also function as a connection point for the motor and sensor support. Despite this, the housing was still a large print. After the print failed halfway, resulting in the loss of a lot of filament, it was decided to print the housing in sections. Despite the reasoning in the design overview, segmenting it would not be a big issue, as it did not involve moving parts. The 4 mm holes seen around

the base's perimeter were made to reinforce the base by using 3 mm threaded shafts and nuts to secure the layers together. The housing was printed in 3 layers, the top layer is the 8 mm section forming the spring housing and walls; the second, the 'floor' section going as far as the base extrusion. The layers can be seen by inspecting the printed housing in Figure 4.12. The middle section experienced some warping in the corners when printing, causing it to rock back and forth even when secured by the rods. This was corrected using a combination of nuts and washers to level out the base. This can be seen in Figure 4.12b.

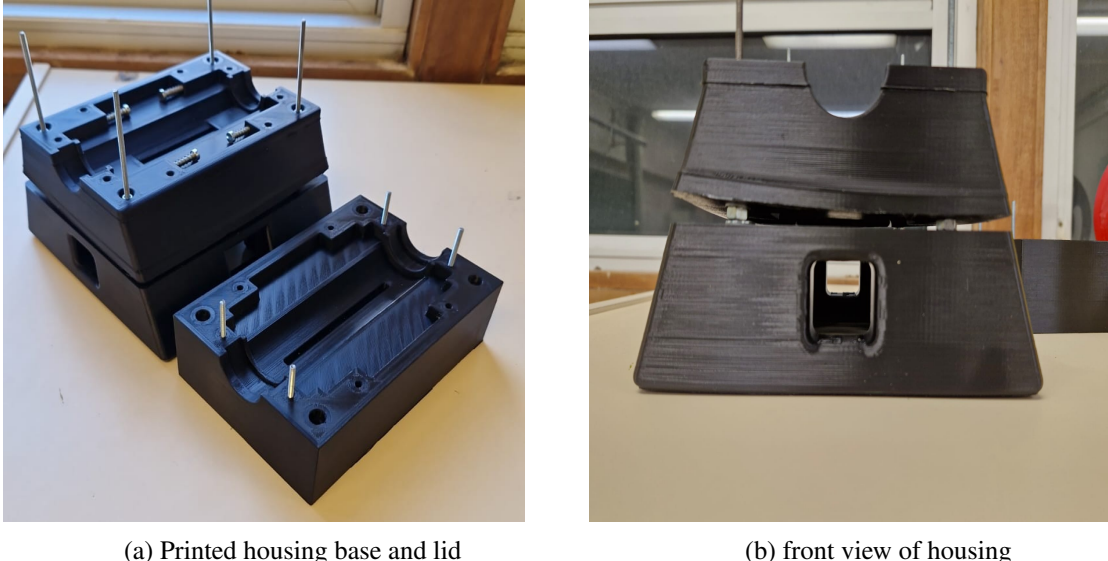


Figure 4.12: Printed housing

4.3.4 Motor and sensor support

The holder is designed to support the motor gear at an appropriate height, enabling free rotation while ensuring constant meshing with the steering wheel gear. It also accurately positions the optical gap sensor beneath the gear, aligning it with the gear slots for reliable detection. The side gaps on the housing provide a secure mounting interface for the hook shape of the mount as shown in Figure 4.13a. A semi-circular cradle on one side accommodates the motor, with an elevated segment to correctly align the motor shaft with the gear. The gear itself is positioned 4 mm above the base of the holder. A slotted section for coupling a potentiometer to the gear shaft is designed on the opposite side. The lateral brackets housing the motor and potentiometer secure these components and maintain gear alignment under operation. Extending from the front of the holder is a flat mounting arm featuring two 3.5 mm holes spaced 93.7 mm from the gear centre, precisely matching the mounting dimensions of the optical gap sensor. These allow the sensor to be fixed directly beneath the gear using 3 mm bolts and nuts, as shown in Figure 4.13b.

4.4 Steering actuation module

The design of the actuation rig is largely based on the dimensions and specifications of the Suzuki Fronx GLX 2024 Model [23] [24]. The dimensions referenced are the wheelbase, track width, minimum turning radius, and tire specifications, which are shown in Table 4.6. The subsystem is designed to be an approximate 1:5 scale model of the Fronx's specs; however, emphasis on functionality and clarity, while keeping accurate steering design principles in mind, is prioritised. As noted in the literature review, SBW is most commonly integrated into rack-actuated steering configurations. For an interactive and informative display model, implementing common practices helps represent how a realistic system would likely function, while highlighting the aspects that make SBW unique and advantageous.

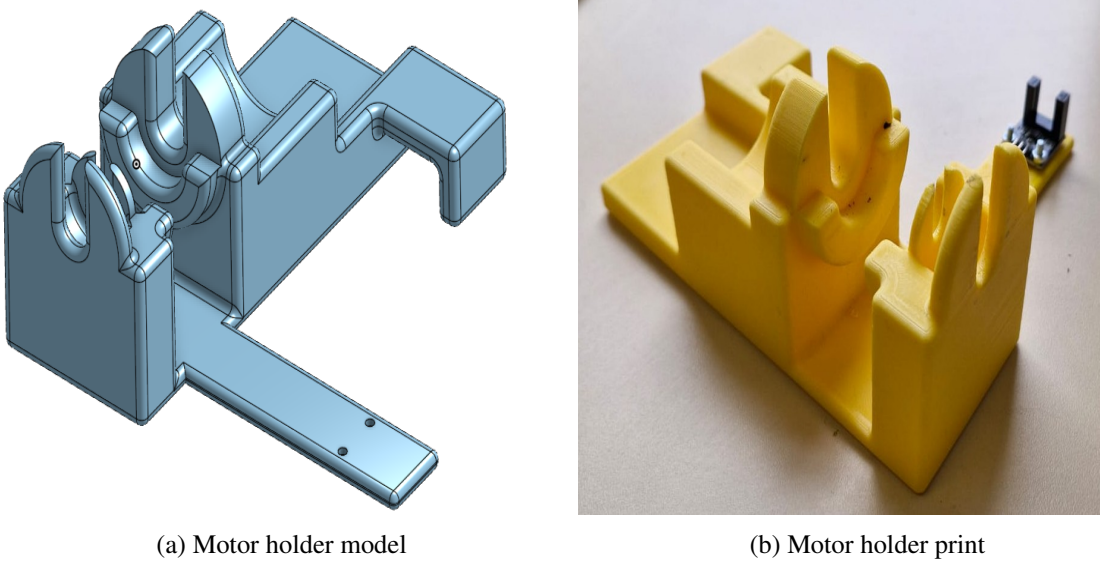


Figure 4.13: Printed housing

Table 4.6: Front axle system parameters

Parameter	Description	Value	Scaled value (1:5)	Unit
l_{wheel_base}	Car Wheelbase	2.52	0.504	m
l_{track_width}	Car track width	1.765	0.353	m
r_{min}	minimum turning radius	4.8	0.96	m
$d_{kingpin}$	Kingpin offset axis	0.883	0.1766	m
r_{wheel}	Wheel radius	0.203	0.0406	m
d_{wheel}	Wheel hub depth	0.152	0.0304	m

The Ackerman principle highlighted in the theory development Section 3 and research papers on the kinetic optimization of the rack and pinion steering-system by Mazilu, A [25] and Pradhan, D; Ganguly, K et.al. [26] are utilized to determine the lengths and calculations that form the basis of this design. The key factors affecting steering performance are: steering arm length and angle; tie-rod length, initial angle displacement and range; rack length; rack-axle offset; track width; wheel-base; and kingpin distance from vehicle centre.

The system is a uni-sided rack and pinion steering configuration with the rack and tie-rods placed ahead of the axle, shown in Figure 4.14. This configuration is chosen as it offers the best stability and effectively uses a compact area. The intricacies of the submodule are expanded further.

4.4.1 Base frame and supports

The base of the actuator is constructed using 20 mm × 20 mm aluminium extrusion profiles, chosen for their structural integrity, clean appearance, and compatibility with modular component assembly. The model's wheelbase is defined as the distance between the outer edges of the end supports along the aluminium frame. The overall frame perimeter measures 333 mm × 180 mm and includes two central support profiles, each 140 mm long and spaced 80 mm apart, which serve as mounting points for the motor support mechanism. The frame is elevated using six 3D-printed support legs—one at each corner and one beneath each central profile. The design of these legs is shown in Figure 4.15.

Due to the limited availability of pre-set nuts compatible with the extrusion profiles, an alternative mounting method was implemented. Each leg has a central cavity to accommodate a 3 mm threaded shaft. A 5 mm washer is placed on top of the leg and secured with an M3 nut. The nut and washer are slotted into the profile. When the nut is tightened, the washer bends slightly, producing a wedge effect that effectively locks the leg against the

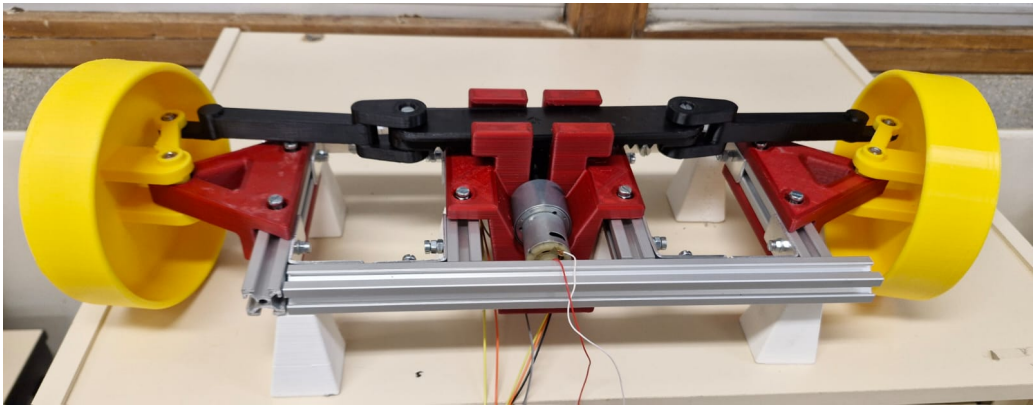


Figure 4.14: Assembled actuation module

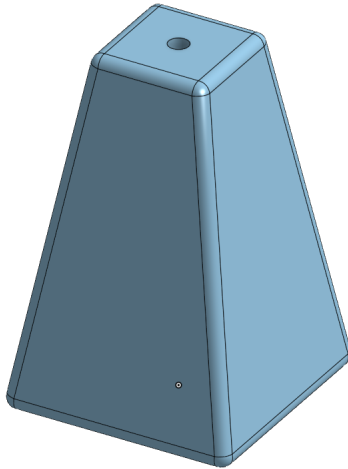


Figure 4.15: Steering actuator leg model

frame, ensuring a secure connection.

The dimensions of the wheel support are determined based on the steering geometry required to achieve the vehicle's minimum turning radius. The Suzuki Fronx executes a turn with a minimum radius of 4.8 m. According to the Ackermann steering principle, the inner wheel must achieve a greater steering angle than the outer wheel during turning. This maximum inner steering angle defines the wheel's rotational limits. Using the schematic in Figure 4.16, Equations 4.7 and 4.8 were derived. When applied to the design parameters listed in Table 4.6, the resulting maximum inner wheel angle is calculated to be 23.21° from the horizontal axis of the turning point (TP). Although the outer wheel requires a smaller steering angle, the support geometry is symmetrically designed to accommodate a full steering range of 46.42° , allowing either wheel to reach the maximum angle if needed.

The support structure draws inspiration from a double wishbone suspension system, as depicted in Figure 4.17b. This design choice not only aligns with conventional automotive principles—reinforcing the engineering relevance of the model—but also reduces material usage through the central cutout. The vertical construction line on the left of Figure 4.17a defines the indent for interfacing with the 20 mm aluminum profile. The support is 30 mm in height, with 10 mm overlapping the profile to ensure proper alignment and 20 mm of thickness on the wheel side to support both the static load and the dynamic forces induced by wheel acceleration and deceleration. The kingpin interface is implemented as a cylindrical recess with a diameter of 16.3 mm and a depth of 12.65 mm, designed to house a 5 mm bearing that serves as the pivot for wheel rotation. The support base includes two mounting slots to accommodate M5 bolts, which secure the support to the profile using pre-set nuts.

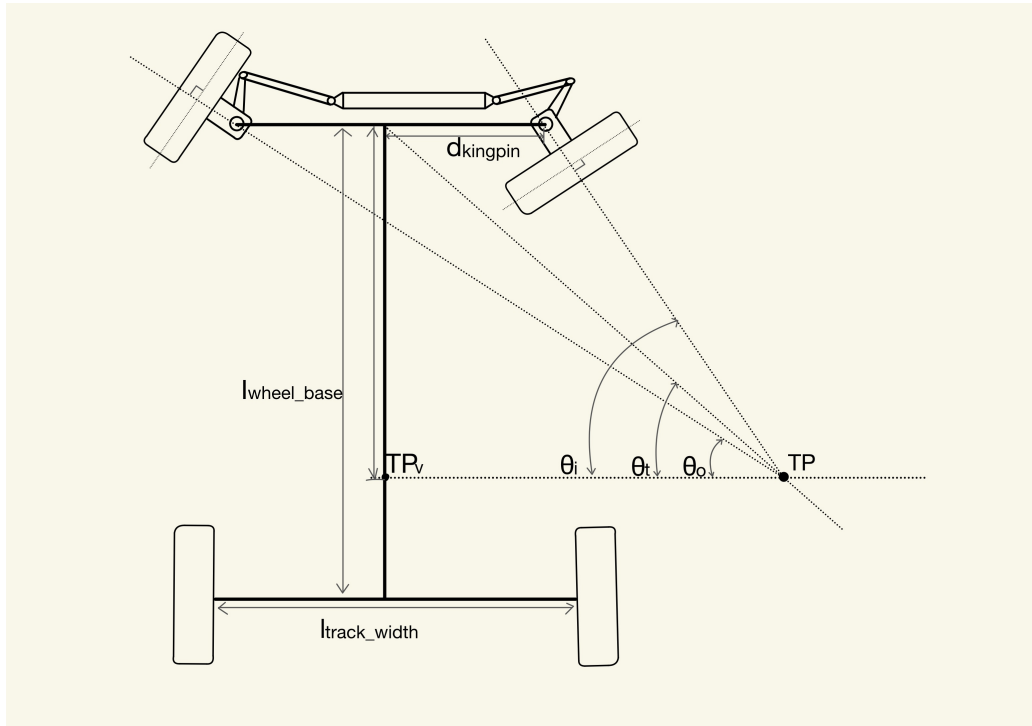


Figure 4.16: annotated steering diagram

$$d_{kingpin} = \frac{l_{track_width}}{2} \quad (4.7)$$

$$\tan(\theta_i) = \frac{\frac{2}{3}l_{wheel_base}}{r_{min} - d_{kingpin}} \quad (4.8)$$

A motor holder was designed similarly to the one used in the steering wheel module. This version, however, features a rail positioned above the pinion gear to secure the rack, maintaining a clearance tolerance of 0.4 mm. Additionally, two side platforms were included to allow the holder to rest securely on the central rails of the base. The design is shown in Figure 4.18.

During assembly, it was observed that the positioning and dimensions of the holder prevented the intended potentiometer, originally planned for detecting rotation, from being installed. To accommodate this constraint, the design was modified to include space for a second optical encoder. This encoder will be used to measure angular displacement based on the Grey code principle, as discussed in Chapter ??.

4.4.2 Steering visualization

For determining the rack and tie rod lengths, Mazilu recommends designing the rack to be as short as possible, while still accommodating the full required steering range, and the tie rods to be as long as possible [25]. Ideally, this could be achieved using a Type 3 steering configuration that uses a centrally located pinion with a central tie-rod take-off. However, given the absence of additional suspension supports in the current model, this configuration raised concerns. Specifically, torque moments during steering and unbalanced loads at extreme turning angles could compromise accuracy and introduce mechanical faults.

To mitigate these risks, the Type 2 configuration, with a central pinion and side tie-rod take-off, was selected. This layout maintains the performance benefits of a Type 1 configuration but leverages the advantages of a steer-by-wire (SBW) system. Since SBW eliminates the need to accommodate a physical steering column, placing the motor and pinion centrally simplifies the design and maximises actuation efficiency with a shorter rack.

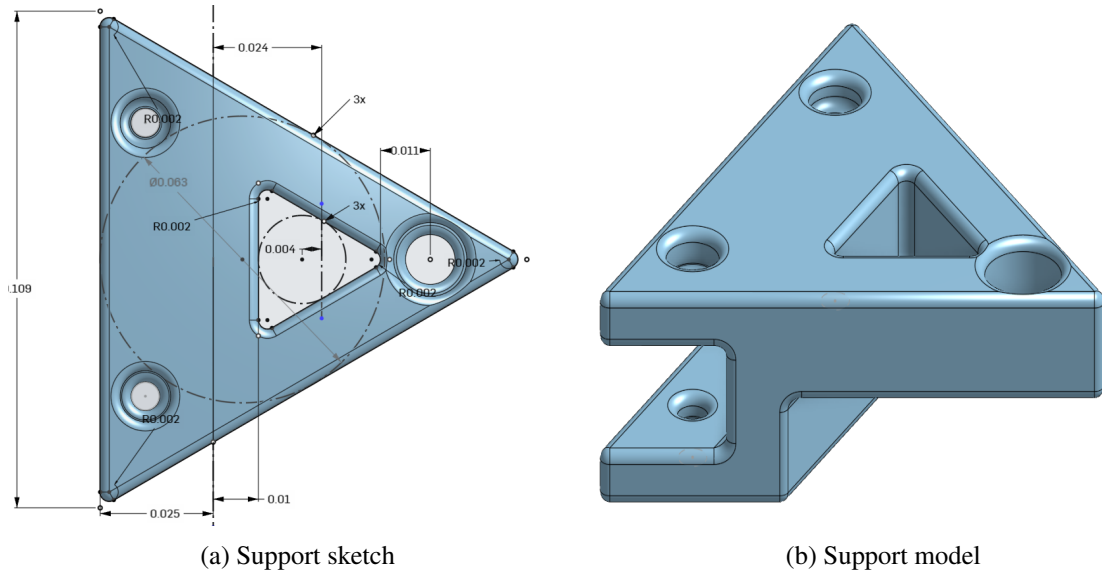


Figure 4.17: Printed housing

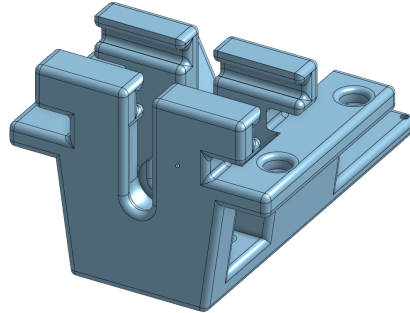


Figure 4.18: Steering actuator motor holder

Rack and pinion design

The initial step in calculating the rack length involves determining the steering arm angle and length. The steering arms are directed toward the instantaneous centre of rotation, which, under dynamic conditions, as stated in the theory development, lies at two-thirds of the wheelbase (l_{wb}) behind the front axle. The angle of the steering arm relative to the horizontal is calculated using Equation 4.9, yielding a steering offset of 62.29° , based on the reference vehicle's parameters.

$$\theta_{sa} = \tan^{-1}\left(\frac{\frac{2}{3}l_{wheel_base}}{\frac{1}{2}l_{track_width}}\right) \quad (4.9)$$

The appropriate steering arm length is determined using Equation 4.10. This equation is derived using the diagram in Figure 4.19. The steering arm is assumed to extend to the centre axis of the hub, ensuring the tie-rod does not interfere with the edge during steering.

$$r_{sa} = \frac{\frac{1}{2}d_{wheel}}{\cos(\theta_{sa})} \quad (4.10)$$

Using this relation, the steering arm length was determined to be 0.164 m.

To achieve the full steering range of 46.42° (0.81025 rad), the wheel must rotate about the kingpin at an angular

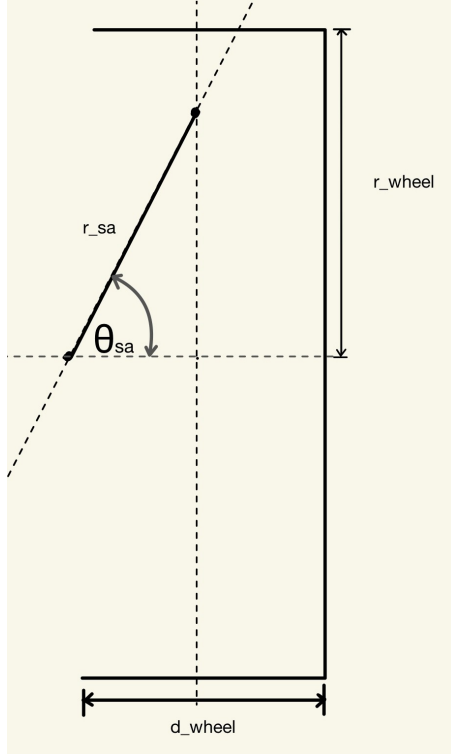


Figure 4.19: Internal wheel hub diagram

velocity ω_{max} of 0.81025 rad/s. The corresponding linear velocity of the tie-rod, calculated using Equation 4.11, is 0.13277 m/s.

$$V_{linear} = r\omega \quad (4.11)$$

Next, the horizontal travel of the tie-rod's end (relative to the kingpin) during left and right turns was calculated using Equation 4.12. The turning angles at the steering arm were adjusted using Equation 4.13, resulting in a left turn angle $\theta_l = 85.5^\circ$ and a right turn angle $\theta_r = 39.08^\circ$

$$\cos(\theta_l) = \frac{d_l}{r} \quad (4.12)$$

$$\theta = \theta_{steering_arm} \pm \theta_{turn} \quad (4.13)$$

This gives a left-turn tie-rod displacement $d_l = 12.85$ mm and a right-turn displacement $d_r = 127.21$ mm. Adding both yields the total rack travel d_{tie} of 0.14 m.

According to Pradhan et al., the angular offset between the rack and tie-rods should be minimized. Assuming near-collinear alignment for simplicity, the minimum required rack tooth length is taken as 0.15 m. Treating the rack like a gear, and assuming a 1:1 gear ratio between the rack and pinion, the rack's tooth length can be equated to the circumference of the pinion. Using Equation 4.14, the radius of the pinion is $\pm 0.024m$. Given the rack's linear speed of 0.13277 m/s, a full turn in one second corresponds to a pinion angular velocity of 5.53 rad/s. This is within the capability of the selected motor, which operates at 6.283 rad/s (± 65 RPM).

$$r_{pinion} = \frac{d_{circumference}}{2\pi} \quad (4.14)$$

Using Equation 3.1, along with a standard pitch of 6 mm and the previously calculated pinion radius, the number

of teeth on the pinion, N_{pinion} , was determined to be 23. This value was then substituted into Equation 3.2 to calculate a module of 2.087, following the same process used for the steering wheel gear calculations. The detailed gear parameters for the pinion are listed in Appendix B.1. Since the rack and pinion operate at a 1:1 gear ratio, the rack uses the same parameters for the gear tooth design.

The rack model is shown in Figure 4.20a. Both ends of the rack were extended by 26.6 mm to accommodate indentations to house 5 mm bearings to connect to the tie rods. The overall dimensions of the rack are 208 mm in length and 27 mm in width. Additionally, two 5 mm × 5 mm guard rails are integrated into the design to provide translational stability. The pinion also serves as the encoder disk. Based on the available surface area and using the same criteria as for the steering gear encoder, 47 slots were incorporated. This allows for a 1° resolution if each pulse is interpreted as an angular step, or 0.5° resolution if angular changes are measured between rising and falling pulse edges. The final pinion design, which includes interfaces for the motor shaft and a potentiometer (similar to the steering wheel motor gear), is shown in Figure 4.20b.

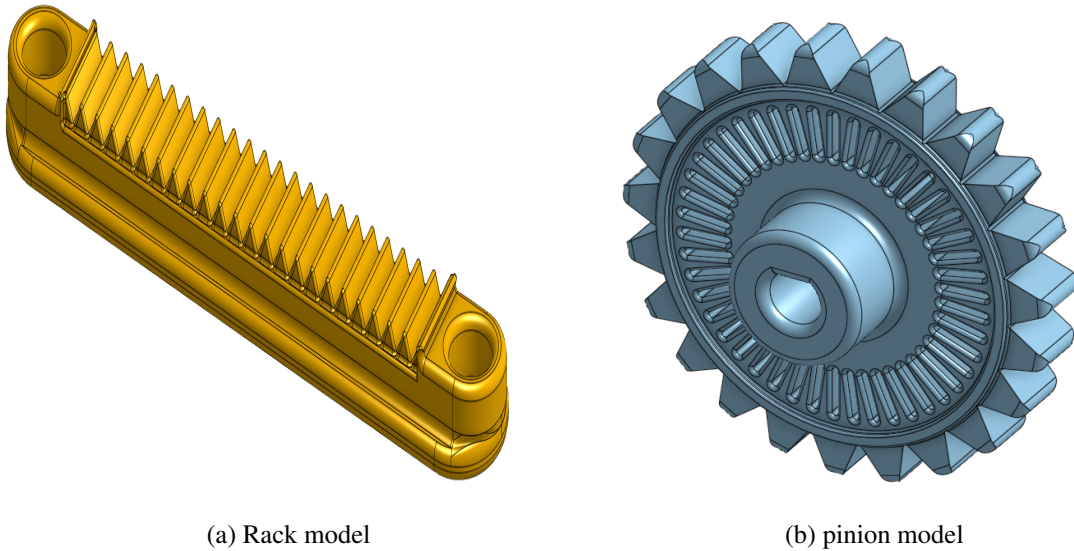


Figure 4.20: Rack and pinion pair

Wheel hubs

The design of the wheel hubs revolved around the steering arm and angle derived earlier. To ensure optimal force transmission without restricting the range of steering motion, the steering arms were designed to be as long as the wheel hub would allow. The initial wheel design followed a 1:5 vehicle scale, producing an 80 mm wheel diameter and a 28 mm steering arm. However, this configuration proved insufficient for an effective presentation and functionality reliability. This would conflict with the model's objective. Consequently, the wheel size was increased to a 150 mm diameter, and the steering arm length was proportionally extended to 47 mm.

The steering arm extends outward from the wheel's kingpin toward the wheel cap. The kingpin axis is offset 40 mm from the wheel surface to allow for a full range of steering motion without mechanical interference from the wheel support. A cylindrical recess at the kingpin accommodates a 5 mm threaded shaft and corresponding fastening hardware, which enable secure rotational attachment to the support structure. Additionally, the end of the steering arm includes a recess designed to house a 3 mm ball bearing, minimising friction at the interface between the tie-rod and the steering arm during steering actuation. Figure 4.21 shows an isometric view of the left wheel hub.

Due to the depth of the support's kingpin recess, custom spacers were designed to ensure proper mechanical contact between the wheel hub and the bearing. These spacers are shown in Figure 4.22. Each spacer is 10 mm in length. The upper spacer features an internal diameter of 6 mm and an external diameter of 13 mm, allowing

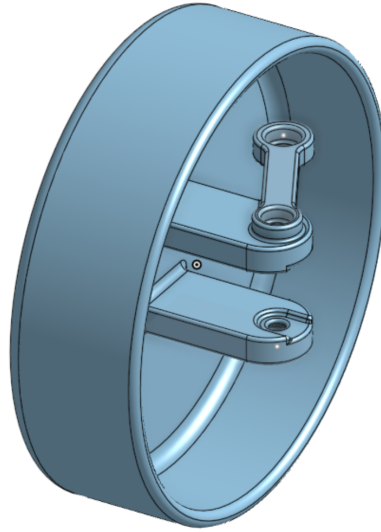


Figure 4.21: Left wheel hub 3D model

it to interface securely with the bearing and the threaded shaft. The lower spacer, which sits beneath the bearing, has an external diameter of 8 mm to maintain alignment within the recess while providing stable axial support.

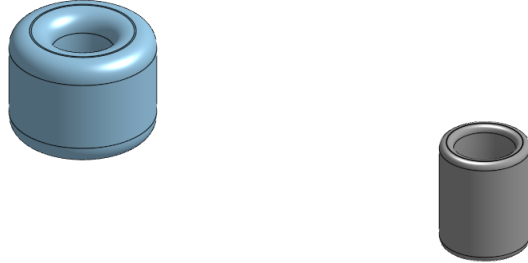


Figure 4.22: Top(left) and bottom (right) support spacers

Tie-rods

The tie-rods are the mechanical links between the steering arms and the rack. Minimising the distance between the rack and the axle, and reducing the angle between the tie-rod and the rack's linear motion path were the two main objectives while designing them. The best compromise has the rack positioned so its centreline sits midway along the vertical distance between the steering arm and the kingpin, as shown in Equation 4.15.

The vertical component of the tie-rod is defined by the offset between the rack and the steering arm. The horizontal component is determined by the distance between the centre of the ball bearings housed in the rack and those in the steering arm. This relationship is illustrated in Figure 4.23. The effective rack length, $d_{rack_effective}$, represents the distance between the centres of the rack's bearings and is 181.5 mm. This value is used in Equation 4.16 to calculate the tie-rod length, resulting in $d_{rack} = 153$ mm.

$$d_{offset} = \frac{d_{y_arm}}{2} \quad (4.15)$$

$$d_{rack} = \sqrt{(d_{y_arm} - d_{offset})^2 + (\frac{1}{2}(d_{track_width} - d_{rack_effective}) + d_{x_arm})^2} \quad (4.16)$$

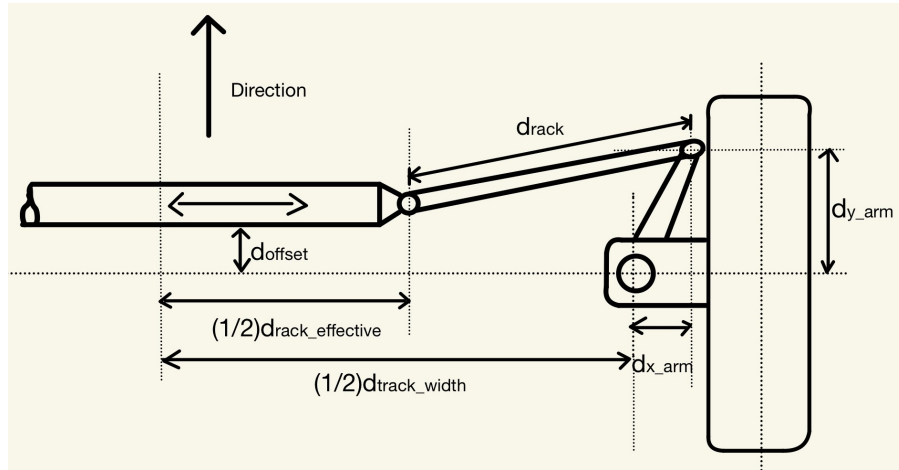


Figure 4.23: Rack and steering arm relation

Figure 4.24 shows the resulting tie-rod model. The left end of the rod connects to the rack using a 5.4 mm through-hole designed to accommodate an M5 bolt and nut. The right end, which attaches beneath the steering arm, features a smaller opening for an M3 fastener. The initial concept featured symmetrical bolt placements (above and below) similar to the rack side, but this arrangement was found to complicate assembly and obstruct internal steering movement. The updated design improves accessibility and allows smoother operation during full turns.

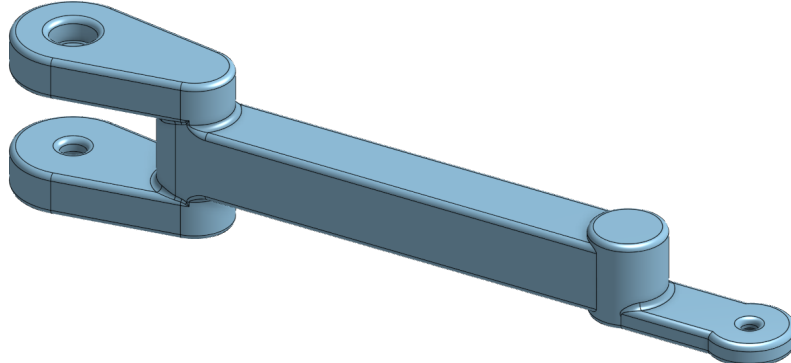


Figure 4.24: Tie-rod model

4.5 Electronic Control Unit (ECU)

As discussed in the literature review, the ECU (Electronic Control Unit) of the steer-by-wire (SBW) system consists of a microcontroller, motor drivers, and various sensors. The primary sensing components are the optical encoders developed for the project, which serve as the main input for angular position detection. The original design intended to use a combination of one optical encoder and one servo potentiometer to measure angular displacement in both the steering wheel and steering actuator modules. However, due to spatial constraints introduced by the motor holder, the steering actuator module now relies on two optical encoders mounted on the pinion for angular measurement. The intent is to use the displacement in their detected signals to implement a grey code algorithm. In theory this should also double the resolution of the encoder.

An Arduino Uno is selected as the microcontroller. The board was already available and thus attributed no cost. The Arduino Uno runs on an ATmega328P and is popular among hobbyists for its processing capacity and versatility. Arduino boards are also well-supported in the MATLAB environment, with numerous integrated

packages enabling real-time data acquisition and control.

Motor drivers are required to precisely regulate the motion and speed of the motors. A comparison of the motor drivers initially considered for this application is provided in Table 4.7.

Table 4.7: Motor driver comparison

	Component Name	Communication method	Current load (A)	Power supply (V)	Price
1	Seeed Studio Grove - I2C Motor Driver with L298	I2C	2 (1 per channel)	from 6 - 15	R482.40
2	MikroElektronika PWM Driver Click Motor Controller for DMP3010LK3	PWM	10	5	R441.40
3	MikroElektronika DC Motor 21 Click DC Motor Driver*	GPIO	0.5	3.3 / 5	R139.90
4	STMicroelectronics Dual Brush DC Motor Driver Expansion Board*	GPIO	1.5	7 - 45	R352.00
5	H BRIDGE 43A HIGH POWER MOTOR DRIVE	PWM	43A	5.5 - 27	R148.00
6	DUAL BRIDGE DC STEP-PER MOTOR DRIVER BOARD	I2C	2 (1 per channel)	from 6 - 15	R180.00
7	L298P MOTOR SHIELD / DRIVER FOR ARDUINO	GPIO	2 (1 per channel)	6 - 15	R234.37

As highlighted in the literature review, MOSFET switching H-drive motor drivers are the preferred choice. They can drive the motor in all quadrants and switch between modes quickly with minimal losses. While feedback torque is not currently implemented, a driver capable of dispersing the current and heat generated due to braking is desired. The 5th motor driver is chosen driver for these reasons. It has an incorporated heat sink and can handle 43 A of current in driving and braking modes. Additionally, the drive has 2 half-drive MOSFET IC chips that provide a signal representative of the current drawn by the motor in driving mode.

Figure 4.25 depicts the layout of the ECU's circuit.

4.6 Control development

Although the system is governed by a single controller, it effectively functions as two interlinked subsystems. The first controls the steering wheel module, which features a control loop to align the steering motor with the intended input direction. This is particularly critical in designs incorporating a torsion bar and torque sensor, where the desired steering angle must be inferred from the applied torque. Due to the mechanical design requiring torque input, manual steering without motor assistance is difficult. This control loop also facilitates the generation of feedback torque to the driver based on the steering actuator's response. In the case of this project, the loop will be implemented simply to allow the motor to track the input.

Traditionally, the second control loop receives the net output angle from the steering module calculated from the net torque detected, and uses it to actuate the steering rack accordingly. It then feeds back the detected steering angle. This angle is normally derived from sensors on the rack and the turning angle is inferred from the car's mechanics. When feedback is incorporated, the difference between the expected angle and the detected angle is used as a reference for the forces acting on the vehicle's tires. This and other factors such as vehicle speed, pitch and yaw, etc. determine the force to feed back to the driver, closing the loop between driver input and mechanical response.

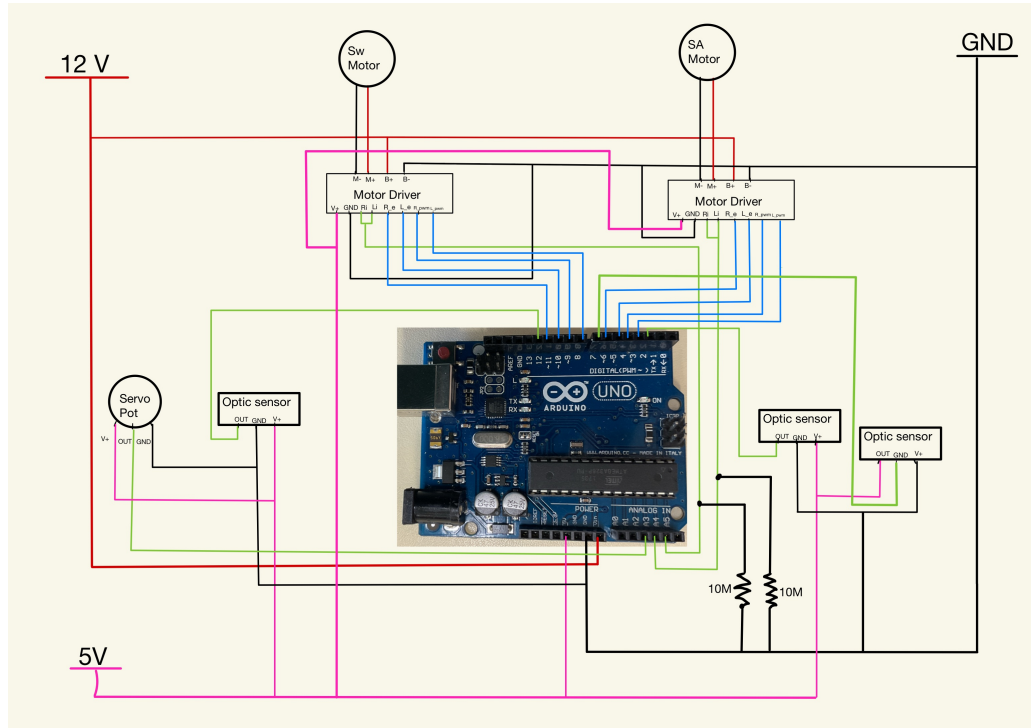


Figure 4.25: ECU circuit layout

To ensure a working prototype would be ready for demonstration at Open Day, the controller is planned to be developed in phases. Initial phases would focus on core functionality, with more complex features added in future iterations. The primary objective for this project phase is to establish a reliable correlation between the steering input and the resulting movement of the rack system.

The system is configured to run at a 10 ms time step.

4.6.1 System modelling

The first step in developing the controller involves creating a model of the system that can be analysed. Both subsystems are modelled based on the schematic presented in Figure 4.26. Due to the lack of precise data and access to advanced measurement facilities, many system parameters have been approximated using standard component values and general material properties. While these approximations may introduce some error when compared to the actual physical system, they are sufficient to design a controller that achieves near-desired performance. The controller can then be fine-tuned once integrated with the physical system to ensure suitability for continuous operation.

Key physical parameters, such as the shaft's moment of inertia about its central axis, were obtained from CAD models developed in OnShape. By assembling the components in their intended configurations and assigning the appropriate materials, the software computes relevant properties, including moments of inertia, centres of gravity, and total mass. Polylactic acid (PLA)—with a density of $1.24\text{g}/\text{cm}^3$, is included in OnShape's materials library, along with mechanical properties such as Young's modulus. These values were used to define system constants such as rotational stiffness, damping coefficients, and other dynamic characteristics. All variable values are available in Appendix B.2. The MATLAB code used for computing SIMULINK controller variables is provided in Appendix D.

Steering wheel model

Equations 4.19–4.22 are derived from the steering wheel schematic shown in Figure 4.26. In this model, the driver's input torque is deliberately neglected. Instead, the control loop is designed to track the steering input

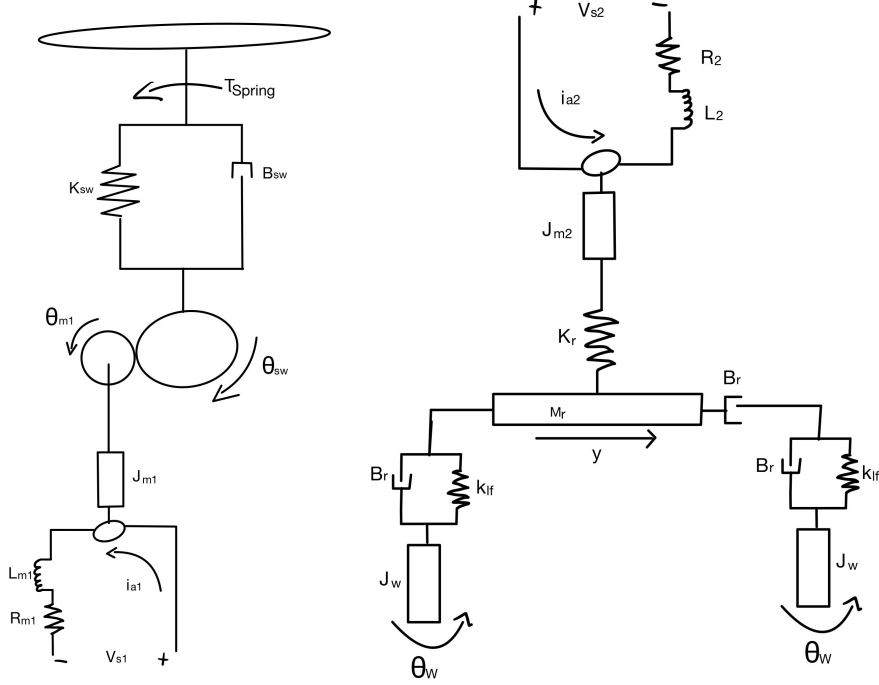


Figure 4.26: System Diagram (Steering wheel left, Steering Actuator right)

angle as accurately as possible, based solely on the motion of the steering wheel, or more precisely, the detected motion at its end. The mass of the steering wheel is modelled as an inertial load, as described by Equation 4.19, while the effects of the springs are captured by Equations 4.17 and 4.18.

$$C_{spr} = (K_{spr} N_{spr} N_{starts}^2 * d_p^2) / (4 * (pi^2)) \quad (4.17)$$

$$T_{springs} = C_{springs} \theta_{sw} \quad (4.18)$$

$$\ddot{\theta}_{sw} = -\frac{\theta_{sw}(C_{spr} - K_{sw}) + B_{sw}\dot{\theta}_{sw} - T_{load}}{J_{sw}} \quad (4.19)$$

$$\dot{i}_{m1} = \frac{R_{m1}i_{m1} - V_{m1} + \dot{\theta}_{m1}k_{em1}}{L_{m1}} \quad (4.20)$$

$$T_{motor} = i_{m1}k_{tm1} \quad (4.21)$$

$$\ddot{\theta}_{m1} = -\frac{1}{J_{m1}} \left(\frac{(C_{spr} + K_{sw})\theta_{m1}}{(Nm^2)} - \left(\frac{B_{sw}}{Nm^2} + B_{m1} \right) \dot{\theta}_{m1} + T_{motor} \right) \quad (4.22)$$

The above equations were then converted into the transfer function shown in Equation 4.23 that could be put in SIMULINK as the plant of the control loop. The full loop is seen in Figure 4.27. As noted in the Literature review, many researchers make use of PID control as the main form of control for the SBW wire systems, with PID control having been briefly explained in Chapter 3. The pin associations for the input and outputs of the system are displayed in Figures C.2 and C.3.

$$\frac{\Theta_{m1}(s)}{V(s)} = \frac{k_{tm1}}{(R_{m1} + L_{m1})(J_{m1}s^2 + (B_{m1} + \frac{B_{sw}}{Nm^2} + \frac{k_{em1}}{R_{m1}+L_{m1}s})s + \frac{(C_{spr}+K_{sw})}{Nm^2}} \quad (4.23)$$

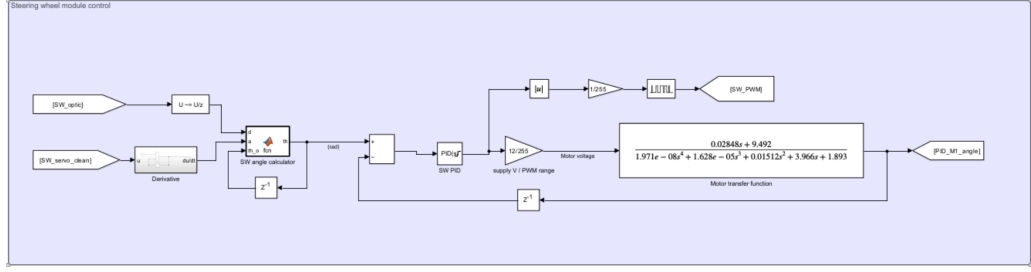


Figure 4.27: Steering wheel control loop

The control loop is provided with input signals from the optical gap sensor and the servo potentiometer. The underlying principle is that as the steering wheel gear rotates, the encoder signal alternates between 0 and 1. This binary signal is passed into a change detector, which outputs a logical 1 each time a transition occurs within a time step.

For the potentiometer, an analogue voltage signal is read and processed through a low-pass filter to attenuate high-frequency noise. As the potentiometer rotates clockwise, the voltage increases; conversely, it decreases when rotating counter-clockwise. The gradient of this signal is used to determine the direction of rotation. It is important to note that the potentiometer's direction of rotation is opposite to that of the steering wheel, due to the mechanical gear configuration.

The filtered signals are then fed into an angle calculation function, the implementation of which is provided in Appendix D, along with sample output data initialized at a starting angle of zero. In summary, the function logic is as follows: if a change in the optical sensor signal is detected and the potentiometer signal is decreasing, the angle is incremented by θ_{inc} , as defined in Equation 4.24. If the potentiometer signal is increasing, the angle is decremented by the same amount. If there is no change in either signals, the output remains the same.

$$\theta_{inc} = 0.9\left(\frac{\pi}{180}\right) \quad (4.24)$$

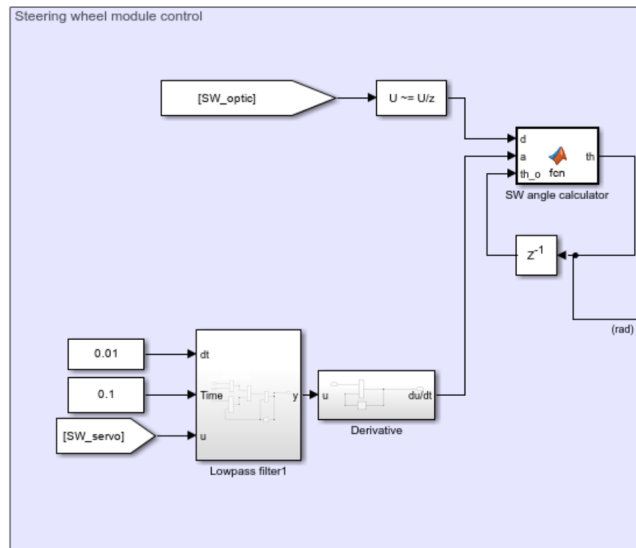


Figure 4.28: Input phase of the Steering wheel controller

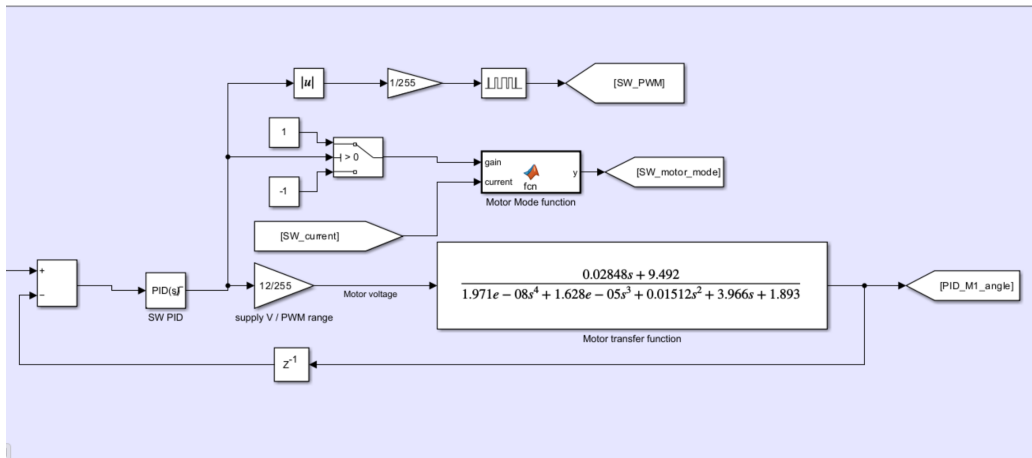


Figure 4.29: Control phase of the Steering wheel controller

The next stage is the processing and control phase, as illustrated in Figure 4.29. To achieve the desired system performance, the PID controller is tuned through an iterative, simulation-based process. The proportional (K_p), integral (K_i), and derivative (K_d) gains are initially estimated using standard tuning methods step response analysis. These values are then refined in simulation to minimize overshoot, reduce settling time, and ensure steady-state accuracy under different input profiles. The objective of the tuning process is to maintain stable tracking of the steering input angle while minimizing oscillation and error in the presence of load disturbances or model inaccuracies. MATLAB/Simulink provides a built-in tuning tool within the PID Controller block, which allows the system's estimated step response to be visualized based on the current plant model and controller gain settings. The controller parameters are adjusted by modifying desired performance characteristics such as response speed and damping, while a real-time estimation of the system response is provided. Although the estimated response is typically optimistic, the tool serves as a valuable reference for visualizing the expected output behaviour and guiding the tuning process.

A common tuning approach is followed whereby a low proportional gain is initially selected and gradually increased to enhance system responsiveness. Integral and derivative gains are then introduced incrementally to eliminate steady-state error and improve transient performance, respectively. Throughout the tuning process, system stability is continuously monitored to avoid oscillation or instability.

During the loop, the absolute value of the PID controller output is converted to a PWM signal and passed to the motor interface. A saturation limit of [255,255] is applied to the PID block output to ensure compatibility with the PWM range output by the Arduino. The sign of the signal is evaluated to determine direction and is routed into the motor mode function block accordingly. Based on the signal polarity and the measured motor current, the Motor Mode Function block determines the appropriate operating mode for the motor. The implementation of this function is provided in Appendix D.

The current threshold used to distinguish operating modes is determined experimentally by subjecting the motor to a load condition and analysing the resulting current waveform. The corresponding current profile is presented in Appendix C.5.

In the context of PID control, T. Park, C. Han, and S. Lee [14] recommend the use of PD control over full PID control for the steering wheel module, as a means of reducing the computational load on the ECU. This approach is initially implemented. Among the variations simulated, the proportional (P) controller yields the most functionally viable result. However, the system exhibits a steady-state error when tracking a step input.

This behaviour is illustrated in Figure 4.30, where a step input of 270° is applied. This input is multiplied by gear ratio of 2.3 to give a tracking reference of 10.84 rad (621°). The system response shows a steady-state offset of approximately 2.9 rad (166.16°), which corresponds to a steering wheel displacement of 72.24° after accounting for the gear ratio. This result is consistent with expectations due to the absence of integral correction in the control loop.

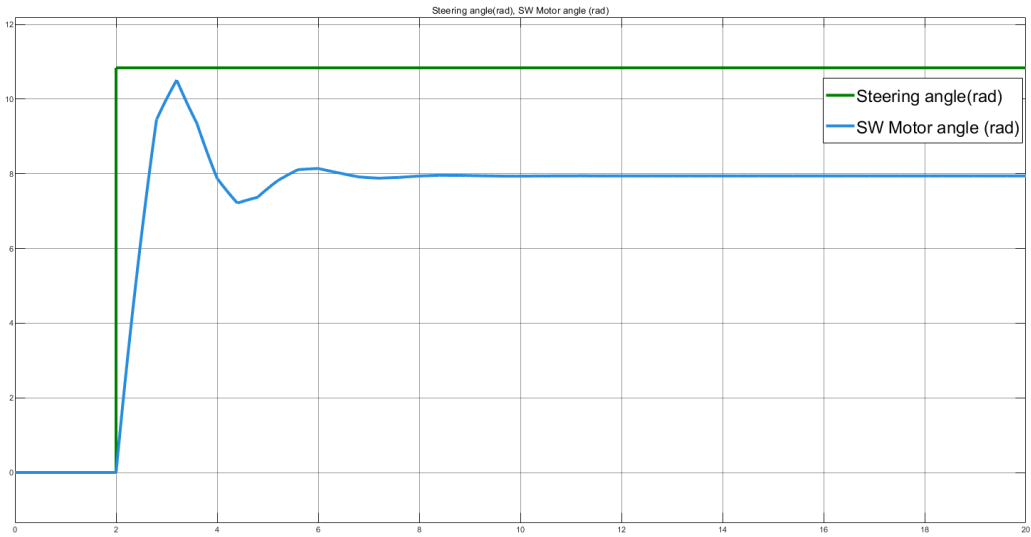


Figure 4.30: PD step response for Steering wheel motor

Although feed-forward techniques are implemented to mitigate the effects of disturbances and enhance tracking accuracy, their effectiveness depends on precise knowledge of the forces acting on the system. As this information is unavailable for the current model, the approach is found to be insufficient, thereby necessitating the incorporation of the integral (I) term into the controller.

As shown in Figure 4.31, a notable improvement in step response tracking is achieved using the PID controller, albeit at the cost of mild oscillations. The motor reaches steady state more rapidly, with a peak overshoot of approximately 2.8 rad ($160.43^\circ/69.75^\circ$ steering.) and settles within 5° of the target in approximately 4.42 seconds. Although the response is not ideal, it is deemed sufficiently stable for integration with the physical system, where further fine-tuning can be conducted as needed.

The gain values used to achieve this response are: $K_p = 11.473$, $K_i = 4.929$, $K_d = 3.344$.

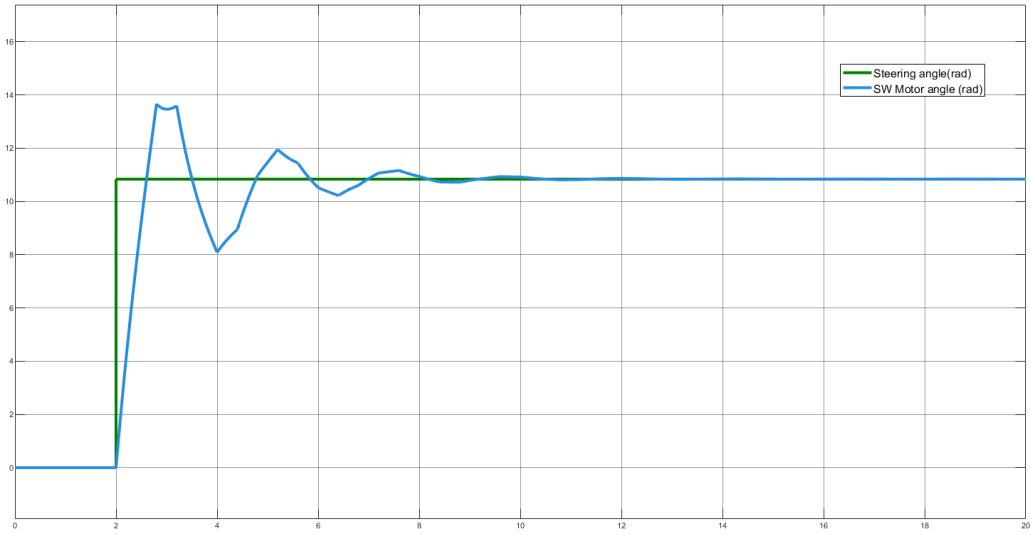


Figure 4.31: PID step response for Steering wheel motor

4.6.2 Steering actuator model

The equations of motion for the actuator are defined by Equations 4.25–4.28. These equations are used to calculate the motor's angular acceleration, the rate of change of motor current, the linear acceleration of the rack,

and the angular acceleration of the wheel. In a similar manner to the steering wheel control, these equations are converted into the transfer functions shown in Equations 4.29–4.31 for implementation in the control loop illustrated in Figure 4.32.

$$\ddot{\theta}_{m2} = -\frac{1}{J_{m2}}(K_r i_{m2} - B_{m2} \dot{\theta}_{m2}) \quad (4.25)$$

$$\dot{i}_{m2} = -\frac{-R_{m2} i_{m2} + V_{m1} + \dot{\theta}_{m2} k_{em1}}{L_{m1}} \quad (4.26)$$

$$\ddot{y} = -\frac{1}{M_r}(B_r \dot{y} + \frac{2k_{lf}y}{r_L^2} - \frac{K_r(\theta_{m2} r_p + y)}{r_p^2}) \quad (4.27)$$

$$\ddot{w} = -\frac{1}{J_f}(B_k p \dot{y} + k_{lf} \theta_w - \frac{K_{lf} y}{r_l}) \quad (4.28)$$

$$\frac{\Theta_{m2}(s)}{V(s)} = \frac{K_r}{J_{m2}(sL_{m2} + R_{m2})s^2 + (B_{m1}(sL_{m2} + R_{m2}) - K_{tm2}K_r)s} \quad (4.29)$$

$$\frac{Y(s)}{\Theta_{m2}(s)} = \frac{\frac{K_r}{r_p M_r}}{s^2 + \frac{B_r}{M_r}s + \left(\frac{2k_{lf}}{M_r r_L^2} + \frac{K_r}{r_p^2 M_r}\right)} \quad (4.30)$$

$$\frac{\Theta_w(s)}{Y(s)} = \frac{\frac{k_{lf}}{r_L}}{J_w s^2 + B_{kp} s + k_{lf}} \quad (4.31)$$

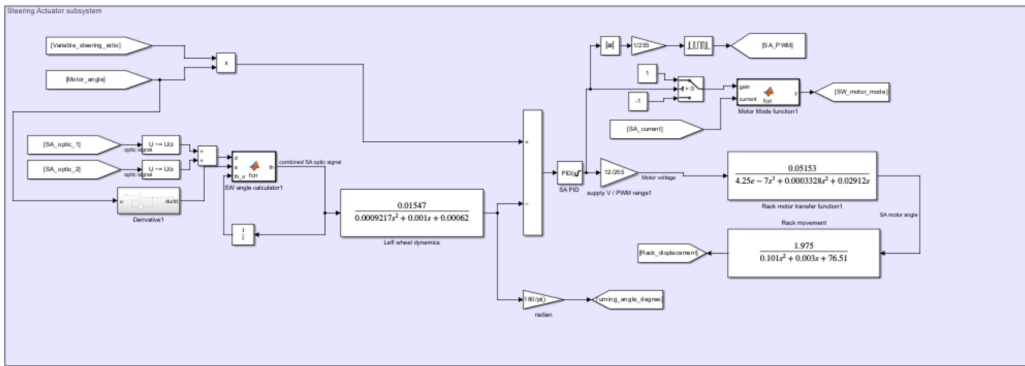


Figure 4.32: Steering actuator loop

The control loop for the actuator is implemented using the same principles as those applied in the steering wheel control loop. The primary distinction lies in the input signals, as shown in Figure 4.33. The reference angle is scaled according to the desired steering ratio. Although this ratio can be modified in future iterations to accommodate different steering ranges, the current objective is to complete one full wheel rotation over a steering range of 720°. This results in a steering ratio of 1:15.5 (i.e., 0.064).

The feedback signal is obtained from the detected rack displacement using two optical gap sensors. While the initial plan involves the application of grey-code logic, the detected signals fail to overlap as expected—illustrated in Figure 3.2, making it difficult to determine the direction of rack movement. To overcome this issue, the gradient of the steering wheel motor signal is used as a directional reference. Since the motor closely tracks the input, its rate of change provides a reliable indication of motion direction. The control phase of the actuator loop is

presented in Figure 4.34, with the generation of the PWM signal and the selection of motor mode carried out in the same manner as in the steering wheel control loop.

For simulation purposes, the motor and rack transfer functions are included to represent system dynamics. In this setup, the output of the rack transfer function is fed into the wheel transfer function. During implementation, these transfer functions are used to compare the expected model behaviour with actual system response, enabling the identification of discrepancies and informing potential adjustments.

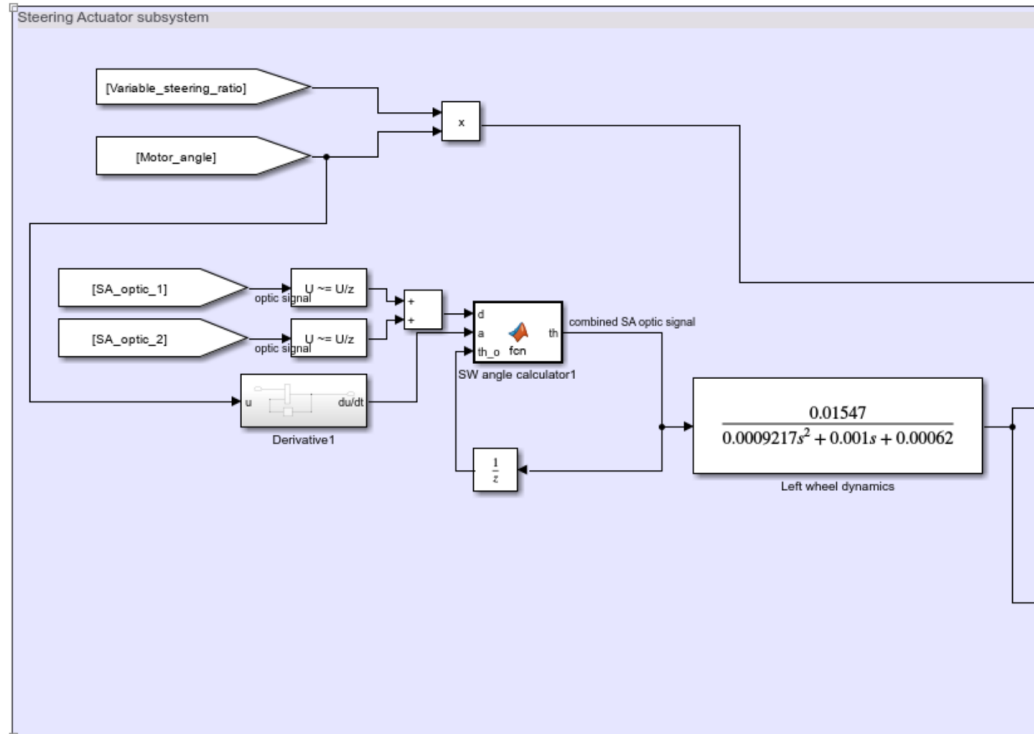


Figure 4.33: Input phase of the steering actuator controller

Based on insights gained from the evaluation of the steering wheel control, the steering actuator is configured with a PID controller from the outset. The best performing step response from this configuration is presented in Figure 4.35. The performance of the output is somewhat unsatisfactory. The signal initially overshoots the reference angle of 17.25° by 14.7% at an angle of 19.79° . While this is a small margin, the time for the signal to settle takes too long, only reaching a 5% error after 14.2s. This signal was attained with the gain values of: $K_p = 6.187$, $K_i = 0.03716$, and $K_d = 19.07$

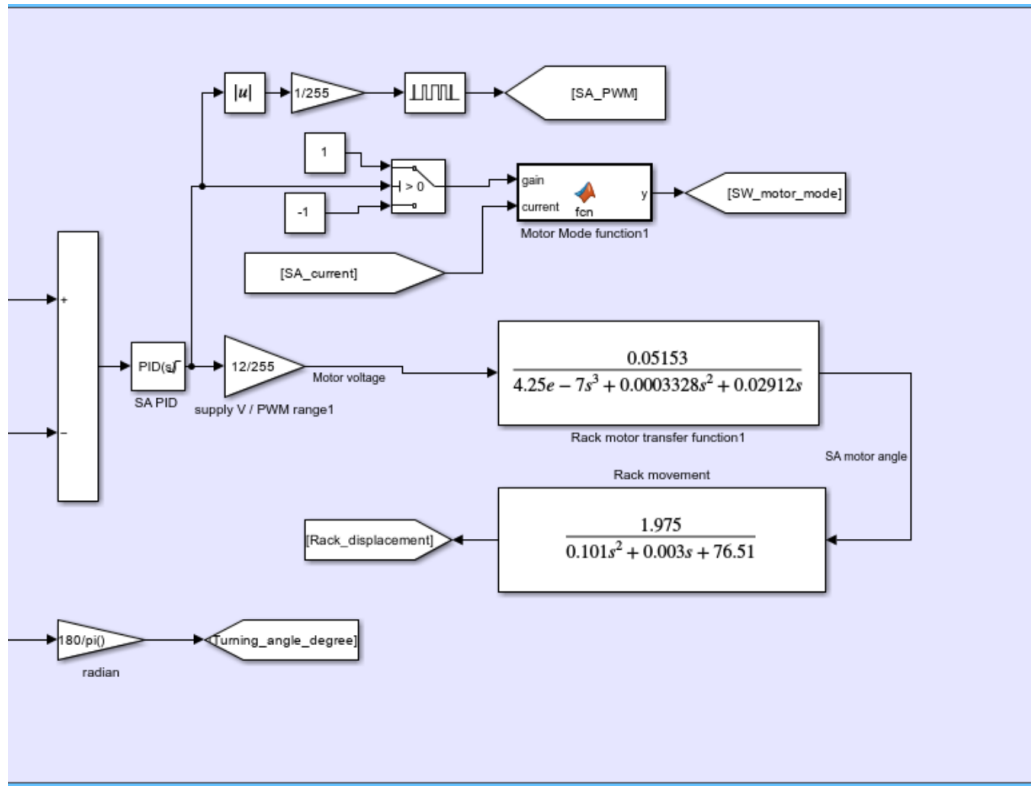


Figure 4.34: Control phase of the steering actuator controller

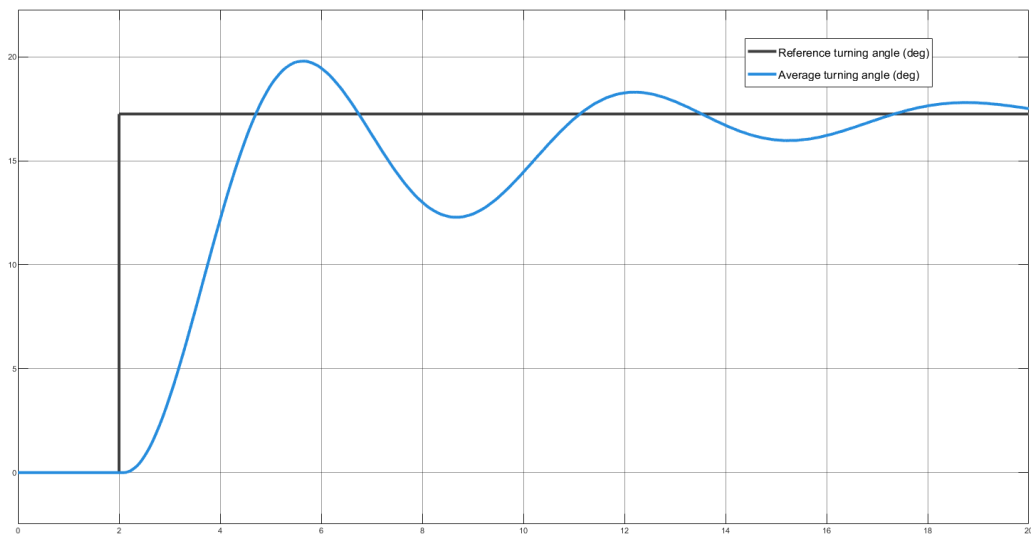


Figure 4.35: Steering actuator step response

Chapter 5

Testing, Results and Discussion

5.1 Testing and Results

The model is designed to fulfil the specifications outlined in Table 4.1. The tests below are conducted to evaluate whether the model meets these objectives. The testing equipment includes a standard Staedtler Noris Club math set protractor, a set square for angular measurements, and a Hewlett-Packard E3630A Triple Output DC Power Supply.

Test 1: Rack System Limit and Steering Accuracy Evaluation (SA-1)

To evaluate the turning range of the rack system, two key properties are tested: the ability of the mechanism to establish hard end stops and the accuracy of the resulting wheel angles. The rack is manually centred to represent a 0° turning angle. A horizontal reference line, normal to the wheel face, is drawn beneath the wheel and a protractor was aligned with it.

The racks is then actuated to its rightmost limit using a motor operating at 12V, the rated maximum voltage expected during operation, and the angular displacement from the reference line is recorded. The process is repeated for the left limit, and for the left wheel. Because the measurement is taken from the wheel face rather than the steering pivot (kingpin), a reference line rather than a single point is used to reduce geometric error due to translation.

A secondary measurement is taken by marking the wheel's extreme position and computing the angle using the Pythagorean theorem. The average of the two readings is compared with the expected steering angle. The results are presented in Table 5.1.

Table 5.1: Rack testing results

Direction	successful limit	Wheel	Average recorded angle($^\circ$)	Calculated turning angle($^\circ$)	Expected angle($^\circ$)	Error($^\circ$)
Right	Yes	Left	62.3	27.07	23.212	3.858
Right	Yes	Right	59.98	30	23.212	6.807
Left	Yes	Left	112.725	22.725	23.212	0.487
Left	Yes	Right	112.94	22.94	23.212	0.2705

Test 2: Steering System Limit and Range Evaluation (SM-4)

This test evaluates the effective turning range of the steering wheel. The wheel is temporarily removed to allow a backdrop paper to be fixed to the housing. It is then reattached, and markers are applied: one on the wheel (using double-sided tape) and one on the paper (with a pen), both aligned in the centred position.

The wheel is rotated manually to the extreme right and left positions, and the positions of the markers are traced onto the sheet. These reference points are transferred to another surface for precise measurement using a protractor and confirmed through geometric methods.

This process is repeated under two conditions: with the spring-return mechanism engaged and disengaged. Results are summarized in Table 5.2.

Table 5.2: Steering limit testing results

Direction	Rotation method	successful limit	Spring present	Average angle(°)	Expected angle(°)	Error(°)
CW	Manual	Yes	No	376	360	16
CCW	Manual	Yes	No	-393	-360	33
CW	Manual	Yes	Yes	373.5	360	13.5
CCW	Manual	Yes	Yes	-388	-360	28

Test 3: Wheel Centring via Spring Mechanism (SM-5)

To test the centring behaviour, the steering wheel is rotated 90°, 180°, 360° in both clockwise and counter-clockwise directions and then released. The wheel's ability to return to the centre is observed and evaluated for consistency and range.

Test 4: Encoder precision(SM-2)

This test assesses the detection resolution of the optical encoders for both the steering wheel and the actuator. The motor is operated at 13 rpm and 22.75 rpm, with two runs at each speed. For the steering wheel, the motor is stopped after a 360° rotation, while the actuator is tested across its full range. Low rotational speeds are selected to enable more accurate visualization and evaluation of sensor performance. Results are shown in Figures 5.1 and 5.2.

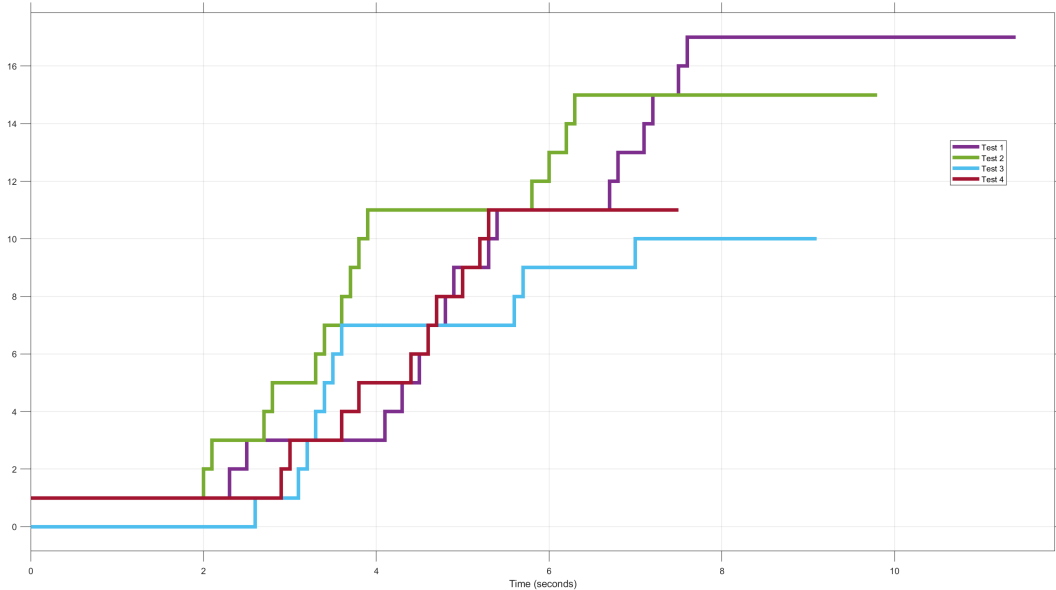


Figure 5.1: Test 4 results for Steering wheel sensor

5.2 Discussion

Test 1: Rack System Limit and Steering Accuracy Evaluation The rack system successfully engages hard mechanical end stops. However, steering accuracy exhibits directional bias—errors during right-hand turns are significantly greater than during left-hand turns. This likely results from mechanical misalignment, possibly due to play in the support bracket that allows more displacement in one direction.

Encouragingly, the system displays partial compliance with Ackermann steering geometry, with the inner wheel consistently achieving a larger steering angle than the outer wheel. Although imperfect, this suggests that the system architecture aligns conceptually with expected behaviour.

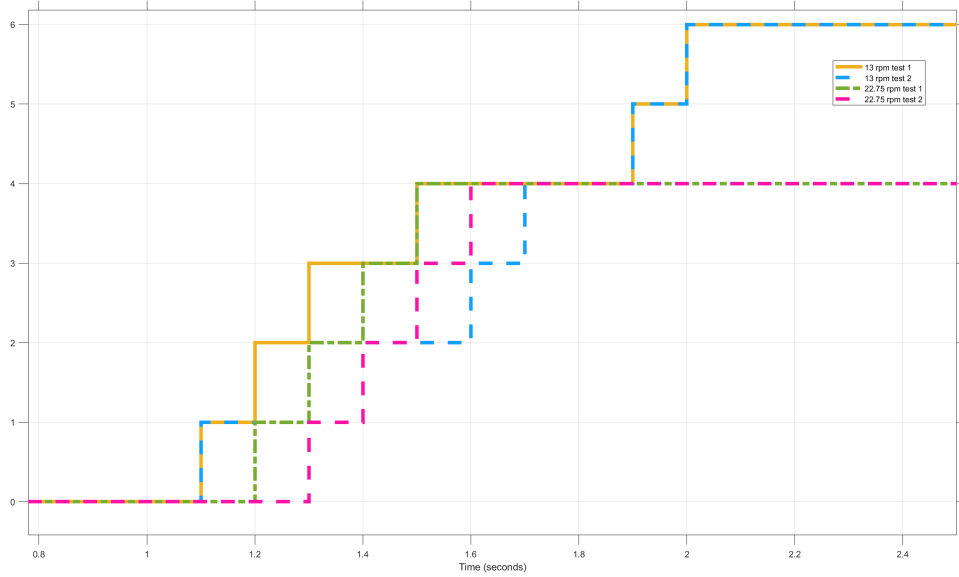


Figure 5.2: Test 4 results for Steering actuator sensor

The achieved turning range exceeded the intended maximum steering angle by 11.2%, surpassing the design target of 46.42°.

Test 2: Steering System Limit and Range Evaluation (SM-4)

All steering range tests confirm that the wheel achieves rotational limits beyond the intended 720° span. In the absence of the spring mechanism, overshoots of 16° (CW) and 33° (CCW) are recorded. With the spring installed, these values reduce slightly, confirming that the springs help moderate extreme movement but do not strictly enforce the design limits. A noticeable amount of play is present between the components in the shaft despite the 3 central rods.

Test 3: Wheel Centring via Spring Mechanism

The spring mechanism fails to return the wheel to centre after release across all tested angles. Even with improved spring housing and alignment using bolts, the springs alone do not induce rotation. Manual nudging is required to initiate return.

Inspection reveals that the lead screw geometry prevents reverse actuation. Even manual attempts to pressure the slider do not translate into rotational motion due to an improper thread angle. In industrial settings, self-back driving screws typically have thread angles around 25, a feature not included in the custom-machined shaft. Stronger springs or a redesign of the screw with proper helix angle would be necessary to support passive centring.

Test 4: angular detection

The optical sensors fail to provide high-resolution readings. The resolution visibly decreases with higher speeds, and tests at a similar speed end with identical final readings. Two causes are identified: either the gaps in the encoder wheel are not consistently detected due to printing quality or motion speed. The second potential cause, discovered belatedly is sample speed. The simulation sample time is set to 10 ms. For 400 ticks per second (to achieve 1° resolution), the required sampling interval would be 2.5 ms. Thus, proper evaluation of the sensor system requires a test environment operating at least 4× the current simulation rate.

5.2.1 Overall system performance

Table 5.3 summarizes the performance of the model against its initial design specifications.

The use of direct angle detection was intended to simplify the scaled-down SBW model, but the results illustrate why torque-based sensing is preferred in real-world systems. Torque detection offers inference of intended motion without relying on mechanical resolution or encoder calibration. Furthermore, actuators capable of resisting motion and driving precise input would have reduced system lag.

The steering input system exhibited structural flex, contributing to a deviation between commanded and actual angles. Although a support frame was included, it proved inadequate under load. This flexure may have led to larger-than-expected steering outputs. Future iterations should employ a stiffer material such as stainless steel for the central beam, or integrate keyed notches to form a locking mechanism and reduce movement.

The lead screw design effectively provided physical hard stops and absorbed end-range energy through the springs. However, the centring mechanism failed due to a poor screw thread profile and insufficient spring force. The late-stage addition of bolts prevented spring force displacement, but did not resolve the lack of reactive torque. A redesign of the screw angle and stronger springs would be required to achieve automatic wheel centring.

Regarding the rack and pinion, several scaling errors are identified. The pinion and rack design are based on the steering arm displacement of a full-sized vehicle, which overestimates rack motion in a scaled model. Additionally, the linear distances from left and right turns were summed rather than subtracted, leading to an oversized rack range. While a redesign was not completed, the increase in wheel size inadvertently corrected some of this misalignment. A smaller pinion would have helped but would have introduced issues with the sensor interface, though this concern is moot given the current sensor performance.

Table 5.3: Specifications assessment

No.	Objective description	Acceptance criteria	Specification met
M-1.	The model must be small	Model should fit in a 600mm x 600mm area	Passed. The final area taken up by the assembled system (see Appendix C) occupied an area of 470mm x 545mm.
M-2.	The model should be low cost	Model components < R3 000	Passed. The total cost of the model (excluding printing filament) was R1 914.64.
SA-1.	The model must have realistic steering capacity	Ackermann-compliant angle within $\pm 10^\circ$ error	Failed. The average error was $\pm 11.2\%$
SA-2.	Actuator system should be sensitive to steering inputs	1° angle resolution (detection and actuation)	Failed. The custom optic sensor did not meet the desired resolution. The actuation precision is inconclusive.
SA-3.	A fast steering speed	Left-to-right turn in 1s	Passed. The actuator was able to complete a turn in 0.8s.
SM-1.	The model must have realistic steering capacity	Limited $720 \pm 5^\circ$ turning range	Passed. The test without the spring system exceeded limits, but the springs limited the range within margins.
SM-2.	The model should be sensitive to steering inputs	1° angle resolution (detection and actuation)	Failed. The accuracy of the sensor did not meet the desired spec. However, individual detection of angles was successful.
SM-3.	A fast steering speed	± 120 rpm steering wheel rotation	Passed. The wheel, driven by the motor completed a full rotation in 1.06 s (within 10% margin)
SM-4.	The model must be rugged	Should endure a scaled input torque (2.5 Nm)	Passed. The model was able to endure various interactions by colleagues as well as tests without any fault.
SM-5.	Replicate common steering experience	Upon release of the steering wheel, it must centralise	Failed. When nudged, the steering wheel would move slightly toward the centre, but could not consistently centralise.
C-1.	The steering response should be smooth	<5% transient state overshoot	Inconclusive. The controller achieved near this in simulation, but a practical test was not possible due to encoder failure.
C-2.	Steering input should be translated to the wheel quickly	<2s delay	Failed. The controller failed to achieve this in simulation, and a practical test was not possible.

Chapter 6

Conclusions and Recommendations

The development of a scaled Steer-by-Wire (SBW) demonstration model did not meet its core objective of creating a working SBW model. However, it has succeeded in providing a tangible, educational prototype that encapsulates the core principles of modern SBW systems. The project involved detailed mechanical design, custom component manufacturing, control system development, and simulation-based validation. Despite several technical limitations and resource constraints, the model achieved functional integration between steering input, electronic control, and rack-based actuation. The structure demonstrated core concepts such as sensor-driven angle detection, PID-based motion control, and feedback loop implementation, making it a valuable educational tool for engineering students and outreach activities.

However, testing revealed shortcomings in system resolution, mechanical rigidity, and return-to-centre behaviour. These issues largely stemmed from compromises in material selection, sensor quality, and print tolerances, necessitated by limited budget, time, and fabrication tools. Nevertheless, the project lays a strong foundation for future iterations with enhanced realism, control fidelity, and robustness.

The SBW model reinforces the viability and value of digitally actuated steering systems, especially in contexts where flexibility, scalability, and integration with autonomous control architectures are essential.

6.1 Future recommendations

Use Industry-Grade CAD Software: It is strongly recommended to use professional mechanical design tools such as SolidWorks or Autodesk Inventor when developing high-precision mechanical components. These platforms offer built-in features for simulating mechanical loads, generating accurate threaded geometries, and validating assembly fit through interference checks. Specifically for components like lead screws, professional tools enable the specification of thread pitch, helix angle, and material properties—ensuring that the screw functions correctly both in linear translation and back-driving modes. Transitioning away from custom tools or generic design software will reduce trial-and-error and increase the reliability of components subjected to complex mechanical interactions.

Redesign Steering Shaft and Centring System: To achieve effective self-centring behaviour, the spring mechanism should be redesigned with the following improvements:

- Preload the springs so that a restoring force is present even at the neutral position. This ensures that small deviations still generate corrective torque.
- Select springs with higher stiffness constants, balancing the need for sufficient return force with the motor's ability to oppose the spring during actuation.
- Replace the existing lead screw with one that includes a proper thread profile designed for bidirectional power transmission. In particular, a self back-drivable thread (e.g., with a 25° helix angle) would allow linear spring compression to result in a restoring rotational torque on the shaft.

These modifications are essential to overcome the current limitation where the spring can compress but cannot induce rotational recovery due to the geometry of the screw.

Improve Sensor Fidelity and Sampling Rate: The existing custom optical gap sensor system proved inadequate for precise angular detection. Future designs should incorporate commercially available rotary encoders with well-defined resolution and documented electrical characteristics. These sensors offer significantly better repeatability, noise immunity, and integration support. Moreover, the microcontroller sampling rate must be increased to meet the desired angular resolution. For instance, achieving 1° resolution at 400 ticks per second requires a sampling interval of no more than 2.5 milliseconds.

Reliable angle detection is critical for accurate control and closed-loop stability.

Enhance Tie-Rod and Rack Scaling: A significant discrepancy was noted in the geometry of the steering linkage. To address this rack travel must be recalculated based on the updated steering angles and the physical limits of the scaled wheels and the tie-rod length and angle should be adjusted to ensure proper transmission of rack motion to the wheels, preserving realistic Ackermann geometry. Subsequently, the pinion should also be redesigned on the same basis. The aluminium profile frame may need to change to match the updated rack and wheel assembly dimensions.

Implement Feedback Torque Loop: Although excluded from this iteration due to complexity, future versions should integrate a basic feedback torque generation mechanism. Even a simplified spring-damper analog or a low-torque algorithm for the present motor system could simulate realistic driver feel.

Structural Improvements: The current frame design, while functional, lacks the alignment consistency needed for long-term use. Some suggested improvements are:

- The motor supports should be incorporate directly into the frame base, rather than relying on adhesive or modular assembly. This will ensure consistent gear alignment and eliminate slippage or misalignment during motion.
- Reinforce the steering shaft support to minimize deflection under load, particularly when torque from the steering wheel or motor is applied.
- Print gears flat on the print bed to minimize warping and ensure accurate meshing. In the current iteration, slight warping of the steering gear led to poor meshing, requiring temporary solutions (e.g., rubber hair tie tensioning) that are not scalable or repeatable.
- Consider using larger, higher resolution printers for large/precision requiring components.

These improvements will enhance mechanical reliability, reduce the need for ad hoc fixes, and improve long-term repeatability.

Bibliography

- [1] T. Hoeltgebraum. (2022, July 22) The history of steering mechanisms — part 1. [Online]. Available: <https://medium.com/@thiagohbaum/the-history-of-steering-mechanisms-part-1-2657ae542c33>
- [2] J. Reimpell, H. Stoll, and W. B. Jurgen, *The automotive chassis : engineering principles*, english ed. ed. Society of Automotive Engineers, 1996.
- [3] S.-W. Oh, H.-C. Chae, S.-C. Yun, and C.-S. Han, “The design of a controller for the steer-by-wire system *,” Tech. Rep.
- [4] N. Ranaweera and G. Donato, “Development and experimental testing of a speed controlled pmsm drive using psim visual programming environment,” Ph.D. dissertation, 08 2019.
- [5] P. A. Simionescu, T. Hoeltgebraum, and D. Martins, “On the evolution of automotive steering mechanisms,” in *Proceedings of the 2022 USCToMM Symposium on Mechanical Systems and Robotics*, P. Laroche and J. M. McCarthy, Eds. Cham: Springer International Publishing, 2022, pp. 116–128.
- [6] T. B. A. museum, “1770 fardier de cugnot,” 5 2025. [Online]. Available: <https://www.tbauto.org/car-collection/1770-fardier-de-cugnot>
- [7] T. Hoeltgebraum. (2022, July 22) The history of steering mechanisms — part 2. [Online]. Available: <https://medium.com/@thiagohbaum/the-history-of-steering-mechanisms-part-2-18091c990f52>
- [8] J. S. Zhao, X. Liu, Z. J. Feng, and J. S. Dai, “Design of an ackermann-type steering mechanism,” *Proceedings of the Institution of Mechanical Engineers, Part C: Journal of Mechanical Engineering Science*, vol. 227, pp. 2549–2562, 11 2013.
- [9] S. Malsbury and J. Hinton, *Electric power assisted steering for small road vehicles*. Society of Automotive Engineers, inc, pp. 43–49.
- [10] K. Suzuki, Y. Inaguma, K. Haga, and T. Nakayama, *Integrated Electro-Hydraulic Power Steering System with Low Electric Energy Consumption*. Society of Automotive Engineers, inc, pp. 19–25.
- [11] A. M. Pawlak, D. W. Graber, and D. C. Eckhardt, *Magnetic Power Steering Assist System - MAGNASTEER*. Society of Automotive Engineers, Inc., pp. 13–18.
- [12] P. Yih and J. C. Gerdes, “Modification of vehicle handling characteristics via steer-by-wire,” *IEEE Transactions on Control Systems Technology*, vol. 13, pp. 965–976, 11 2005.
- [13] M. Kurishige, R. Nishiyama, N. Inoue, S. Wada, and T. Kifuku, “A new eps control strategy to improve steering wheel returnability,” in *SAE 2000 World Congress*, 2000.
- [14] T. J. Park, C. S. Han, and S. H. Lee, “Development of the electronic control unit for the rack-actuating steer-by-wire using the hardware-in-the-loop simulation system,” *Mechatronics*, vol. 15, pp. 899–918, 10 2005.
- [15] G. Zhu, H. Yang, and F. Yu, *Controller Design for an Automobile Steer-By-Wire System*. Institute of Electrical and Electronics Engineers, 2019.
- [16] M. Live, “Tesla cybertruck steer-by-wire system,” 4 20224. [Online]. Available: <https://www.youtube.com/watch?v=daZVl2VuxD8&list=PLKiPZRFdZJBQofIhgO09lIx9ID0XuOaWw&index=8>
- [17] D. Cesiel, M. C. Gaunt, and B. Daugherty, “Development of a steer-by-wire system for the gm sequel development of a steer-by-wire system for the gm se,” Tech. Rep., 2006.

- [18] K. Eisenhauer, J. Andrew, J. Baxter, D. Boyton, and S. Robinson, *Opto-electronic torque, Absolute Angle and Rate Sensor for EPAS and EHPAS Steering Applications*. Society of Automotive Engineers, inc, pp. 35–41.
- [19] R. Hazelden, *High integrity optical torque sensor for electronic power steering systems*. Society of Automotive Engineers.
- [20] W. F. Milliken, D. L. Milliken, and M. Olley, *Chassis design : principles and analysis*. Professional Engineering Pub., 2002.
- [21] “Gear dimension calculator,” 2025. [Online]. Available: https://evolventdesign.com/pages/blank-calc?srsltid=AfmBOopf3U0BHvxignBMDHrEfCoKbCfJR8Hgj_j1Rda6nLRetGWmR0NX#google_vignette
- [22] nackhabitat. (2025, April 11) Sharing a cool tip that i learned well over a year ago, but wasn't able to put into use until today. and it ended up working perfectly. shout out to whoever made a short video about this a long time ago because you helped me! diy 3dprinting tips 3dprint bambulabs 3ddesign. [Online]. Available: <https://www.instagram.com/reel/DISnjzWAL87/?igsh=MWVzb3JoY3ZzOTFnYw%3D%3D>
- [23] C. Select, 04 2025. [Online]. Available: <https://www.centurionselect.co.za/suzuki/specification/fronx/#driving-amenities>
- [24] Wheel-size.com, “2024 suzuki fronx wheel fitment guide,” 04 2025. [Online]. Available: <https://www.wheel-size.com/size/suzuki/fronx/2024/>
- [25] A. Mazilu, “Kinematic optimization of the rack and pinion steering-system of an automobile: An example,” Tech. Rep., 2016. [Online]. Available: <https://www.researchgate.net/publication/311309543>
- [26] D. Pradhan, K. Ganguly, B. Swain, and H. Roy, “Optimal kinematic synthesis of 6 bar rack and pinion ackerman steering linkage,” *Proceedings of the Institution of Mechanical Engineers, Part D: Journal of Automobile Engineering*, vol. 235, pp. 1660–1669, 5 2021.

Appendix A

Github

<https://github.com/MasNet610/Steer-by-wire>

Appendix B

Parameter values

B.1 Gear values

Table B.1: Gear specifications for pinion, steering wheel, and steering motor

Specification	Pinion Gear	Steering Wheel Gear	Steering Motor Gear
Number of Teeth	23	87	39
Module (mm)	2.0867	1.8966	1.8966
Pressure Angle (°)	30	30	30
Gear Type	External	External	External
Outside Diameter (mm)	52.1675	168.7974	77.7606
Pitch Diameter (mm)	47.9941	165.0042	73.9674
Root Diameter (mm)	42.7774	160.2627	69.2259
Addendum (mm)	2.0867	1.8966	1.8966
Dedendum (mm)	2.6084	2.3708	2.3708
Working Depth (mm)	4.1734	3.7932	3.7932
Whole Depth (mm)	4.6951	4.2674	4.2674
Circular Pitch (mm)	6.5556	5.9583	5.9583
Tooth Thickness (mm)	3.2778	2.9792	2.9792
Base Circle Diameter (mm)	41.5641	142.8978	64.0576
Undercut	No	No	No

B.2 Modelling

B.3 Bill of Materials

Table B.2: Parameters Table

Parameter	Description	Value	Unit
d_p	Screw pitch	0.008	m
N_{starts}	Number of screw starts	2	-
K_{spr}	Spring constant	0.08	N/m
K_r	Rack lumped torque stiffness	30.96	Nm/rad
B_r	Rack damping coefficient	0.5	Henry
M_r	Rack lumped mass	0.794688	kgm^2
K_{lf}	Rack linkage stiffness	0.00062	kgm^2
r_L	Offset of kingpin axis	0.04007805	m
r_p	Pinion gear radius	0.02608375	m
B_{kp}	King pin damping coefficient	0.004	Kgm^2
J_w	Lumped front wheel inertia	0.00058442	Kgm^2
J_{sw}	Shaft inertia	0.0025	Kgm^2
K_{sw}	Shaft lumped torque stiffness	2174.530464	Nm/rad
N_{m1}	Gearing ratio	2.3	-
R_1	Motor resistance	14.8	ohm
L_1	Motor inductance	0.0444	Henry
K_{m1}	Motor constant	0.641333333	Nm/A
J_{m1}	Motor inertia	0.00001	Kgm^2
B_{m1}	Motor damping	0.001587777	Nm/(rad/s)
k_{em1}	Back emf constant	0.38	V/(rad/s)
V_{sm}	Supplied voltage (PWM signal)	-	V
R_2	Motor resistance	8.5	ohm
L_2	Motor inductance	0.0425	Henry
K_{m2}	Motor constant	0.396666667	Nm/A
J_{m2}	Motor inertia	0.00001	Kgm^2
B_{m2}	Motor damping	0.005827519	Nm/(rad/s)
k_{em2}	Back emf constant	1.64	V/(rad/s)
V_r	Supplied voltage (PWM signal)	-	V

Table B.3: Parts list for the Steer-by-Wire model

Part Name	Part Number	Supplier	Link	Price (ZAR)	Qty	Total (ZAR)
MOTOR GEARED 12VDC 1A6 270RPM 6mm DIA=37mm	GB37Y360 12V	Mantech	Link	288.65	1	288.65
MOTOR GEARED 12VDC 0A3 65RPM	EGB-365S-15130	Mantech	Link	496.85	1	496.85
H BRIDGE 43A HIGH POWER MOTOR DRIVE	—	Mantech	Link	148.00	3	444.00
DEEP GROOVE BALL BEARING 3X10X4MM ZZ CN BTC	—	BMG	Link	27.80	2	55.60
DEEP GROOVE BALL BEARING 5X16X5MM OPEN CN	—	BMG	Link	10.05	6	60.30
DEEP GROOVE BALL BEARING 17X35X10MM 2RS C3 BTC	—	BMG	Link	16.95	2	33.90
RS PRO Stainless Steel Compression Spring	821-289	RS Components	Link	183.00	1	183.00
OPTICAL GAP / SLOT SENSOR BOARD G=10mm	170202	Mantech	Link	19.23	3	57.69
STRUT PROFILE PG20 20X20 4 SLOTS	1.11.20.020020.04	Moduasm	Link	102.65	1.3	133.45
PRE-SET NUT PG15 PG20	2.11.06.M5	Moduasm	Link	8.06	20	161.20
Total						R1 914.64

Appendix C

Additional pictures

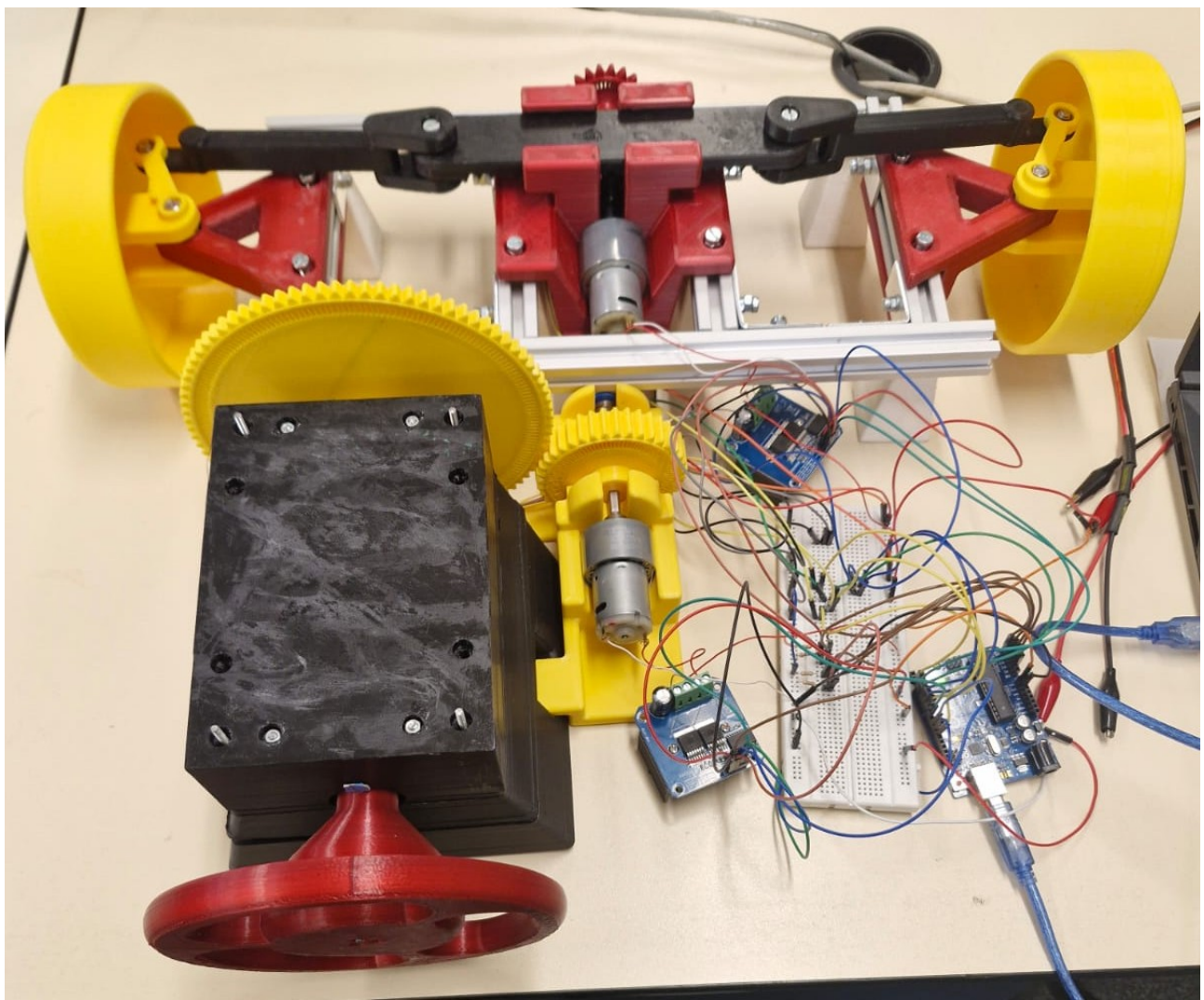
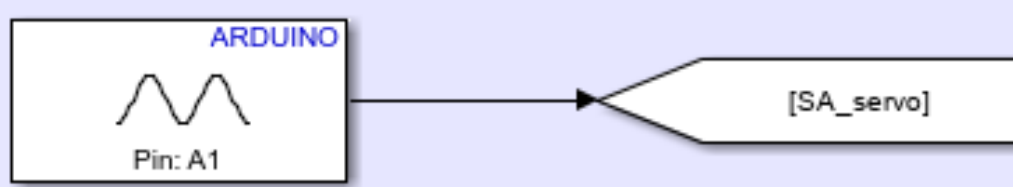
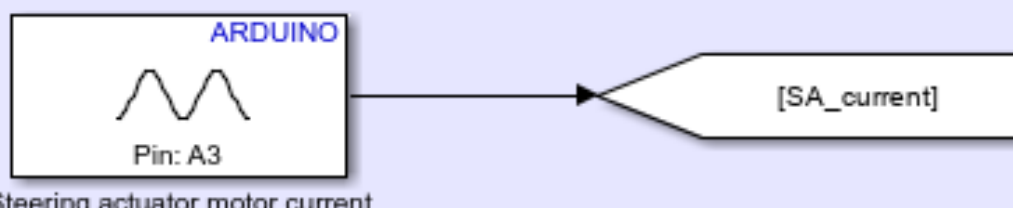
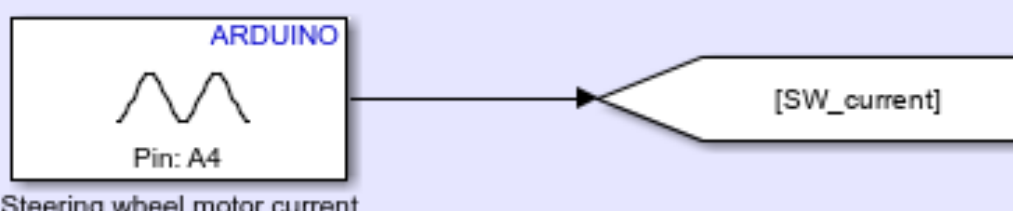
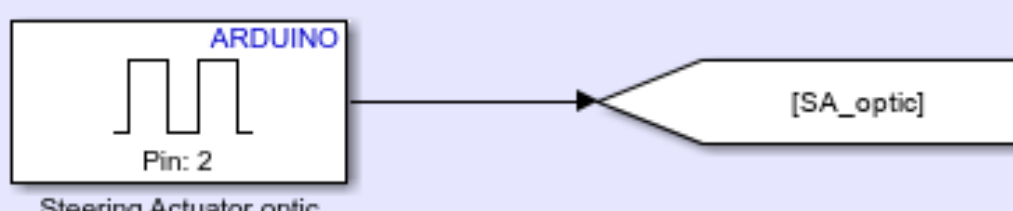


Figure C.1: Fully assembled SBW Model

Inputs



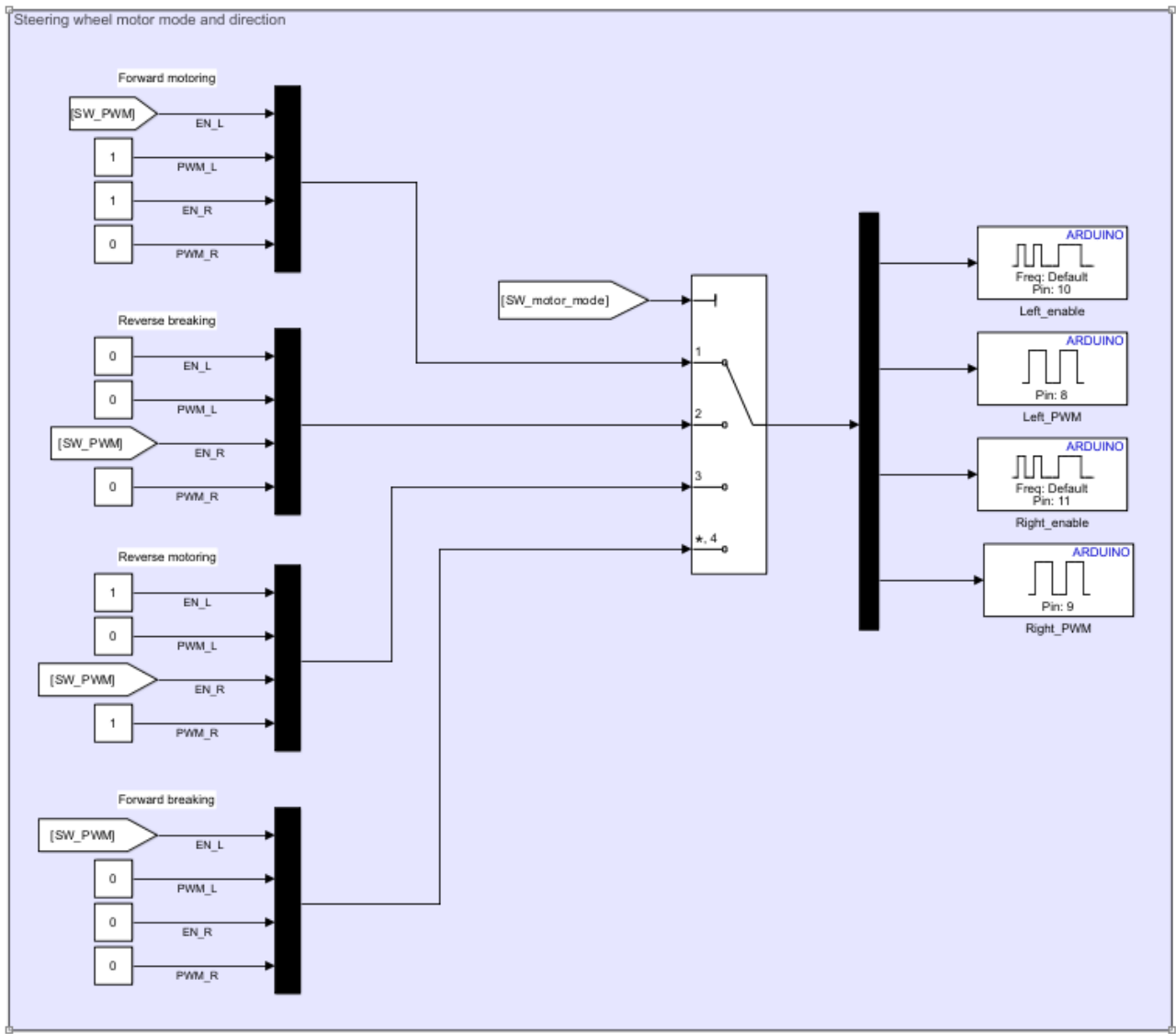


Figure C.3: Steering wheel motor driver commands

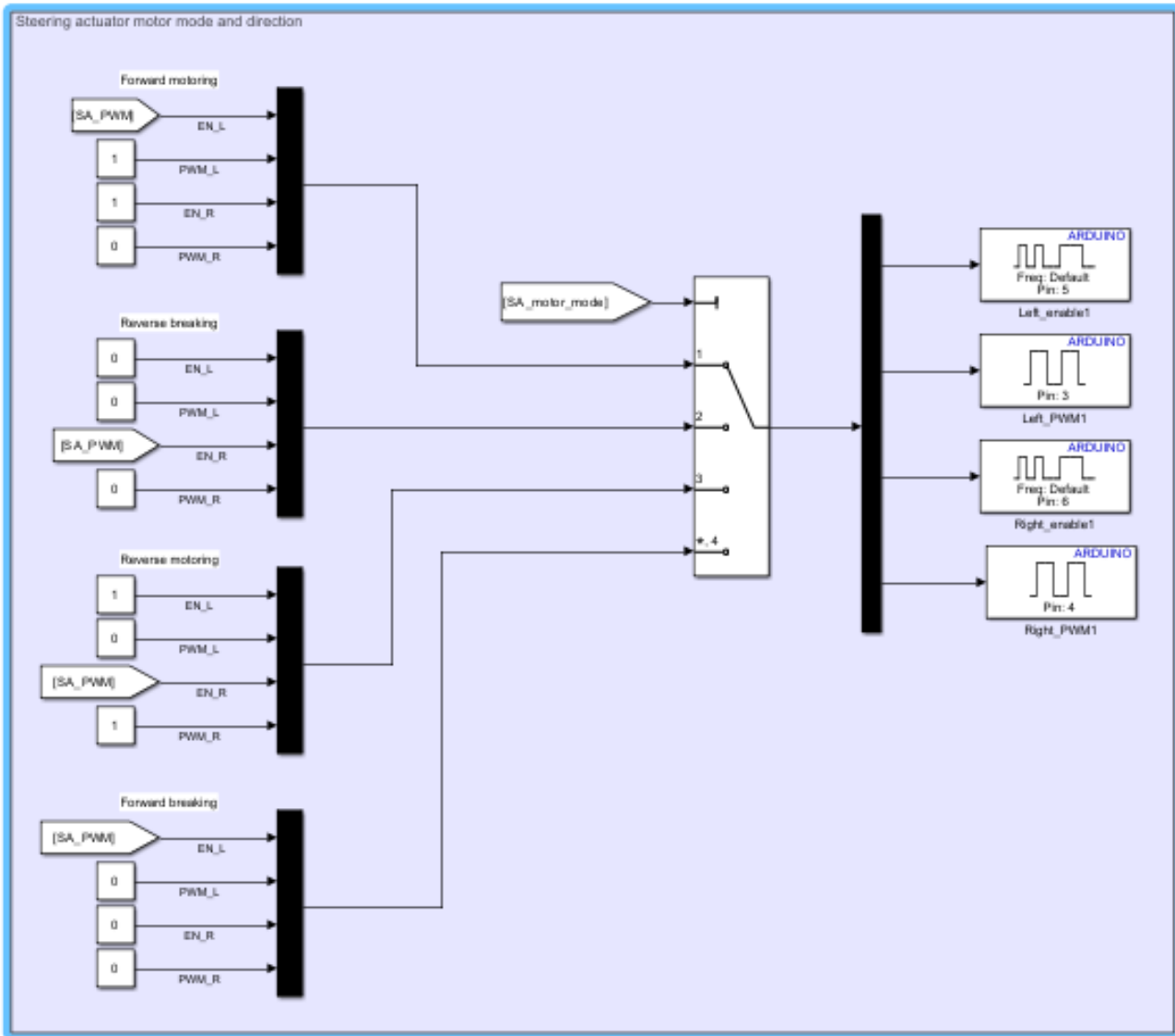


Figure C.4: Steering Actuator motor driver commands

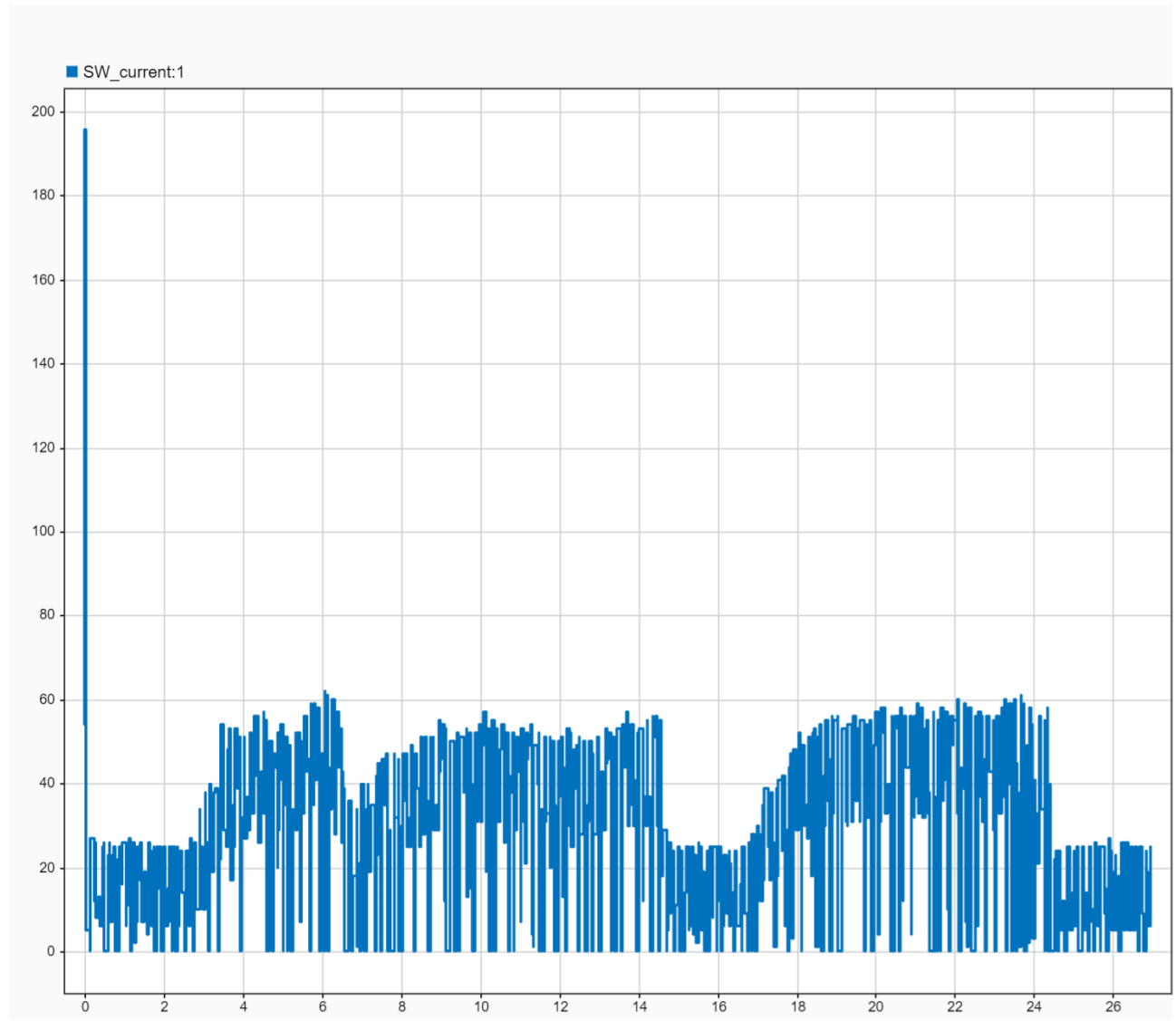


Figure C.5: Current analysis of motor under stress

Appendix D

Matlab Controller calculations

```
1 %% Steer By Wire system modeling
2 %% Steering wheel System
3 % System variables
4
5 syms th_sw dth_sw ddth_sw th_m1 dth_m1 ddth_m1 i_m1 di_m1 V_m1 x s
6
7 syms J_sw K_sw B_sw J_m1 B_m1 C_spr Nm d_l K_spr d_p N_starts N_spr T_load k_tm1 k_em1 R_m1
    ↪ L_m1
8 syms M_motor_gear J_motor_gear J_linear G_PLA l_shaft r_bushing M_shaft grav_cons u_PLA
9 % Symbolic equation derivation
10 % *Steering wheel EOM*
11
12 ddth_sw = (1/J_sw)*(T_load - B_sw*dth_sw - C_spr*th_sw - K_sw*th_sw)
13 % Motor current equation
14
15 di_m1 = (1/L_m1)*(-R_m1*i_m1 - k_em1*dth_m1 + V_m1)
16
17 T_motor = k_tm1*i_m1;
18 %%
19 % *Steering motor EOM*
20
21 ddth_m1 = -(C_spr + K_sw)*th_m1/(Nm^2 * J_m1) - (B_sw/Nm^2 + B_m1)/J_m1*dth_m1 + T_motor/
    ↪ J_m1
22 % Symbolic TFs
23 % These were used for PID control
24
25 TF_m1_current = -(s*k_em1*th_m1 + V_m1)/(s*L_m1 + R_m1)
26 TF_motor1 = (k_tm1/(s*L_m1 + R_m1))/ (J_m1*s^2 + (C_spr + K_sw)/(Nm^2) + (B_sw/(Nm^2) + B_m1
    ↪ + (k_tm1*k_em1)/(s*L_m1 + R_m1))*s)
27 % State Space equations
28
29 x = [th_m1 dth_m1 i_m1]
30 u = [V_m1]
31
32 A_m1 = [0 1 0; -(C_spr + K_sw)/(J_m1*Nm^2) (-B_m1 + B_sw/Nm^2)/J_m1 k_tm1/J_m1; 0 k_em1/
    ↪ L_m1 -R_m1/L_m1]
33 B_m1 = [0 ; 0 ; -1/L_m1]
34 C_m1 = eye(3);
35 D_m1 = zeros(3,1);
36 % Variables
37 % Variable list
```

```

38
39 G_PLA = 3.5e9; %PLA shear modulus
40 l_shaft = 0.24671219; %shaft length
41 M_motor_gear = 0.08116938; %Motor gear mass
42 J_motor_gear = 0.00004883; %Motor gear moment of inertia
43 J_linear = 0.00128838; %Moment of inertia of colinear shaft components
44 N_m1 = 2.3; %Gearing ratio. 1 turn of SW is 2.3 of Motor
45 k_tm1 = 0.641333333; % Motor constant
46 R_m1 = 14.8; %Motor resistance
47 L_m1 = 0.0444; % Motor inductance
48 k_em1 = 0.38; %Back emf constant
49 J_m1 = 10e-6; %Motor inertia
50 B_m1 = 0.00159; %Motor damping
51 u_PLA = 0.35; %High estimated friction coefficient
52 B_sw = 0; %Shaft damping
53 M_shaft = 0.57593742; %rotating shaft mass
54 Nm = 2.3; %Gear ratio
55 K_spr = 80; % Spring constant (0.08 N/mm)
56 N_spr = 8; %Number of springs
57 N_starts = 2; %Screw starts
58 d_p = 0.008; % Screw pitch
59 r_bushing = 0.017; %Bushing radius
60 r_sliding = ((0.017/2)+5.5e-3); %friction radius for shaft slider
61 grav_cons = 9.8; %gravitational acceleration
62 s = tf('s');
63 % Variable calculation
64 % Calculation of spring constant C_spr
65
66 d_l = d_p * N_starts; % Screw lead calculation
67 x = d_l * (th_sw/(2*pi())); %spring compression distance
68 F_spr = (N_spr*(K_spr*(x))); %Force due to spring compression
69 T_spr = (F_spr * d_l)/(2*pi());
70
71 C_spr = (K_spr*N_spr*N_starts^2*d_p^2)/(4*(pi^2))
72 %%
73 % Shaft moment of inertia
74
75 distance = (0.07396740/2) + (0.16500420/2);%radii of the two meshed gears
76 J_motor_gear_offset = J_motor_gear + M_motor_gear*distance^2; %parallel axis theorem
77 J_sw = J_linear + (J_motor_gear_offset) %Shaft moment of inertia
78 %%
79 % Shaft stiffness is based on rotation friction
80
81 F_spring_friction = u_PLA*F_spr; %The friction force due to the spring acting
82 F_normal_shaft = M_shaft * grav_cons; %Normal force of the shaft
83 F_shaft_friction = u_PLA*F_normal_shaft; %Friction due to shaft rotation
84 K_sw = (F_shaft_friction*r_bushing)+(F_spring_friction*r_sliding);
85 K_sw = double(subs(K_sw, th_sw, 1))
86 % Valued equation derivation
87 % Valued TFs
88 % These were used for PID control

```

```

89
90 TF_motor1 = (k_tm1/(s*L_m1 + R_m1))/ (J_m1*s^2 + (C_spr + K_sw)/(Nm^2) + (B_sw/(Nm^2) + B_m1
91   ↪ + (k_tm1*k_em1)/(s*L_m1 + R_m1))*s)
92 % State Space values
93 x = [th_m1 dth_m1 i_m1]
94
95 A_m1 = [0 1 0; -(C_spr + K_sw)/(J_m1*Nm^2) (-B_m1 + B_sw/Nm^2)/J_m1 k_tm1/J_m1; 0 k_em1/
96   ↪ L_m1 -R_m1/L_m1]
96 B_m1 = [0 ; 0 ; -1/L_m1]
97 C_m1 = eye(3);
98 D_m1 = zeros(3,1);
99
100 Q_m1 = eye(3);
101 R_m1 = 1;
102
103 mul = 1.5e2; %1e5 safe
104 mul_R = 1;
105     %X Y TH DX DY DTH
106 Q_m1 = Q_m1.*[1*mul, 0.01*mul, 0.01*mul];
107 R_m1 = R_m1.*mul_R;
108
109 Klqr_m1 = lqr(A_m1,B_m1,Q_m1,R_m1)
110
111 A_cl_m1 = A_m1-B_m1*Klqr_m1;
112
113 K_dc_m1 = D_m1 - C_m1*inv(A_cl_m1)*B_m1
114 %%
115 %
116 %% SA system
117 % System variables
118
119 syms V_m2 dth_m2 th_m2 ddth_m2 y dy ddy s th_w dth_w ddth_w i_m2 di_m2 ddi_m2
120
121 syms B_r M_r k_lf r_L r_p B_kp I_f R_m2 L_m2 K_tm2 J_m2 B_m1 E K_r ia_m2 dia_m2 J_w k_em2
122 % Symbolic equations
123 % Motor EOM
124 % Paper "Development of estimation force feedback torque control algorithm for
125 % driver steering feel in vehicle steer by wire System: Hardware in the loop"
126
127 ddth_m2 = -B_m1*dth_m2/J_m2 + K_r*ia_m2/J_m2
128
129 dia_m2 = -R_m2*ia_m2/L_m2 + K_tm2*dth_m2/L_m2 + V_m2/L_m2
130 % Rack and tire transfer function
131 % Paper "Development of estimation force feedback torque control algorithm for
132 % driver steering feel in vehicle steer by wire System: Hardware in the loop"
133
134 ddy =(1/M_r)*((-2*k_lf*y/r_L^2)-(K_r*y/r_p^2)-B_r*dy + (K_r*th_m2/r_p))
135
136 ddth_w = (1/I_f)*((-k_lf*th_w + (k_lf*y/r_L) - B_kp*dth_w))
137 % Symbolic TFs

```

```

138
139 TF_motor2 = simplify(K_r/ (J_m2*(s*L_m2+R_m2)*s^2 + (B_m1*(s*L_m2+R_m2) - K_tm2*K_r)*s))
140
141 TF_rack = simplify((K_r/(r_p*M_r))/(s^2 + B_r*s/M_r + (2*k_lf/(M_r*r_L^2) + K_r/(r_p^2*M_r)))
142   ↪ ))
143
144 TF_Wheel = simplify((k_lf/r_L) / (J_w*s^2 + B_kw*s + k_lf))
145 % State Space equations
146 % Motor SS
147 x = [th_m2 dth_m2 i_m2]
148 u = [V_m2]
149
150 A_m1 = [0 -(B_m1/J_m2) K_r/J_m2; 0 1 0; 0 -k_em2/L_m1 -R_m2/L_m2]
151 B_m1 = [0 ; 0 ; 1/L_m1]
152 C_m1 = eye(3);
153 D_m1 = zeros(3,1);
154 %%
155 % Rack SS
156
157 x = [y dy]
158 u = [th_m2]
159
160 A_m1 = [0 1; (1/M_r)*((-2*k_lf/r_L^2)-(K_r/r_p^2)) -(B_r/M_r)]
161 B_m1 = [0 ; K_r/(M_r*r_p)]
162 C_m1 = eye(2);
163 D_m1 = zeros(2,1);
164 %%
165 % Tire SS
166
167 x = [th_w dth_w]
168 u = [y]
169
170 A_m1 = [0 1; -(k_lf/J_w) -(B_kw/J_w)]
171 B_m1 = [0 ; k_lf/(J_w*r_L)]
172 C_m1 = eye(2);
173 D_m1 = zeros(2,1);
174 % Variables
175 % Variable list
176
177 s = tf('s');
178 R_m2 = 8.5; %Motor resistance
179 L_m2 = 0.0425; %Motor inductance
180 K_tm2 = 0.39667; %Motor constant
181 k_em2 = 1.64; %Back emf constant
182 J_m2 = 0.00001; %Motor inertia
183 B_m1 = 0.00583; %Motor damping
184
185 E = 2340000000; %Youngs modulus
186
187 r_p = 0.05216750/2; %Pinion gear radius

```

```

188 %K_r = 30.96; %Lumped torque stiffness (skeptical)
189 M_r = 0.101; %Rack mass
190 B_r = 0.003; %Estimated rack damping coefficient due to friction
191 k_lf = 0.00062; %Rack linkage stiffness (Ball bearings)
192 B_kp = 0.001; %Kingpin damping coefficient (PLA friction)
193 r_L = 0.04007805; %Offset of kingpin axis
194 % Variable calculation
195 % Lumped torque stiffness
196
197 F_rack_lumped_normal = 0.20928123 * grav_cons;%Normal force of the rack system
198 F_rack_friction = u_PLA*F_rack_lumped_normal; %Friction due to shaft rotation
199 K_r = (F_shaft_friction*r_p)
200 %%
201 % Wheel inertia
202
203 J_w = 0.00058442; %Lumped front wheel inertia
204 M_wheel = 0.29270232; %Wheel mass
205 J_w = J_w + M_wheel*(-0.00644323 - 0.02750000)^2 %parallel axis theorem
206
207 % Valued TFs
208
209 TF_motor2_valued = simplify(K_r/ (J_m2*(s*L_m2+R_m2)*s^2 + (B_m1*(s*L_m2+R_m2) - K_tm2*K_r)*
210 %<-- s))
211 TF_rack_valued = simplify((K_r/(r_p*M_r))/(s^2 + B_r*s/M_r + (2*k_lf/(M_r*r_L^2) + K_r/(r_p
212 %<-- ^2*M_r))))
213 TF_Wheel_valued = simplify((k_lf/r_L) / (J_w*s^2 + B_kp*s + k_lf))
214 % State Space equations
215 % Motor SS
216
217 x = [th_m2 dth_m2 i_m2]
218 u = [V_m2]
219
220 A_m1 = [0 -(B_m1/J_m2) K_r/J_m2; 0 1 0; 0 -k_em2/L_m1 -R_m2/L_m2]
221 B_m1 = [0 ; 0 ; 1/L_m1]
222 C_m1 = eye(3);
223 D_m1 = zeros(3,1);
224 %%
225 % Rack SS
226
227 x = [y dy]
228 u = [th_m2]
229
230 A_m1 = [0 1; (1/M_r)*((-2*k_lf/r_L^2)-(K_r/r_p^2)) -(B_r/M_r)]
231 B_m1 = [0 ; K_r/(M_r*r_p)]
232 C_m1 = eye(2);
233 D_m1 = zeros(2,1);
234 %%
235 % Tire SS
236

```

```

237 x = [th_w dth_w]
238 u = [y]
239
240 A_m1 = [0 1; -(k_lf/J_w) -(B_kp/J_w)]
241 B_m1 = [0 ; k_lf/(J_w*r_L)]
242 C_m1 = eye(2);
243 D_m1 = zeros(2,1);

```

Listing D.1: PID Controller calculations

```

function th = fcn(d, a, th_o)

detector_slots = 200;

if th_o == null
    th_o = 0;
end

if ((d == true) && (a > 0))
    th = th_o + ((360/(2*detector_slots))* (pi/180));
elseif ((d == true) && (a < 0))
    th = th_o - ((360/(2*detector_slots))* (pi/180));
else
    th = th_o;
end

function y = fcn(gain, current)

if ((current > 45) & (gain > 0)) %Forward motoring, but meeting resistance
    y = 2; %reverse braking
elseif ((current < 45) & (gain > 0)) %Forward motoring
    y = 1;
elseif ((current < 45) & (gain < 0)) %Reverse motoring
    y = 3;
elseif ((current > 45) & (gain < 0)) %Reverse motoring but meeting resistance
    y = 4;
end

```

Appendix E

AI prompts

Prompt: 'I keep running into this error in MATLAB, what is it referring to?"Error using + (line 63)
Invalid operand. Variables of type "sym" cannot be combined with other models."

The error appears to happen due to a symbolic variable I am using that I've associated a value to, howe

Response: "Thanks for sharing the error. Here's a breakdown of what MATLAB is telling you:

Error:

pgsql

Copy

Edit

Error using + (line 63)

Invalid operand. Variables of type "sym" cannot be combined with other models.

Interpretation:

This error means you're trying to add (+) a symbolic variable (sym) to something that's not compatible , or another data type that doesn't mix with symbolic expressions.

Example that causes this:

matlab

Copy

Edit

syms k

G = tf(1, [1 2 3]);

H = G + k; % ERROR: can't add symbolic variable to transfer function

Even if you've done:

matlab

Copy

Edit

k = 5; % assigns numeric value

It might still be symbolic if k was previously declared with syms.

Fixes:

Ensure symbolic variables are converted before using them numerically:

matlab

Copy

Edit

k_num = double(k); % convert symbolic to numeric

result = G + k_num;

Avoid mixing symbolic and model objects:

If you're using symbolic variables just to define parameters, use `subs()` to substitute them before using.

Example:

```
matlab
Copy
Edit
syms k
A = [0 1; -k -2];
k_val = 100;
A_num = double(subs(A, k, k_val));
Clear old symbolic definitions if needed:
If MATLAB is "remembering" a symbolic type from earlier, reset it:
```

```
matlab
Copy
Edit
clear k
k = 100; % Now purely numeric
To diagnose quickly:
Run:
```

```
matlab
Copy
Edit
whos k
It will show if k is still of type sym.
```

If you paste the specific code snippet where this is happening, I can give you an exact fix. But based on your message, it sounds like you're accidentally trying to add a symbolic variable to a model object."

Prompt: "damping coefficient of ball bearings"

Response: "The damping coefficient of ball bearings is not typically specified directly by bearing manufacturers. Instead, they are designed to minimize friction and energy loss, and their damping is usually very low. However, in engineering models, you often need an approximate damping coefficient to account for internal friction, lubricant effects, and other factors."

General Notes:

Damping in ball bearings arises from:

Lubricant shear

Internal friction

Micro-slip between balls and raceways

Seal drag (if sealed bearings)

Typical Approximations:

There's no single fixed value, but here are common approaches:

1. Empirical Values (Ball Bearing Damping Coefficient):
Typical estimates for damping coefficients

B (in Nm·s/rad) range:

Type Damping Coefficient (Nm·s/rad)

Small precision bearings

10

6

10

6

to

10

4

10

4

Medium-sized bearings

10

5

10

5

to

10

3

10

3

With lubrication drag Up to

10

2

10

2

These are order-of-magnitude estimates. Actual damping can vary based on speed, preload, and lubrication.

2. Proportional Damping (if modeling dynamically):
If you have mass

M or inertia

J, and you want critical or underdamped behavior:

=
2

B=2
KJ

Where:

is damping ratio (e.g., 0.01 to 0.05 for lightly damped systems)

K is stiffness (e.g., contact stiffness of bearing + shaft)

J is rotational inertia

3. Estimating via Manufacturer Data:

If you have bearing specs (like from SKF, NSK, etc.), some give:

Starting torque

Friction torque vs. speed curves

From friction torque

T
f

, you can approximate:

B

T
f

Where

is operating speed in rad/s. This gives a linearized viscous damping coefficient.

If you just need a number:

For a typical medium-sized bearing (say 8-15 mm bore) with light lubrication:

matlab

Copy

Edit

B_bearing = 1e-4; % Nm·s/rad

This is reasonable for system-level simulations.

Let me know your bearing size/type, and I can give a better estimate or help extract from manufacturer

Prompt: "This table is spilling off of my page. How can you set the appropriate column sizes for me"\begin{table}

\centering
\caption{Specifications assessment}
\begin{tabular}{|l|l|l|l|l|}
\hline
No.& Objective description & Acceptance criteria & Specification met\\
\hline
\hline
M-1. & The model must be small & Model should fit in a 600mm x 600mm area & Passed. The final (See Appendix \ref{app:Pictures} occupied an area of 470mm x 545mm) \\
\hline
M-2. & The model should be low cost & Model components < R3 000 & Passed. The total cost of the model was R3 000. \\
\hline
SA-1. & The model must have realistic steering capacity & Ackermann compliant angle within \$10^{\circ}\$ & Passed. \\
\hline
SA-2. & Actuator system should be sensitive to steering inputs & 1\$^\circ\$ angle resolution (detected by a custom optic sensor) & Failed. The custom optic sensor did not meet the desired resolution. The actuation precision is inconclusive. \\
\hline
SA-3 & A fast steering speed & Left-to-right turn in 1s & Passed. The actuator was able to complete a full turn in 1 second. \\
\hline
SM-1. & The model should be sensitive to steering inputs & 1\$^\circ\$ angle resolution (detected by a custom optic sensor) & Failed. The accuracy of the sensor did not meet the desired spec. However, individual detection of angles was successful. \\
\hline
SM-2. & A fast steering speed & 120rpm steering wheel rotation & \\
\hline
SM-3. & The model must be rugged & Should endure a scaled input torque (2.5 Nm) & Passed. \\
\hline
SM-4. & replicate common steering experience & Upon release of the steering wheel, it must center. The steering wheel would move slightly toward the centre when nudged, but could not consistently return to the center. \\
\hline
C-1. & The steering response should be smooth & <5% transient state overshoot & Inconclusive. The simulation results showed overshoot, but it was not quantified. \\
\hline
C-2. & Steering input should be translated to the wheel quickly & <2s delay & Inconclusive. The simulation results showed a delay, but it was not quantified. \\
\hline
\end{tabular}
\label{tab:Model_test_results}
\end{table}"


```
\label{tab:Model_test_results}
\end{table}
```

Notes:

This table uses X columns to allow automatic text wrapping within the page width.

The xcolor package is used for the \textcolor{red}{...} part.

Consider defining a custom column for fixed-width text (e.g., p{3cm}) if you want even more control.

Let me know if you'd like to adjust column widths manually or switch to landscape orientation."

```
Prompt: "Hey chat, I have this table, but it is too wide, can you make the first column wrap to save space?"  
\begin{table}[htbp]  
\centering  
\footnotesize  
\caption{Parts list for the Steer-by-Wire model}  
\begin{tabularx}{0.9\textwidth}{|c|l|l|X|r|r|r|}  
\hline  
\textbf{Part Name} & \textbf{Part Number} & \textbf{Supplier} & \textbf{Link} & \textbf{Price (ZAR)} &  
\hline  
MOTOR GEARED 12VDC 1A6 270RPM 6mm DIA=37mm & GB37Y360 12V & Mantech & \href{https://www.mantech.co.za/ProductInfo.aspx?P=MOTOR GEARED 12VDC 1A6 270RPM 6mm DIA=37mm & GB37Y360 12V & Mantech & \hline  
\hline  
MOTOR GEARED 12VDC 0A3 65RPM & EGB-365S-15130 & Mantech & \href{https://www.mantech.co.za/ProductInfo.aspx?P=MOTOR GEARED 12VDC 0A3 65RPM & EGB-365S-15130 & Mantech & \hline  
\hline  
H BRIDGE 43A HIGH POWER MOTOR DRIVE & --- & Mantech & \href{https://www.mantech.co.za/ProductInfo.aspx?P=H BRIDGE 43A HIGH POWER MOTOR DRIVE & --- & Mantech & \hline  
\hline  
DEEP GROOVE BALL BEARING 3X10X4MM ZZ CN BTC & --- & BMG &  
\href{https://bmgyworld.net/bmg/en/ZAR/All-Categories/Bearings/Ball/Deep-Groove/Single-Row/623-ZZ-BTC/p/623\%20ZZ\%20BTC}{Link} & 27.80 & 2 & 55.60 \\  
\hline  
DEEP GROOVE BALL BEARING 5X16X5MM OPEN CN & --- & BMG &  
\href{https://bmgyworld.net/bmg/en/ZAR/All-Categories/Bearings/Ball/Deep-Groove/Single-Row/625/p/625}{Link} & 16.95 & 2 & 33.90 \\  
\hline  
DEEP GROOVE BALL BEARING 17X35X10MM 2RS C3 BTC & --- & BMG &  
\href{https://bmgyworld.net/bmg/en/ZAR/All-Categories/Bearings/Ball/Deep-Groove/Single-Row/6003-2RSC3-BTC/p/6003\%202RSC3\%20BTC}{Link} & 16.95 & 2 & 33.90 \\  
\hline  
RS PRO Stainless Steel Compression Spring & 821-289 & RS Components & \href{https://za.rs-online.com/webapp/wcs/stores/servlet/Product_0_821289/}{Link} & 183.00 & 1 & 183.00 \\  
\hline  
OPTICAL GAP / SLOT SENSOR BOARD G=10mm & 170202 & Mantech & \href{https://www.mantech.co.za/ProductInfo.aspx?P=OPTICAL GAP / SLOT SENSOR BOARD G=10mm & 170202 & Mantech & \hline  
\hline  
STRUT PROFILE PG20 20X20 4 SLOTS & 1.11.20.020020.04 & Moduasm & \href{https://moduasm.co.za/product/strut-profile-pg20-20x20-4-slots-1-11-20-020020-04-2/}{Link} & 102.65 & 1.3 & 133.45 \\  
\hline  
PRE-SET NUT PG15 PG20 & 2.11.06.M5 & Moduasm & \href{https://moduasm.co.za/product/pre-set-nut-pg15-pg20-2-11-06-m5-2/}{Link} & 8.06 & 20 & 161.20 \\  
\hline  
\multicolumn{6}{|r|}{\textbf{Total}} & \textbf{R1 914.64} \\  
\hline  
\end{tabularx}
```

```
\label{tab:partslist}
\end{table}''
```

Response: "To make the first column wrap and save space in your table, replace the column type c (centered) or a flexible X type from the tabularx package.

Here's the adjusted table with the first column changed to p{3.5cm}, which wraps long content neatly:

```
latex
Copy
Edit
\begin{table}[htbp]
\centering
\footnotesize
\caption{Parts list for the Steer-by-Wire model}
\begin{tabularx}{0.9\textwidth}{|p{3.5cm}|l|l|X|r|r|r|}
\hline
\textbf{Part Name} & \textbf{Part Number} & \textbf{Supplier} & \textbf{Link} & \textbf{Price (ZAR)} & \\
\hline
MOTOR GEARED 12VDC 1A6 270RPM 6mm DIA=37mm & GB37Y360 12V & Mantech & \href{https://www.mantech.co.za/ProductInfo.aspx?...}{Link} & 27.80 & 2 & 55.60 \\
\hline
MOTOR GEARED 12VDC 0A3 65RPM & EGB-365S-15130 & Mantech & \href{https://www.mantech.co.za/ProductInfo.aspx?...}{Link} & 27.80 & 2 & 55.60 \\
\hline
H BRIDGE 43A HIGH POWER MOTOR DRIVE & --- & Mantech & \href{https://www.mantech.co.za/ProductInfo.aspx?...}{Link} & 27.80 & 2 & 55.60 \\
\hline
DEEP GROOVE BALL BEARING 3X10X4MM ZZ CN BTC & --- & BMG &
\href{https://bmgyworld.net/bmg/en/ZAR/All-Categories/Bearings/Ball/Deep-Groove/Single-Row/623-ZZ-BTC/p/623%20ZZ%20BTC}{Link} & 27.80 & 2 & 55.60 \\
\hline
DEEP GROOVE BALL BEARING 5X16X5MM OPEN CN & --- & BMG &
\href{https://bmgyworld.net/bmg/en/ZAR/All-Categories/Bearings/Ball/Deep-Groove/Single-Row/625/p/625}{Link} & 27.80 & 2 & 55.60 \\
\hline
DEEP GROOVE BALL BEARING 17X35X10MM 2RS C3 BTC & --- & BMG &
\href{https://bmgyworld.net/bmg/en/ZAR/All-Categories/Bearings/Ball/Deep-Groove/Single-Row/6003-2RSC3-BTC/p/6003%20RSC3%20BTC}{Link} & 16.95 & 2 & 33.90 \\
\hline
RS PRO Stainless Steel Compression Spring & 821-289 & RS Components & \href{https://za.rs-online.com/webapp/wcs/stores/servlet/ProductDetail?sku=0821289}{Link} & 183.00 & 1 & 183.00 \\
\hline
OPTICAL GAP / SLOT SENSOR BOARD G=10mm & 170202 & Mantech & \href{https://www.mantech.co.za/ProductInfo.aspx?...}{Link} & 27.80 & 2 & 55.60 \\
\hline
STRUT PROFILE PG20 20X20 4 SLOTS & 1.11.20.020020.04 & Moduasm & \href{https://moduasm.co.za/product/strut-profile-pg20-20x20-4-slots-1-11-20-020020-04-2}{Link} & 102.65 & 1.3 & 133.45 \\
\hline
PRE-SET NUT PG15 PG20 & 2.11.06.M5 & Moduasm & \href{https://moduasm.co.za/product/pre-set-nut-pg15-pg20-2-11-06-m5-2}{Link} & 8.06 & 20 & 161.20 \\
\hline
\multicolumn{6}{|r|}{\textbf{Total}} & \textbf{R1 914.64} \\
\hline
\end{tabularx}
\label{tab:partslist}
```

\end{table}

You can adjust the p{3.5cm} width if it's still too tight or too loose. Let me know if you'd like to allow line breaks or if you want the table to rotate to landscape."